LUND UNIVERSITY

Linnæus University

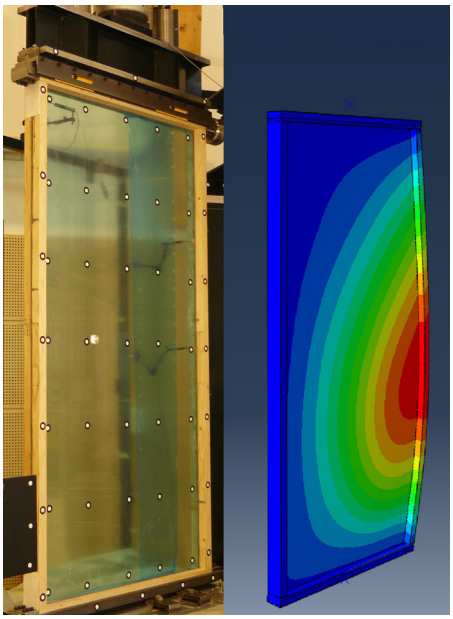

# BUCKLING OF A LOAD BEARING TIMBER-GLASS SHEAR WALL
## Development of a Finite Element Model

GREGER NEIJBERT

Structural Mechanics

*Master's Dissertation*

DEPARTMENT OF CONSTRUCTION SCIENCES

DIVISION OF STRUCTURAL MECHANICS

ISRN LUTVDG/TVSM--13/5189--SE (1-84) | ISSN 0281-6679

MASTER'S DISSERTATION

# BUCKLING OF A LOAD BEARING TIMBER-GLASS SHEAR WALL

## Development of a Finite Element Model

GREGER NEIJBERT

Supervisor: **ERIK SERRANO**, Professor; Dept. of Building and Energy Technology, Linnaeus University, Växjö.

Examiner: **KENT PERSSON**, PhD; Div. of Structural Mechanics, LTH, Lund.



Printed by Media-Tryck LU, Lund, Sweden, August 2013 *(Pl)*.

For information, address:

Department of Building and Energy Technology, Linnaeus University, SE-351 95 Växjö, Sweden.
Homepage: http://lnu.se

Division of Structural Mechanics, LTH, Lund University, Box 118, SE-221 00 Lund, Sweden.
Homepage: http://www.byggmek.lth.se

# Abstract

In a European collaborative research project a timber-glass shear wall element has been developed. This consists of a 10×1200×2400 mm thick glass pane of standard float glass with an LVL-frame adhesively bonded to the glass along its perimeter .In previous research several laboratory tests of these types of shear walls were performed. The tests, performed for various modes of loading, indicated that the shear walls collapsed due to buckling

The aim of this master thesis has been to further analyse the stability of the timber-glass shear wall element. The results from laboratory tests were evaluated and the shear wall element was analysed with the finite element method using a modelling and analysis computer software. The finite element model was calibrated to match the results from the experiments in terms of failure loads, assuming failure was due to instability in the shear wall element. Further analyses were made on the influence of various parameters (e.g. material and geometry) on the structural behaviour. Of special interest has also been to investigate the load bearing capacity when combining vertical and horizontal loads.

The results show that the buckling load was decreased when using a less stiff adhesive. The elastic stiffness of the timber studs had a larger relative impact on the stability of the shear wall element, than the elastic modulus of glass. The buckling shape also turned out to be dependent on the ratio between the stiffness of glass and the stiffness of the vertical timber studs. In a combined load case two interaction formulas were fitted to the results of the analysis.

The buckling analyses was in the end, after a lot of work, a good tool to use when estimating the critical load limit of the timber glass shear wall. However, the boundary conditions have showed to be of great importance in order to get an accurate result.

# Sammanfattning

I ett europeiskt samarbetsprojekt har ett skjuv-väggelement av glas och trä utvecklats. Detta element består av en 10×1200×2400 stor glasskiva av standard glas, med en träram av 45×45mm LVL limmad längs kanterna. I tidigare studier har flera laboratorietester utförts på dessa typer av skjuv-väggelement. Provningarna, som har utförts med olika typer av belastningsfall, indikerar att skjuv-väggen kollapsade på grund av instabilitet, buckling.

Syftet med detta examensarbete har varit att ytterligare analysera stabiliteten i detta vägg-element av glas och trä i samverkan. Resultatet från laboratorietester har utvärderats och väggelementet har också analyserats med finita elementmetoden med en modellerings- och analysprogramvara. Inverkan av materialegenskaper har också analyserats ytterligare. Av särskilt intresse har också varit att undersöka lastkapaciteten vid en kombination av vertikal och horisontal lastpåverkan.

Resultaten visar att knäcklasten minskar markant vid användning av ett mindre styvt lim. Den elastiska styvheten hos träet visar sig ha en större relativ inverkan på lastförmågan jämfört med den elastiska styvheten hos glaset. Bucklingsformen visade sig vara beroende av förhållandet mellan styvheterna hos glaset och träet. Vid det kombinerade lastfallet kunde två olika interaktions samband utformas.

Bucklingsanalysen visar sig, efter mycket nedlagt arbete, vara en bra metod för att utvärdera lastförmågan hos väggelementet. En mycket betydelsefull faktor för att erhålla korrekta resultat var modellens upplagsvillkor.

# Preface

This master thesis was carried out during the spring of 2013. The work has been conducted at Linnaeus University, Department of Building and Energy Technology.

First I would like to thank Professor Erik Serrano at Linnaeus University for giving me the opportunity to carry out my master thesis work within this research area. I also thank Erik for his generous dedication and support, without his knowledge and advise this project would not have been possible to complete. I am also very grateful to Dr. Johan Vesby at Linnaeus University, and Dr. Kent Persson at LTH Division of Structural Mechanics for their expertise and advice which they have shared with me through our discussions.

Finally I want to thank my family and friends for their great support throughout my education.

Växjö, Juni 2013
Greger Neijbert

# Contents

# 1 Introduction

Timber and glass are materials with a wide range of uses. Both timber and glass have been used a long time back, and due to the technical development the usage area has expanded and today the materials are found in a variety of good products. In architecture glass has long been an appreciated material, especially for its transparent properties. With glass one can enlighten the indoor environment, which is an important factor for our indoor wellbeing. Thanks to technical development it has become possible to build large glass façades to a reasonable cost, and today it is rather a demand than a request that the building has a large light inlet and a transparent appearance.

Timber has been used in construction since mankind built the first hut and timber is an excellent building material, not only because of its good strength qualities but also for its aesthetically expression and that it is considered as an environmental friendly building material. A natural step in the development would be to combine timber and glass and allowing them to complete each other's properties.

Laminated glass façade have been used a long time, but until now only serving as an outer shell on a supporting structure. In modern architecture it is not uncommon that entire walls are replaced by large glass panes. But a house wall element must carry the vertical loads from roofs and other overlaying loads and stabilize the house sideway against wind loads. When this wall is replaced by a glass façade an additional load carrying system is required. The vertical loads are then often carried by columns and beams, and the stabilizing structure are made up by wind diagonals or carried by interior walls. A good idea to save on materials and costs would be to use the glass as a structural element.

## 1.1 Topic introduction

In a European research project dealing with load bearing timber-glass building components, a shear wall element able to carry load both vertically and horizontally has been studied. The research project was carried out in cooperation between Glafo AB and Linnæus University, with the official name 'Glass and timber – Innovative building components with added value'. In previous research several tests of these types of shear walls were performed. The execution of these tests is presented in [1] but the results have not been further analysed.

The shear wall elements tested consisted of an LVL-frame adhesively bonded to the glass along its perimeter using two different adhesives, one silicone and one acrylate adhesive. The glass pane used was 10x1200x2400 mm. The glass material was a standard float glass. Three types of load cases were used, vertical, horizontal and combined vertical-horizontal loading. Displacements were measured with potentiometers and with a non-contact 3D-deformation measuring system, Pontos™.

In the experimental test there were no visual cracks in the glass before the maximum load was reached. The elements failed suddenly by cracking of the entire glass sheet. The glass fell out in large pieces and the timber-frame could not hold the remaining glass or carry the load level reached.

## 1.2 Aim and limitations

The aim of this master thesis is to further analyse the stability of the timber-glass shear wall element. The results from tests performed at Linnæus University will be used to evaluate the out-of-plane displacements for different load cases. The shear wall elements under loading will also be analysed with the finite element method using a modelling and analysing computer FE-program. The FE-model will be calibrated to match the results from experiments in terms of failure loads assuming failure is due to instability in the shear wall element.

Once a reasonably good fit to experimental data is obtained further analyses will be made on the influence of various material parameters on the structural behaviour of the timber-glass shear wall.

Of special interest is also to investigate the load bearing capacity when combining vertical and horizontal loads. Results from this analysis could serve as a background for development of design formulae for timber-glass composite shear walls.

To be able to perform accurate calculations and have a functional FE-model it is important to get a good knowledge of the materials glass, wood and the adhesive that holds these together. A theoretical background of failure due to instability of structures is also important to obtain. This is achieved by an introductory literature review.

## 1.3 Outline of the thesis

The first part aims at giving the reader a background of materials, the concept of a timber-glass shear wall and an introduction to the theory used dealing with buckling phenomena (instability) and the finite element method. Materials that are used to build up the shear wall element: timber, glass and adhesive are presented in chapter 2, were also earlier research of timber-glass composite products are mentioned. In chapter 3 the timber-glass shear wall element analysed in this thesis is presented more thoroughly. In chapter 4 the theory of instability of a plate, the finite element method and the FE software Abaqus is described.

The second part, chapter 5, aims at describing how the FE-model was developed and presents the method used to gain the results of this thesis.

In the third part (chapter 6-8) the results from calculations are presented and discussed. Finally suggestions for further work are made.

References used are presented in the final chapter. The appendix section shows graphs and tables from experiments and FE-calculations, the former being used as input for the model development, the latter being the results from the various analyses performed.

# 2 Materials in the shear wall element

## 2.1 Timber

Timber is one of the oldest building materials used by mankind. Timber in its natural form has a lot of embedded properties that makes it an excellent building material. It is capable of transferring both tension and compression and has a high strength to weight ratio. Timber is also easy to process into different shapes and to connect with other timber elements.

The natural growth of timber creates a variety of structures and characteristic defects. This is often aesthetically appealing but it also creates problems in timber construction. Timber is thus not a homogeneous material and defects like knots must be considered as these reduce the strength of timber. When, for example timber is exposed to tension, a knot can be regarded as a hole, resulting in eccentric loading as the fibers circle the knot. Defects vary in shapes, sizes and number and a board with many knots is weaker than a board with fewer knots. Other examples of defects are fissures. [2]

The strength of the timber is besides the number of defects dependent of several other parameters like species, density and the slope of the grain. To be able to take advantage of the potential capacity of timber it is normally graded into different strength grades. The properties are determined in a nondestructive manner either by visual inspection or by mechanical grading. Visual strength grading was developed in the US during the 1920s and is a manual process performed by a qualified grader. The timber is graded into different classes based on type, size and frequency of defects. Today there are also scanning techniques developed to simplify and improve the process. Machine strength grading is a technique that evaluates the timber properties on the principle that strength is related to stiffness. Each timber piece is tested to provide parameters, so called indicating properties, that are compared with statistical data, the most common parameters are modulus of elasticity and density. [3]

Timber always contains a certain amount of water. The moisture content (MC) indicates the mass of water in percent of the mass of the completely dry timber. The timber moisture content strives to be in balance with the surrounding environment and changes with the relative humidity of the surrounding air. This also leads to a change in dimension and strength. Timber shrinks as the moisture content decreases and swells as it increases, the strength increases when moisture content decreases and vice versa. Flawless timber with a moisture content of 6-23% changes as an example its compressive strength parallel to the fiber direction by 5% at 1% change in moisture content. Experiments have also shown that the load duration has an effect on strength. [2] In the design of timber structures a conversion factor, $k_{mod}$, is used to take climate and load duration into account when establishing the strength property. [4]

Timber is an anisotropic material, i.e. the properties vary depending on the direction of the material compared to an isotropic material like steel in which the properties are the same in any direction. The tree trunk structure gives rise to a material which can be regarded as cylindrically orthotropic. The properties vary along three different directions, the main

directions are the longitudinal (fiber direction), radial and tangential direction [2], see Figure 2.1 below.

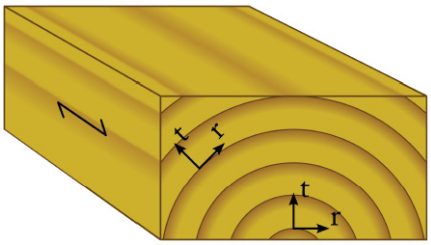


*Figure 2.1 Idealized material orientations of timber. The radial and tangential directions are denoted r and t, respectively, on the end-grain surface. (Image originates from [1] )*

The highest strength is achieved in the longitudinal direction. Flawless softwood timber, e.g. Norway spruce (*Picea abies*) has a tensile strength in the range of 100 MPa, however the defects have a large impact and structural timber has a characteristic tensile strength of 10-35 MPa. The load-deformation curve is almost linear up to failure [2] and for structural timber the modulus of elasticity varies between 7-14 GPa depending on its grade. [4]

Tensile strength across the fibers is very low compared to the longitudinal direction, with characteristic values being as low as 0.4 MPa for structural timber [4]. Loading in tension perpendicular to grain should therefore in general be avoided, and stress transfer in this direction should only be used as a secondary effect. For example tensile stresses occur across the fiber direction when a curved glulam beam is loaded in bending [2]. The elastic modulus perpendicular to grain varies between 230-470 MPa for structural timber [4].

The compressive strength parallel to the fiber direction is 40-50 MPa for defect free timber [2] and ranges from 16 to 26 MPa for structural timber [4]. To determine the compressive strength, test specimens are used where there is no risk of buckling. Failure occurs when the fibers collapse and buckles forming kinks. During this kinking the load bearing capacity typically decreases with 20% [2]. The modulus of elasticity is the same as in tension. Perpendicular to the fibers the deformation is often more interesting than the compressive strength, as no real failure occurs.

Most commonly the shear action in timber is related to the three othotropic planes, longitudinal-radial, longitudinal-tangential and radial-tangential (also known as rolling shear). Loading in longitudinal shear (longitudinal-radial or longitudinal-tangential) is the most common in timber structures. From a practical point of view it is not possible for an engineer to distinguish between the two when designing structures, therefore the lowest value of shear strength is used in codes. In structural design codes the shear strength can vary depending on if the load applied is a torque or shear force, and the geometry of the cross section may also have an influence [2]. The characteristic value of shear strength in structural timber is in Eurocode 5 3-4 MPa [4], this is half of what Carling [2] specifies for flawless timber. Shear strength of timber is strongly dependent on the presence of cracks, knots on the other hand have a reinforcing effect [2]. The shear modulus for structural timber varies between 440-

880MPa [4] (longitudinal shear). The shear modulus in rolling shear is typically of one order of magnitude less, 40-60 MPa.

### 2.1.1 Timber products

Timber is available in several different types of building materials in different forms. For obvious reasons, sawn timber is available in limited dimensions, but this problem was solved in the late 1800s by gluing several boards to each other. The product is called Glued Laminated Timber (GLT). The mean strength of GLT is not much higher than that of solid timber but the defects of the timber are more uniformly distributed in GLT which reduces the variance of the structural properties, resulting in higher characteristic values and design values. Since the development of GLT several other useful products have been developed, such as plywood, high density fiber boards, oriented strand board etc. In many of the developed products some kind of adhesive is used for binding timber together in different forms, the timber may consist of solid boards or sawdust.

Laminated veneer lumber – LVL, is produced using similar principle as for GLT. Thin veneers (2-4mm) are peeled off the log, which first has been steamed in hot water. After drying the veneers these are glued together and formed to structural panels with a thickness of 20-90 mm and a size of maximum 3000 x 24000 mm. When the adhesive has cured the panels are sawn to desired board dimensions. For standard LVL the layers are oriented with the fibers in the same direction. Similar to GLT, the LVL shows a less variability in structural properties and is a strong material with relatively high modulus of elasticity and high bending, compression, tension, and shear strength. [3]

### 2.1.2 Stiffness properties of timber

Timber is assumed to be an elastic and orthotropic material in the FE-model to be developed. As described above this means that it has different properties in three directions that correspond to longitudinal, radial and tangential directions. The timber frame of the shear wall used is made of laminated veneer lumber, LVL. The material parameters for the LVL used in the experiment must be estimated to create a proper model.

In [5] Ormarsson uses the following parameters for stiffness properties of timber. The given values are assumed to be equivalent with Norway spruce.

*Table 2.1 Elastic stiffness parameters for timber, according to Ormarsson [5]*

| | | | |
|---|---|---|---|
| Elastic Stiffness parameters | $E_l = 9700$ MPa | $E_t = 220$ MPa | $E_r = 400$ MPa |
| | $G_{lt} = 250$ MPa | $G_{lr} = 400$ MPa | $G_{rt} = 25$ MPa |
| | $\nu_{lt} = 0.6$ | $\nu_{lr} = 0.35$ | $\nu_{rt} = 0.55$ |

The refined timber product LVL has higher modulus of elasicity. In [6] Blyberg uses the following values for the LVL when I-beams with a web of glass and flanges of LVL are modeled in a four-point bending test.

*Table 2.2 Elastic stiffness parameters for LVL timber, according to [6]*

| | | | |
|---|---|---|---|
| Elastic Stiffness Parameters | $E_l = 16\ 060$ MPa | $E_t = 440$ MPa | $E_r = 440$ MPa |
| | $G_{lt} = 440$ MPa | $G_{lr} = 440$ MPa | $G_{rt} = 44.4$ MPa |
| | $\nu_{lt} = 1.1$ | $\nu_{lr} = 1.1$ | $\nu_{rt} = 0.39$ |

In discussion with supervisor Professor Erik Serrano the values for LVL presented in Table 2.3 were estimated. The values are a combination of the values according to the manufacturer's material specification and values for normal structural timber (spurce or pine).

*Table 2.3 Estimated elastic stiffness parameters of LVL timber used in experiments on the timber-glass shear walls (E. Serrano)*

| | | | |
|---|---|---|---|
| Elastic Stiffness Parameters | $E_l = 13\ 800$ MPa | $E_t = 430$ MPa | $E_r = 130$ MPa |
| | $G_{lt} = 440$ MPa | $G_{lr} = 440$ MPa | $G_{rt} = 44.4$ MPa |
| | $\nu_{lt} = 0.5$ | $\nu_{lr} = 0.5$ | $\nu_{rt} = 0.5$ |

## 2.2 Glass

Glass is a highly valuable material with aesthetically appealing properties. The foremost advantage of glass is its transparency, this was the first material that let the light shine through walls in to a building without letting in wind or water. This property is probably the most appreciated and used in almost all buildings. As a result of the technical development, there are many new application areas for glass today, among these it is a highly interesting material for structural, i.e. load bearing, applications within building construction.

The special characteristics of glass depend on the way it is formed and the structure of the atoms in the material. All materials appear in solid, liquid or gas state. In a solid state the atoms are bound to each other in a determined manner, in liquid or gas state the atoms are more free to move. Many materials in nature like sand or metals are crystalline solid materials with an ordered atomic structure. When these materials are heated they melt to a liquid, and when the melt cools down the atoms return again to the same ordered structure. The glass melt has a very high viscosity and when it cools the atoms remain in an unordered fashion which gives the characteristic transparency. Crystalline materials shrink fast when they crystallize to a solid material, this occurs at the melt temperature. Glass melt does not have a distinct melting point and the transition to a solid state is gradual. The high viscosity and gradual transition to the solid state gives the opportunity to form glass in a unique way. [7]

Glass is mainly made of oxides and in regular glass the most common base is silica sand which is mixed with soda and limestone, called soda-lime silica glass. By combining different oxides to this mass different properties can be added. [7]

#### *Techniques of making glass*

Since the first making of glass, different techniques have been developed to process the material. The first glass panels were created with the technique of a blowpipe that creates a glass bubble. By then making a small hole and spinning the blowpipe a circular glass panel is formed which can be cut to different shapes. The method of making glass panels has developed over time and in the mid 1950's the technique of "float glass" was developed in Enlgand [8], a technique which is still used today. When the technique of making glass was refined and production costs dropped glass became more available to everyone. Architects of today use glass to create astonishing building facades or other creations, which was impossible before the development of float glass.

The name "float glass" indicates the process used to produce the glass panels. The materials are mixed and heated to a melted mass which is then poured on to a bed of molten tin on which it floats. This creates two plane surfaces. The molten glass is slowly cooled down and cut to desired dimensions [8]. Annealed glass is regular float glass that is produced with a cooling process that is slow enough to avoid eigenstresses in the glass.

### 2.2.1 Mechanical properties

Glass is an isotropic material and when loaded as well as unloaded it responds with perfectly linear behavior. Glass is indeed also a strong material, but it is at the same time very brittle and breaks easily if any cracks or scratches are present. The material breaks suddenly when the load limit is reached without any plastic deformations. In comparison to steel there is no yielding i.e. any larger deformations before a structural collapse. This is not a desired property in a building structure, where the structure should give some sorts of warning that its loading capacity is being reached. Steel material show yielding so that larger deformations occur and wood squeaks and cracks, but glass can break suddenly without any warning, like concrete without reinforcement [8]. A safe structure should be capable of carrying the load even after a major part of the system has collapsed, a property called a redundancy. The absence of redundancy must be considered when using glass as a structural material.

Glass has a high theoretical strength of up to 100 GPa, but the actual strength is difficult to define and the design strength value for short term loading is 22.5 MPa [9]. The molecular structure of glass doesn't have the capability to stop an arising crack and a crack that appears due to tensile stress grows until it meets a free edge [8]. Specially made glass without any surface imperfections can have a tensile strength up to 7000 MPa, but soda-lime silica glass of similar composition made by industrial methods only has a tensile strength of 25 to 70 MPa [10]. Another factor that affects the strength is the roughness of the edges on the glass, a flat surface is much stronger. Veer [9] shows that the edge finish is a dominating factor in determining the glass strength.

The rate of deformation and time of stress impact has also a high importance on the strength of glass. Glass has a tendency to fail under static fatigue, and unexpected failure can occur at lower loads than what's expected. It is stronger when loaded rapidly rather than slow, but does not stand thermal or mechanical shocks. [10]

### *Material Data*

Table 2.4 below shows a summary of the properties of annealed glass according to Glafo [7].

*Table 2.4 Properties of glass according to Glafo [7]*

| | | |
|---|---|---|
| Density (ρ) | 2500 | $kg/m^3$ |
| Young's modulus (E) | 70-75 | GPa |
| Shear modulus | 20-30 | GPa |
| Poissons ratio | 0.23 | - |
| Thermal expansion coeff. (α) | $9 \cdot 10^{-6}$ | /K |
| Compressive strength | 880-930 | MPa |
| Tensile strength | 30-90 | MPa |
| Bending strength | 30-100 | MPa |

In a British pocket book for structural engineers [11] ,Cobb gives values according to Table 2.5

*Table 2.5 Properties of glass according to Cobb [11]*

| | | |
|---|---|---|
| Density (ρ) | 25-26 | $kN/m^3$ |
| Young's modulus (E) | 70-74 | GPa |
| Poissons ratio | 0.22-25 | - |
| Thermal expansion coeff. (α) | $8 \cdot 10^{-6}$ | /K |
| Compressive strength | 1000 | MPa |
| Tensile strength | 45 | MPa |

### *Reinforced and strengthened glass*

To further increase the strength of glass generally two methods are used, toughening and laminating. Toughening of glass is a physical process, but the material itself is unchanged. The glass panel is first heated to about 600 degrees, and then the panel's surfaces are ventilated with air with temperature of about 20 degrees. When the panel is cooled down it shrinks and becomes hard on the outside, but the inside is still warm and cools off slower. As the inside cools and thereby shrinks compressive stress is created on the outside layer of the panel, and tensile stress is created in the inner parts. The compressive stress closes scratches and cracks in the outer layer and these can´t grow and cause a collapse. Normal (annealed) float glass breaks into large pieces with sharp edges but the thermally strengthened glass breaks into many small pieces.

Laminating is another technique to make glass safer. The method is to glue two or more glass panels together. To make the joint invisible the mostly used methods is to laminate with a transparent foil of PVB (polyvinyl butyrate). [8] The laminated glass has the advantage that it holds the glass together even if a crack appears which can generate a remaining structure with some post breakage load bearing capacity after fracture has occurred. Kott describes the failure of a laminated glass pane with two glass panes and one layer of PVB in three stages. In stage 1 both panes carry the load, until a fracture appears in one of the panes which is the beginning of stage 2. In stage 2 all the load is carried by the intact pane. The final stage begins when all panes are cracked but the structure has not collapsed. The cracked glass cannot carry tensile stresses so the PVB now acts as tension reinforcement and the glass transmits compression stresses. [12]

## 2.3 Adhesives

The adhesive bond is developed by a process of adhesion and cohesion. The adhesive has to stick to (adhesion) the two different materials (adherends) and in the final state become sufficiently solid so that it remains intact when subjected to stresses (cohesion).

The adhesion, i.e. ability to stick to the surfaces, can be generated by chemical bonds, mechanical interlocking or a combination of these. The chemical bounding is generated when the adhesive reacts chemically with the adherend, and creates a surface property named tackiness. The mechanical interlocking produces the joint by a cementing process where the adhesive penetrates into pores, holes, scratches etc. of the surface connecting the materials.

The ability to remain intact when subjected to stresses, i.e. cohesion, is developed in the adhesive during the curing, i.e. the hardening process. The cohesive forces are a function of cross linking within the adhesive and the number of side chains on the long chain molecules of the adhesive.

The curing process of adhesives occurs in different ways. It can be e.g. by the evaporation of a solvent, the formation of crystal or by crosslinking between molecules. In curing by evaporating the adhesive is a high viscosity polymer carried by an organic solvent or water. When the solvent evaporates the tacky adhesive remains to carry the stresses, often the evaporation is helped by exposing it to open air and when ready, the pieces are pressed together, these adhesives are commonly called contact adhesives.

There are a large number of different materials glued together in the industry. Since there must be compatibility between the adherends and the adhesive, this also requires a large number of various adhesive products that can attach to the materials and tie them together. If the two adherend materials are chemically totally different a conversion process is often required to change the surface chemistry and enable the adhesive to stick to both surfaces, an example of such a process is the use of primers.

When hardened the chemical constituents of the adhesive govern its mechanical properties. If it has a high glass transition temperature it can be brittle, if the molecular chains are capable of bending and rotating it is more rubbery. Many adhesives are sensitive to environmental

changes, such as moisture, temperature and light (especially UV-light) etc. The strength of the adhesive bond is therefore dependent on the service environment. It is also dependent on the type of solvent and the bond thickness. [10]

To withhold well working joints using adhesives there are some design approaches to keep in mind. The obvious one is of course that the bonding surface area should be as large as possible. The joint should be designed to counteract forces in the plane of the adhesive, i.e. work in shear. It is important to avoid peeling stresses were the adhesive can be very week, in some overlap joint shear stresses produce tensile stress at the edges which initiates peeling. [10]

### 2.3.1 Adhesives for timber glass applications

Since glass is a brittle material it is important to connect glass and timber in a way that avoids stress concentrations in the glass. Adhesives have the ability to transmit loads from timber to glass in a uniform manner if a flexible adhesive is used instead of more commonly used rigid adhesive.

The most common adhesives used today are silicone, silanes, polyurethanes or acrylates. The silicone adhesives have in general a relatively low characteristic strength but they have a very good resistance against environmental factors. Acrylates in general have a higher strength but lose their strength at temperatures over 50°C or at high humidity. [13].

In [14] a study of three different adhesives is presented, the main aim of this study was to analyze some adhesives that could be used for connecting glass and timber in load bearing structures. The adhesives included were: a highly deformable silicon adhesive with a thick bond line, a stiff polyurethane adhesive with a thin bond line and an acrylate adhesive with mechanical property between the two others. The adhesives were tested in shear and tensile stress with the mean values of strength (stress at failure) according to Table 2.6

*Table 2.6 Mean values of strength for adhesives tested in [14]*

| Adhesive | | Tensile strength (MPa) | Shear strength (MPa) |
|---|---|---|---|
| Silicone | (Sikasil SG-20) | 0.77 | 0.93 |
| Acrylate | (SikaFast 5215) | 3.04 | 4.48 |
| Polyurethane | (Prefere 6000) | 1.56 | 3.82 |

The strength of the polyurethane had a large variance indicating that this type of bond was more sensitive to disturbances than the other two. In the concluding remark it is stated that the silicone adhesive is well suited to distribute loads, but its low strength means that a large contact area is required. Therefore the acrylate adhesive would be the most appropriate adhesive to investigate further. A negative property of this adhesive though is its thermal stability. With a glass transition temperature of 52°C the stiffness of the acrylate adhesive could be reduced in a building due to solar energy. [14]

In [13] Winter states that the most suitable adhesives to be used in a façade construction would be the silicone adhesive. Although their strength is lower they have a much more consistent behavior under effect of moisture and temperature, and the creep behavior is lower. Long term effects of silicones are also well known since they have been used in structural glazing during decades.

The Young's modulus of different adhesives varies. Of the adhesives further mentioned in this thesis Silicone adhesive, e.g. Sikasil SG-20 has a Young's modulus of approximately 1 MPa according to the product data sheet. For the acrylate adhesive, SikaFast 5215, Young's modulus is about 80 MPa. There are however also adhesives with higher E-modulus of up to 20 GPa, e.g. epoxy [10].

## 2.4 Timber/glass composites

The hotel Palafitte in Switzerland was built with timber-glass I-beams to support the roof. The I-beams were made with timber flanges and a glass web which gives a light impression and lets the light shine through to create a bright atmosphere in the building. There are studies that investigate the behavior of these elements when exposed to higher loads. One important property that was observed was that a redundancy can be obtained in these types of composite elements. In a study at Linnæus University in Sweden [1] 14 I-beams specimens were tested for stiffness during lower loads and the ultimate load until failure. The tests evaluated three modifying parameters; adhesive type, flange groove width and the roughness of the corners in the glass section. The I-beams were tested in four-point bending with lateral support along the beam to prevent lateral torsional buckling. In all of the beams the first crack appeared in the glass at a load much lower than the maximum load level. The increase of load from first crack until maximum load was above 100% for all beams. At failure, several cracks had appeared and the wood flanges had also failed.

In [15] Niedermaier presents a study of glass panels that can be used as stiffening elements in light-weight timber structures for example to with-stand the wind loads. The glass panel was glued to a timber frame and stabilized the frame through its shear stiffness. The construction also enabled the possibilities of integrating other important technical features such as thermal insulation. The fundamental influence on the deformation behavior of the panels was shown to be due to the type of adhesive and due to the geometry of the glued joints. Since the elements of facades are exposed to different climates the adhesives were tested in different temperatures, also the effect of fatigue strength must be considered.

A research project of "Holzforschung Austria" (HFA) has resulted in a patented structural timber-glass-composite element system, and two building have been raised for further studies on long-term behavior and durability. One of these buildings is a two storey house, were the assembly and production process had a very positive outcome. With good results after the long-term tests mass production of these kinds of buildings could be possible. [13]

# 3 Shear wall element

In this chapter the background and concept of a shear wall element will be described. Earlier tests of a shear wall element conducted at Linnæus University will then be described and summarized. The results from these tests will later on be used to evaluate the models analyzed in a computer FE-program.

## 3.1 The conceptual design of the shear wall element

The shear wall element was designed within the research project described in the introduction. The shear wall is intended to carry loads vertically and horizontally and be able to function as a load carrying façade element.

The built up of the entire wall element consist of three parts. In the mid plane there is a load carrying core of glass, on both sides there is a timber frame attached to the core, and thus the load bearing core is embedded in the timber along its perimeter. On the outside, attached with steel profiles, there is a 4 + 4 mm thick laminated glass. The steel profiles create enough space so that solar control equipment can be installed. On the inside an insulated glass unit is inserted into a wooden frame that is screwed to the load carrying mid part timber frame. The design is developed with considerations both for energy efficiency and the risk of sabotage.

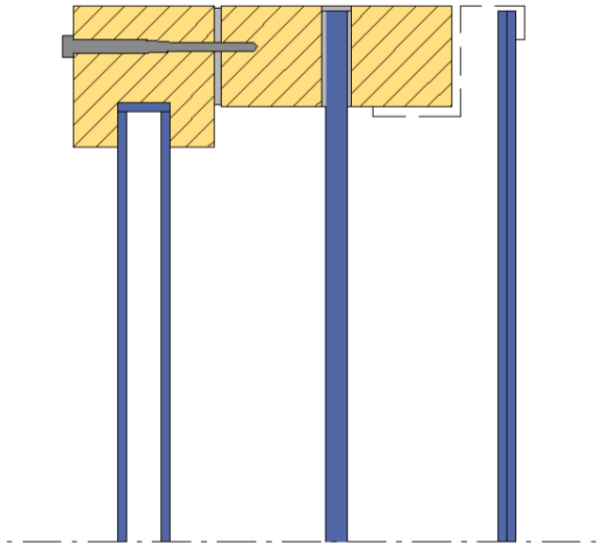

*Figure 3.1 Conceptual section of shear-wall element*

## 3.2 Methods and materials in previous experiments on shear wall elements

The load carrying structure is only the mid glass core and the timber frames, the other parts are not intended to add any strength to the load carrying system. Therefore when these shear wall elements were tested only the mid pane and the timber frame were built and tested.

In the laboratory at Linnæus University 10 shear wall elements were tested with the dimensions according to Figure 3.2.

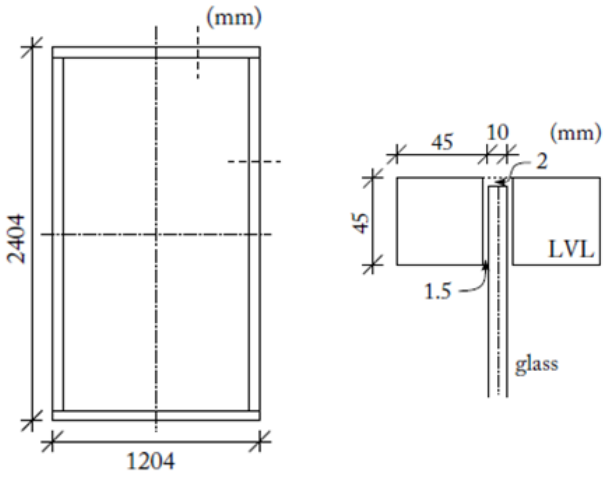


*Figure 3.2 Geometry of the shear wall element [1]*

Three of the specimens were glued with a silicone adhesive (Sikasil SG-500), the others were glued with an acrylate adhesive (Sikafast). The elements were tested in three load cases to study the behavior in vertical, horizontal and combined vertical and horizontal loading. Figure 3.3 below shows the load cases. The gray objects are the load application and support devices. P1 to P6 shows the location of the potentiometers used in the test to measure the displacements.

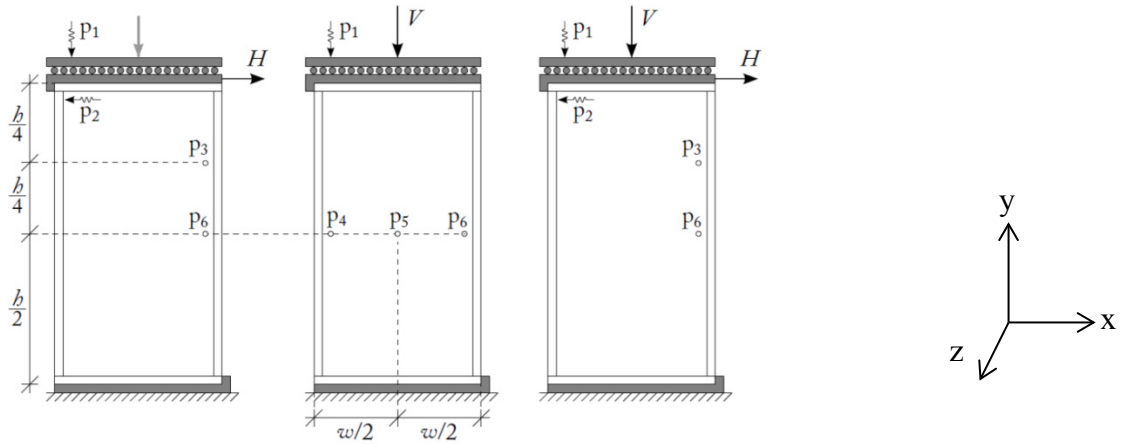


*Figure 3.3 Load cases and displacement measurement points for horizontal load (left), vertical load (mid) and combined vertical-horizontal load(right) [1]*

The upper and the lower support were both free to rotate about the horizontal (x) axis. Both the upper and lower supports were locked in the out of plane (z) direction. In the vertical load case the horizontal translation (y-direction) in the upper load applying device was locked. In the horizontal load case the upper loading device functioned as a hold-down support. Figure 3.4 below shows a more detailed image of the supports holding the shear wall element in place.

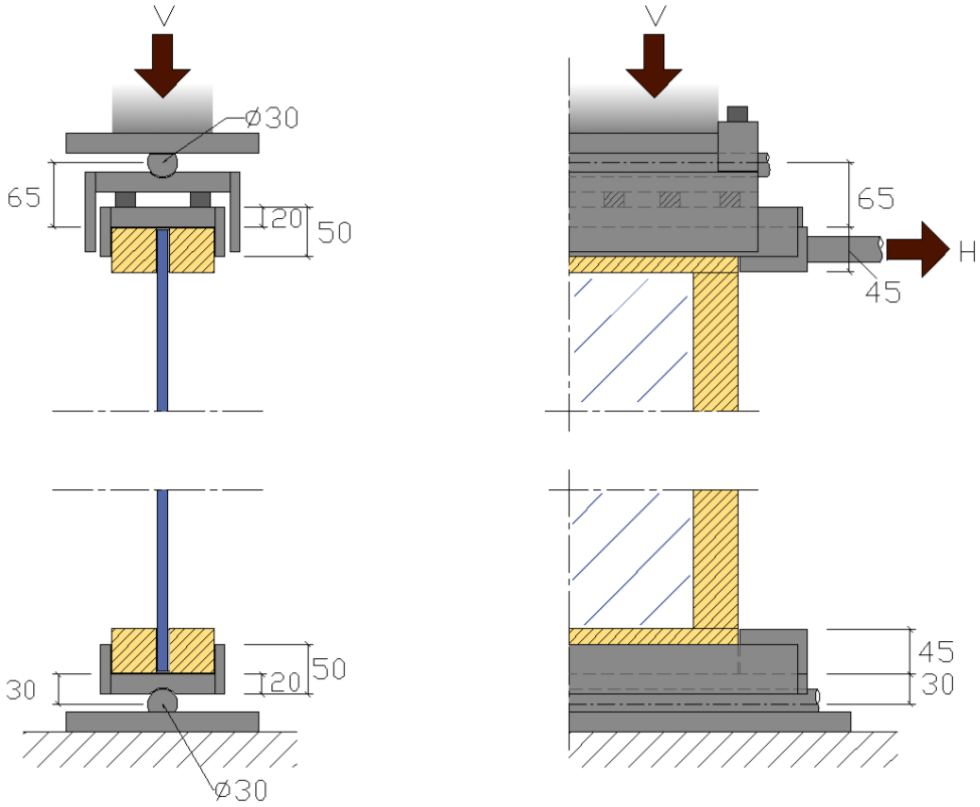


*Figure 3.4 Supports of the shear wall elements at experiments at Lineaus University.*

The displacements during test were also measured by a non-contact 3D-deformation measuring system (Pontos$^{TM}$). The system consists of two digital cameras, arranged in different angels towards the test object, and from a series of images during the test the system can determine displacements at discrete points marked on the element with stick-on labels.

## 3.3 Results from previous experiments on shear wall elements

Observations from the test performed shows that there was no post cracking capacity in any of the specimens, as was the case for the I-beams discussed in 2.4. When the glass pane cracked a large proportion of the glass fell out and the entire shear wall element failed.

Table 3.1 below shows the maximum loads obtained for all of the tested shear wall elements.

*Table 3.1 Maximum loads in kN for tested specimens*

| Load case | Acrylate specimens | | Silicone specimens | |
|---|---|---|---|---|
| | Horizontal | Vertical | Horizontal | Vertical |
| Horizontal | 67.8<br>71.3 | -<br>- | 41.4 | - |
| Vertical | -<br>-<br>- | 211<br>168<br>170 | - | 130 |
| Horizontal and vertical | 36.4<br>57.7 | 105<br>132 | 36.2 | 70.6 |

In Figure 3.5 below the results are plotted in a graph. These results have then been the basis in forming a superellipse curve to describe the relation between vertical and horizontal force at the point of failure. The superellipse curve is described in equation (3.1)

$$\left(\frac{V}{V_{cr}}\right)^m + \left(\frac{H}{H_{cr}}\right)^m = 1 \qquad \textbf{(3.1)}$$

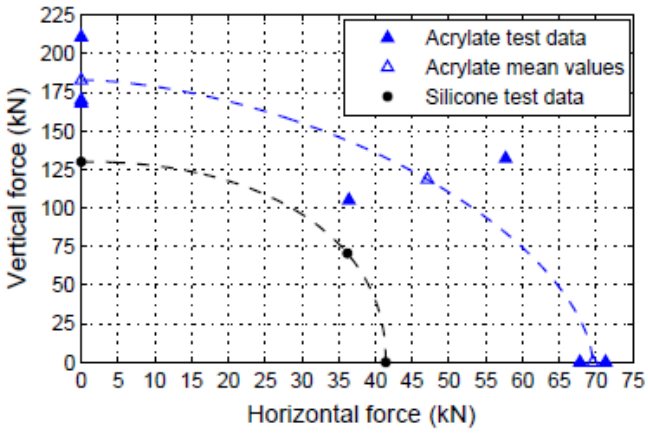


*Figure 3.5 Maximum load diagram. The dashed lines are the superellipse curves fitted to the results according to eq (3.1). For acrylate m=1.7, and for silicon m=2.2. [1]*

The measurements (load cells, potentiometers and the Pontos system) were studied to evaluate the load-displacement relations and the shape of the buckling modes. This would later serve to correlate the FE model. Graphs from this analysis, not presented here, can be found in Appendix A.

The buckling shapes were estimated through analysing Pontos data and experimental results and are illustrated in Figure 3.6.

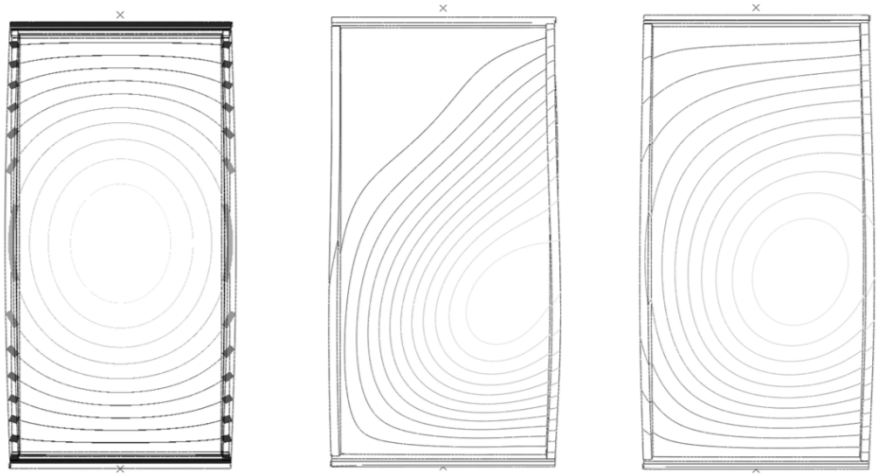

*Figure 3.6 Estimation of buckling modes (out of plane displacement) at vertical (left), horizontal (middle) and combined (right) load case.*

Studying the graphs from the experiments the applied vertical to horizontal load ratios can be estimated. In the combined load case, the loads were applied in a vertical to horizontal ratio of about 1 to 0.4. In the horizontal load case, the vertical force, serving as hold down support, was applied with the vertical to horizontal ratio of about 0.15 to 1.

# 4 Theory

## 4.1 Theory of buckling

When an ideal structure is exposed to compression forces there is a limit of how large the stresses can be for the structure to maintain its initial shape. In an elastic stable structure the infinitesimally increase of load gives an infinitesimal increase of the deformations. In an unstable state the infinitesimal increase of load instead means that the structure deforms in a progressive manner, this often means a collapse of the structure. Structures that are sensitive for instability problems are slim structures exposed to large compressive forces, such as columns, walls and steel profiles with slender webs etc.

For example a perfectly straight column that is loaded with a normal stress at its ends deforms linear until a certain load level, $P_{cr}$, where the structure cannot hold its initial straight line resulting in a transverse deflection. This form of instability phenomenon is called buckling. The point where the straight line no longer can be kept is called the bifurcation point, this is illustrated in Figure 4.1.

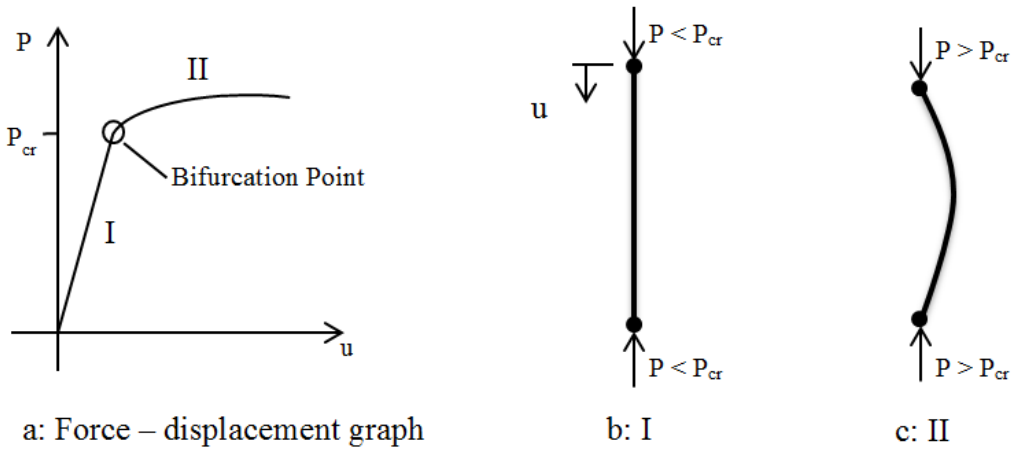


*Figure 4.1Illustration of bifurcation point*

The critical load $P_{cr}$ for an initially perfectly straight and homogeneous column exposed only to compression forces can be determined according expression (4.1), formed by Leonard Euler (1707-1783). Euler derived the critical load of a column for four different basic boundary conditions, these are called the “Euler buckling modes” (the derivation will not be shown here, the interested reader is referred to example [16] or [17]). These basic modes can be applied to calculate the buckling load of more advanced structures by identifying parts of the structure that belong to the basic modes. [17]

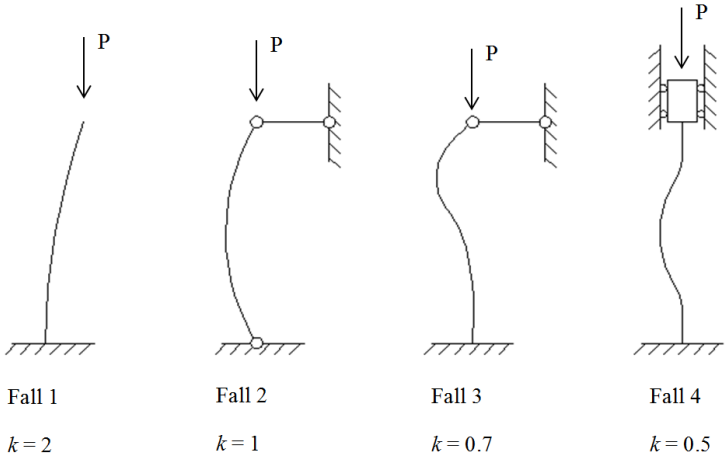


*Figure 4.2 Euler buckling modes*

$$P_{cr} = \frac{\pi^2 \cdot EI}{(kL)^2} \tag{4.1}$$

A plate is described as a two dimensional element, with the thickness $t$ much smaller than the width $b$ and length $a$. The mid-plane of the plate passes through the middle of the plate. A plate, simply supported on two opposite sides as shown in Figure 4.3, can be regarded as a column with a very large width. According to Euler buckling theory the critical buckling load of a plate, with boundary conditions according to Figure 4.3, can be calculated with (4.2).

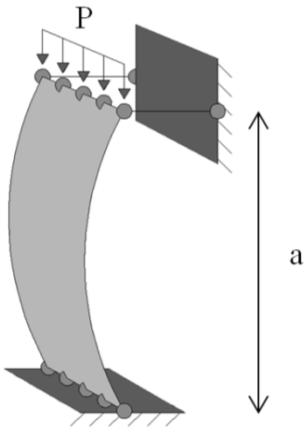


*Figure 4.3 Plate, simply supported on two opposite sides, loaded in its plane*

$$P_{cr} = \frac{\pi^2 \cdot EI}{a^2} \cdot \frac{1}{(1 - v^2)} \tag{4.2}$$

The multiplication with variable $1/(1 - v^2)$ in (4.2) takes the larger width of the plate into consideration. [18]

For a plate supported along three or four sides, the buckling occurs when the compression forces result in out of plane displacements of a point on the plate. Unlike a column that becomes unstable such plates can, in theory, carry more load after the critical point. This fact

is some time used in design of slim steel structures, but will not be treated in this thesis work because of the brittle behavior of glass and lack of redundancy described in 2.2 above.

The theory that describes the behavior of a plate is often divided into two different parts. The first part determines the load level of the bifurcation point and the second part calculates the behavior after the bifurcation point and the ultimate load level. [18]

The first part uses linear-elastic analysis to calculate the critical level. This calculation can be solved either by solving the differential equation for a plate or through the strain energy method. The following derivation for the buckling of a plate is made according to Timoshenko & Geer [16]. For a more detailed derivation the interested reader is referred to this book.

Assume that a plate deforms slightly in the transverse direction during application of forces in its middle plane, i.e. there is no lateral load. It is then possible to calculate the magnitudes of the forces that are required to keep the plate in this deflected state. The equilibrium equation for a plate loaded only in its plane with small transverse displacements is then described by the differential equation:

$$\frac{\partial^4 w}{\partial x^4} + 2\frac{\partial^4 w}{\partial x^2 \partial y^2} + \frac{\partial^4 w}{\partial y^4} = \frac{1}{D}\left(N_x \frac{\partial^2 w}{\partial x^2} + N_y \frac{\partial^2 w}{\partial y^y} + 2N_{xy}\frac{\partial^2 w}{\partial x \partial y}\right) \qquad \textbf{(4.3)}$$

where $w$ is the lateral displacement and $D$ describes the plates flexural rigidity given in (4.4), $N_x$ , $N_y$ , $N_{xy}$ [N/m] are the normal forces and the shear force in the respective directions.

$$D = \frac{E \cdot t^3}{12 \cdot (1 - v^2)} \qquad \textbf{(4.4)}$$

where; t= thickness, $v$ = poisons ration.
The strain energy method can be used to study the plate energy at the bifurcation point, i.e. compere the internal energy U from bending with the external work T done by the acting forces in the middle plane. The internal strain energy that is stored in a deformed plate is given by the differential equation:

$$U = \frac{1}{2} \cdot D \iint \left[\left(\frac{\partial^2 w}{\partial x^2} + \frac{\partial^2 w}{\partial y^2}\right)^2 - 2 \cdot (1 - v) \cdot \left(\frac{\partial^2 w}{\partial x^2} \cdot \frac{\partial^2 w}{\partial y^2} - \left(\frac{\partial^2 w}{\partial x \partial y}\right)^2\right)\right] dxdy \qquad \textbf{(4.5)}$$

The work conducted by external forces is given by the differential equation:

$$T = -\frac{1}{2} \iint \left[N_x \frac{\partial^2 w}{\partial x^2} + N_y \frac{\partial^2 w}{\partial y^y} + 2 \cdot N_{xy} \frac{\partial^2 w}{\partial x \partial y}\right] dx\, dy \qquad \textbf{(4.6)}$$

When U > T the plate remains stable in its flat form, at U < T the plate has past the critical loading point and is in an unstable state, i.e. buckling has occurred. The bifurcation point can be obtained by setting the internal energy equal to the work done by external forces:

$$U = T \qquad \textbf{(4.7)}$$

### 4.1.1 Buckling of simply supported plate under uniform compression.

Consider the plate in Figure 4.4 compressed in its middle plane by a uniformly distributed force $N_x$ [N/m].

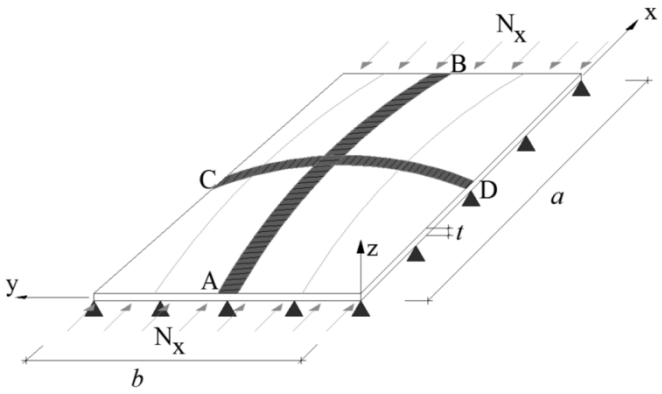


*Figure 4.4 Simply supported plate under uniform compression*

In this case there is no loading in the y- or xy-direction i.e:

$$N_y = N_{xy} = 0 \qquad \textbf{(4.8)}$$

If $N_x$ is gradually increased the equilibrium condition of the plate becomes unstable and buckling occurs. The critical value of $N_x$, i.e. $N_{cr}$, can be found using the strain energy method.

The boundary condition gives:

- At $x = 0$ and $x = a$,
  $w = \dfrac{\partial^2 w}{\partial x^2} = 0$
- At $y = b$ and $y = 0$
  $w = \dfrac{\partial^2 w}{\partial y^2} = 0$

These boundary conditions imply that the deflection of the rectangular plate can be described by a double trigonometric series on the form:

$$w = \sum_{m=1}^{\infty}\sum_{n=1}^{\infty} a_{mn} \sin\frac{m\pi x}{a} \sin\frac{n\pi y}{b} \quad m, n = 1,2,3, \ldots \qquad \textbf{(4.9)}$$

Substituting the expression of *w* according to (4.9) into equation (4.5) for U and (4.6) for T, setting $U - T = 0$, and applying the prescribed boundary conditions the following expression is obtained:

$$\left[D\left(\left(\frac{m\pi}{a}\right)^2 + \left(\frac{n\pi}{b}\right)^2\right)^2 + N_x\left(\frac{m\pi}{a}\right)^2\right] \cdot a_{mn} \sin\frac{m\pi x}{a} \sin\frac{n\pi y}{b} = 0 \qquad \textbf{(4.10)}$$

This expression must be valid for all values of *x* and *y* on the plate, therefore the first part of the equation must also equal zero. After rearranging, an expression for the critical force is formed:

$$N_x = \frac{D\left(\left(\frac{m\pi}{a}\right)^2 + \left(\frac{n\pi}{b}\right)^2\right)^2}{\left(\frac{m\pi}{a}\right)^2} \qquad \textbf{(4.11)}$$

The combination of *m* and *n* now must be combined so that $N_x$ reaches a minimum value. In [16] it is shown that the lowest critical level is reach when the shape of the buckled plate has the form of one half sinus wave over the width, i.e. at $n = 1$. Setting $n = 1$ and rearranging gives:

$$N_{cr} = \left(\frac{mb}{a} + \frac{a}{mb}\right)^2 \cdot \frac{D\pi^2}{b^2} = k_{cr} \cdot \frac{D\pi^2}{b^2} \qquad \textbf{(4.12)}$$

The first part of this expression is a dimensionless parameter called the buckling load coefficient, $k_{cr}$.

$$k_{cr} = \left(\frac{mb}{a} + \frac{a}{mb}\right)^2 \qquad m = 1,2,3 \ldots\ldots \qquad \textbf{(4.13)}$$

With the expression (4.4) for the plates flexural rigidity D inserted in (4.12) and by knowing that:

$$\sigma_x = \frac{N_x}{t} \qquad \textbf{(4.14)}$$

the more well-known expression for the critical stress of plate buckling can be formed:

$$\sigma_{cr} = k_{cr} \cdot \frac{\pi^2 \cdot E}{12 \cdot (1 - \nu^2) \cdot \left(\frac{b}{t}\right)^2} \qquad \textbf{(4.15)}$$

The buckling load coefficient. $k_{cr}$ given by (4.13) is a function of the panel's aspect ratio and the number of half sinus waves in the loading direction. The minimum value is $k_{cr} = 4.0$ for a given mode. This means that for a plate with the plate aspect ratio $a/b = 4$ the mode with lowest critical stress has m=4 half sinus waves in the loading direction. [18]

The stability of the plate is dependent on the width to thickness ratio, as shown in (4.15). This can be explained by thinking of the strip A-B in Figure 4.4as a column which is supported by the strip C-D. The stiffer the strip C-D is (i.e. the smaller width to thickness ratio) the more stress can be applied before the A-D column becomes unstable and buckles.

### 4.1.2 Plates with other support and load conditions

The longitudinal edges are often connected to another element so that they in some extent are prevented to rotate freely. This means that the bending resistance in the transvers strip, for example C-D in Figure 4.4, is much stiffer than in the simply supported case and the critical stress level at the bifurcation point will be able to increase. Expression (4.15) can still be used to calculate the critical stress by adjusting the buckling coefficient $k_{cr}$ and thus taking this extra stiffness into account. The same approach can be used in other load conditions, for example at shear stress. Hence the buckling load coefficient $k_{cr}$ is a function of the support and load conditions. [18]

#### *Plate under shear loading*

The plate in Figure 4.5 is loaded in shear stress. Consider the square element in the left figure, oriented 45° to the edges. The compressive stresses cause local buckling in this element and global buckling in the plate.

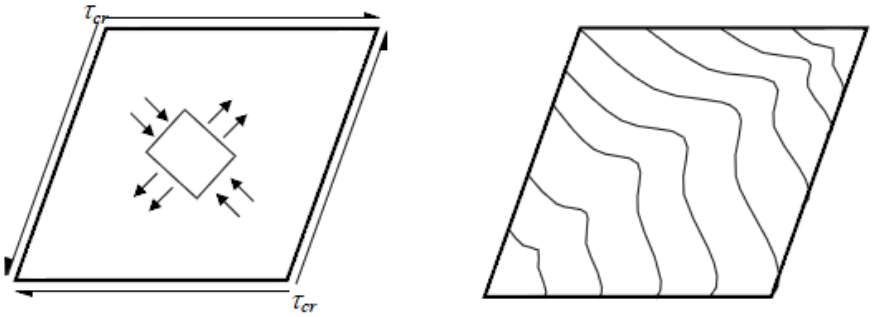


*Figure 4.5 Plate in shear stress*

(4.15) can be used for shear stress $\tau_{cr}$ , which gives

$$\tau_{cr} = k_\tau \cdot \frac{\pi^2 \cdot E}{12 \cdot (1-\nu^2) \cdot \left(\frac{b}{t}\right)^2} \qquad \textbf{(4.16)}$$

In [18] Åkesson describes that the buckling coefficient at the critical shear stress level varies with the plate aspect ratio according to (4.17) and (4.18).

$$k_\tau = 5.34 + \frac{4}{\left(\frac{a}{b}\right)^2} \quad \text{for} \quad \frac{a}{b} \geq 1 \qquad \textbf{(4.17)}$$

$$k_\tau = 4 + \frac{5.34}{\left(\frac{a}{b}\right)^2} \quad \text{for} \quad \frac{a}{b} \leq 1 \qquad \textbf{(4.18)}$$

#### *Plate under edge bending.*

For a plate simply supported around all edges subjected to edge bending stress, illustrated in Figure 4.6, the critical value of the edge bending stress $\sigma_b$ is given by

$$\sigma_{b.cr} = k_b \cdot \frac{\pi^2 \cdot E}{12 \cdot (1 - \nu^2) \cdot \left(\frac{b}{t}\right)^2} \qquad \textbf{(4.19)}$$

with ratio a/b → ∞, the buckling coefficient can be set to $k_b = 23.9$

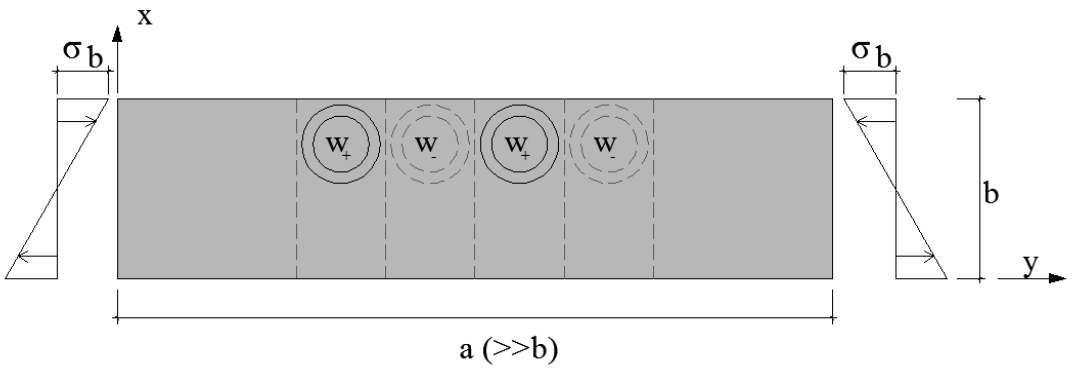


*Figure 4.6 Plate subjected to edge bending stress*

### *Combination of stresses*

Figure 4.7 illustrates a plate, simply supported around all edges, subjected to the combination of axial compressive stress ($\sigma$), edge bending compressive stress ($\sigma_b$) and shear stress ($\tau$).

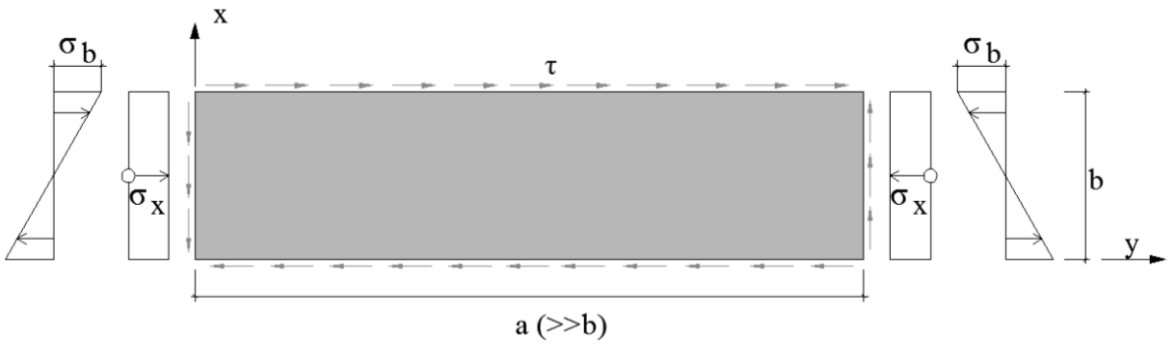


*Figure 4.7 Simply supported plate subjected to combined loads.*

In [17] the bifurcation point in a combined load case as illustrated in Figure 4.7 is determined by:

$$\left(\frac{\sigma}{\sigma_{cr}}\right) + \left(\frac{\sigma_b}{\sigma_{b,cr}}\right)^2 + \left(\frac{\tau}{\tau_{cr}}\right)^2 = 1 \qquad \textbf{(4.20)}$$

$\sigma_{cr}$ is the critical axial compressive stress level, described in 4.1.1
$\sigma_{b,cr}$ is the critical bending compressive stress level.
$\tau_{cr}$ is the critical shear stress level.

It should be emphasized that the interaction equation (4.20) applies only for the support and loading conditions given in Figure 4.7. With other types of support, loading condition or panel

aspect ratio the interaction equation may change. The complexity of this phenomenon is well documented in [19] where the interaction between $\sigma/\sigma_{cr}$ and $\tau/\tau_{cr}$ for various combinations of different supports, loads and panel aspect ratios are given. Figure 4.8 illustrates an example of this, showing interaction curves between $\sigma/\sigma_{cr}$ and $\tau/\tau_{cr}$ for a plate with restrained edges and panel aspect ratio $\emptyset = a/b < 1$.

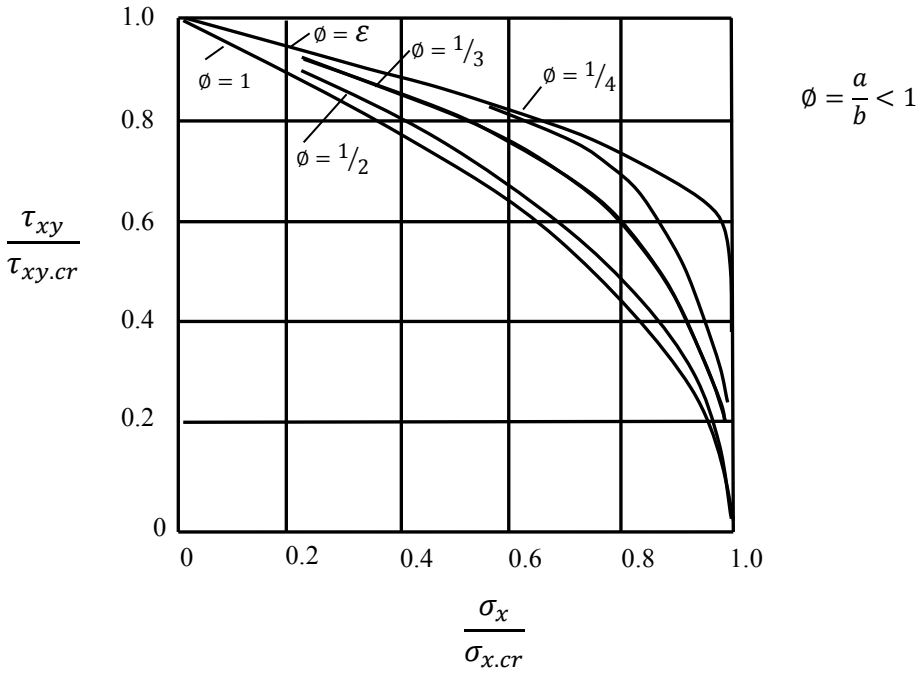


*Figure 4.8 Ineraction curves between shear and compression, under restrained edges and* $\emptyset < 1$

In interaction equation (4.20) the exponent of $\sigma/\sigma_{cr}$ is set to 1, and the exponents of $\tau/\tau_{cr}$ and $\sigma_b/\sigma_{b,cr}$ are in this case 2. A different approach is e.g. the superellipse equation used for the empirical fit shown in equation (3.1) where all exponents are set to the same value. When determining the interaction between different stresses from experimental results different approaches are thus available.

### *Initial plate imperfections*

The theoretical value for the critical stress assumes that the plate initially is a perfectly plane structure, with a homogeneous material without flaws and behaving isotropically. In reality however this is obvious rarely the case. Both geometrical imperfections and residual stresses affect the amount of extra load that the plate element can carry. The initial imperfections can be compared to an existing load which is added to the external load.

## 4.2 Finite element method

Within the fields of engineering basically all models formulated to explain a physical phenomenon take the form of differential equations. Usually these problems are complex and the differential equation is too complicated to be able to solve with a classical analytical method. The *finite element (FE) method* is a numerical approach to solve a general differential equation in an approximate manner. In the early 1960s the FE-method took its form and began to spread widely within the field of engineering.

In modeling physical phenomena, these are often formulated to hold on a specific region, for example a beam or plate. The region can be described as one-, two- or three-dimensional. The FE method divides the region into smaller parts, and the set of all small elements are called *finite element mesh*. Instead of directly making an approximation over the entire region, the FE-method makes the approximation for the smaller elements. With the behavior of the single elements determined, the elements of the entire region are put together under determined conditions for an approximation over the entire region. Although the approximated solution may vary in a non-linear fashion over the entire region, the approximation within the small elements can be linear or quadratic and are still able to catch the variation over the region with a high accuracy. The smaller the elements, i.e. the finer the mesh, a more accurate approximation will be obtained, at the expense of more calculations and, therefore, more computer resources.

The approximation of how the variable varies over the element is an interpolation over the element, where the variable is assumed to be known at certain points, so called *nodal points*. The nodal points are often placed at the boundaries of the element. The FE method can be applied both to *boundary value problems*, e.g. the deflection of a beam, and to *initial value problems* e.g. transient heat conduction.

### 4.2.1 FE formulation of three-dimensional elasticity

The derivation of the FE formulation for three dimensional elasticity is presented here following Ottosen & Petersson [20]. The unknown functions within the problems of solid mechanics are in general the displacements in the x-, y- and z-direction. With these solved for the nodal points of a FE mesh the strains and stresses can be determined within the structure of interest. Before we can set up the FE formulation the basic properties and notations for stresses and strains are stated.

***Stresses***

On a continuous body two kinds of forces are assumed to be present; body forces (force per unit volume) and surface forces (force per unit surface).

Consider an infinitesimal, internal or external, surface d$A$ on the body, with a unit normal vector $\mathbf{n}$ acting out of the body and the force d$\mathbf{P}$ acting on d$A$ out of the body. The surface force (per unit surface) on d$A$ is termed the traction vector $\mathbf{t}$, and has components in x-, y- and z-directions. $\mathbf{t}$ is given by;

$$\mathbf{t} = \frac{\mathrm{d}\mathbf{P}}{\mathrm{d}A} \quad \mathrm{d}A \to 0; \quad \mathbf{t} = \begin{bmatrix} t_x \\ t_y \\ t_z \end{bmatrix} \ [\mathrm{N/m^2}] \tag{4.21}$$

The traction vector **t** is related to the unit normal vector **n**, and thus a different surface cut thru the same point will have a different traction vector. If the normal vector **n** is in the direction of the x-,y- and z-axis respectively the corresponding traction vector, denoted $\mathbf{s}_x$, $\mathbf{s}_y$ and $\mathbf{s}_z$ respectively, is given in components along the coordinate axis. Combined together these special traction vectors form the so called *stress tensor* **S**.

$$\mathbf{s_x} = \begin{bmatrix} \sigma_{xx} \\ \sigma_{xy} \\ \sigma_{xz} \end{bmatrix}, \mathbf{s_y} = \begin{bmatrix} \sigma_{yx} \\ \sigma_{yy} \\ \sigma_{yz} \end{bmatrix}, \mathbf{s_z} = \begin{bmatrix} \sigma_{zx} \\ \sigma_{zy} \\ \sigma_{zz} \end{bmatrix}, \qquad \mathbf{S} = \begin{bmatrix} \mathbf{s}_x^{\mathrm{T}} \\ \mathbf{s}_y^{\mathrm{T}} \\ \mathbf{s}_z^{\mathrm{T}} \end{bmatrix} = \begin{bmatrix} \sigma_{xx} & \sigma_{xy} & \sigma_{xz} \\ \sigma_{yx} & \sigma_{yy} & \sigma_{yz} \\ \sigma_{zx} & \sigma_{zy} & \sigma_{zz} \end{bmatrix} \tag{4.22}$$

The components are termed stress components, $\sigma_{xx}$, $\sigma_{yy}$ *and* $\sigma_{zz}$ are called normal stresses and $\sigma_{xy}$, $\sigma_{xz}$, $\sigma_{yx}$, $\sigma_{yz}$, $\sigma_{zx}$ and $\sigma_{zy}$ are called shear stresses. It can be shown that $\sigma_{xy} = \sigma_{yx}$ , $\sigma_{xz} = \sigma_{zx}$ and $\sigma_{yz} = \sigma_{zy}$ , therefore **S** is symmetric. With the stress tensor **S** known the traction vector can be described for an arbitrary unit normal vector.

$$\mathbf{t} = \mathbf{Sn} \quad \text{,where } \mathbf{n} = \begin{bmatrix} n_x \\ n_y \\ n_z \end{bmatrix} \tag{4.23}$$

The equilibrium of an arbitrary part of the body includes the body force, denoted **b**, that acts in the region *V* and the traction vector **t** that acts on the boundary surface S. Equilibrium requires that;

$$\int_S \mathbf{t}\,\mathrm{d}S + \int_V \mathbf{b}\,\mathrm{d}V = \mathbf{0} \tag{4.24}$$

which can be written in three separate equations

$$\begin{aligned} \int_S t_x\,\mathrm{d}S + \int_V b_x\,\mathrm{d}V &= 0 \\ \int_S t_y\,\mathrm{d}S + \int_V b_y\,\mathrm{d}V &= 0 \\ \int_S t_z\,\mathrm{d}S + \int_V b_z\,\mathrm{d}V &= 0 \end{aligned} \tag{4.25}$$

With (4.22)and(4.23) $t_x = \mathbf{s}_x^{\mathrm{T}}\mathbf{n}$ ,which gives for the first equation of (4.25):

$$\int_S \mathbf{s}_x^{\mathrm{T}}\mathbf{n}\,\mathrm{d}S + \int_V b_x\,\mathrm{d}V = 0 \tag{4.26}$$

Using the Gauss divergence theorem (4.26) can be reformulated to:

$$\int_V (\text{div}\,\mathbf{s}_x + b_x)\,\mathrm{d}V = 0 \qquad \textit{(4.27)}$$

And as (4.27) holds for an arbitrary region $V$ this gives

$$\text{div}\,\mathbf{s}_x + b_x = 0 \qquad \textit{(4.28)}$$

Equation two and three of (4.25) is reformulated in the same manner. By using the definition of the divergence of the vector and inserting $\mathbf{s}_x, \mathbf{s}_y, \mathbf{s}_z$ according to (4.22) the following expression is obtained, which describes the equilibrium condition for the body:

$$\begin{aligned}
&\frac{\partial \sigma_{xx}}{\partial x} + \frac{\partial \sigma_{xy}}{\partial y} + \frac{\partial \sigma_{xz}}{\partial z} + b_x = 0 \\
&\frac{\partial \sigma_{yx}}{\partial x} + \frac{\partial \sigma_{yy}}{\partial y} + \frac{\partial \sigma_{yz}}{\partial z} + b_y = 0 \qquad \textit{(4.29)} \\
&\frac{\partial \sigma_{zx}}{\partial x} + \frac{\partial \sigma_{zy}}{\partial y} + \frac{\partial \sigma_{zz}}{\partial z} + b_z = 0
\end{aligned}$$

The stress components are organized in the matrix $\boldsymbol{\sigma}$, and the matrix differential operator $\widetilde{\nabla}$ is used to form the simpler notation in compact matrix form:

$$\widetilde{\boldsymbol{\nabla}}^{\mathbf{T}}\boldsymbol{\sigma} + \mathbf{b} = \mathbf{0} \qquad \textit{(4.30)}$$

where:

$$\widetilde{\boldsymbol{\nabla}}^{\mathbf{T}} = \begin{bmatrix} \frac{\partial}{\partial x} & 0 & 0 & \frac{\partial}{\partial y} & \frac{\partial}{\partial z} & 0 \\ 0 & \frac{\partial}{\partial y} & 0 & \frac{\partial}{\partial x} & 0 & \frac{\partial}{\partial z} \\ 0 & 0 & \frac{\partial}{\partial z} & 0 & \frac{\partial}{\partial x} & \frac{\partial}{\partial y} \end{bmatrix}, \sigma = \begin{bmatrix} \sigma_{xx} \\ \sigma_{yy} \\ \sigma_{zz} \\ \sigma_{xy} \\ \sigma_{xz} \\ \sigma_{yz} \end{bmatrix} \qquad \textit{(4.31)}$$

### *Strains*

When the body deforms the coordinates of a point changes from (x, y, z) to ($x+u_x$, $y+u_y$, $z+u_z$). The displacement components $u_x$, $u_y$ and $u_z$ are collected in the displacement vector **u**. Displacements of ($x+d_x$, $y+d_y$, $z+d_z$) then becomes **u** + d**u**, and using the chain rule d**u** is:

$$\mathbf{u} + \mathrm{d}\mathbf{u} = \begin{bmatrix} u_x \\ u_y \\ u_z \end{bmatrix} + \begin{bmatrix} \mathrm{d}u_x \\ \mathrm{d}u_y \\ \mathrm{d}u_z \end{bmatrix} = \begin{bmatrix} u_x \\ u_y \\ u_z \end{bmatrix} + \begin{bmatrix} \frac{\partial u_x}{\partial x}\mathrm{d}x + \frac{\partial u_x}{\partial y}\mathrm{d}y + \frac{\partial u_x}{\partial z}\mathrm{d}z \\ \frac{\partial u_y}{\partial x}\mathrm{d}x + \frac{\partial u_y}{\partial y}\mathrm{d}y + \frac{\partial u_y}{\partial z}\mathrm{d}z \\ \frac{\partial u_z}{\partial x}\mathrm{d}x + \frac{\partial u_z}{\partial y}\mathrm{d}y + \frac{\partial u_z}{\partial z}\mathrm{d}z \end{bmatrix} \qquad \textit{(4.32)}$$

The partial derivatives, e.g. $\partial u_x/\partial x$, are called displacement gradients and in general these gradients are small in compered to unity. This simplifies the expression of the normal strains so that they may be written as:

$$\varepsilon_{xx} = \frac{\partial u_x}{\partial x} \; ; \varepsilon_{yy} = \frac{\partial u_y}{\partial y} \; ; \varepsilon_{zz} = \frac{\partial u_z}{\partial z} \tag{4.33}$$

Also when evaluating the shear strain small deformations are assumed ($\sin\theta \cong \theta$) and these can be written as:

$$\gamma_{xy} = \frac{\partial u_x}{\partial y} + \frac{\partial u_y}{\partial x} \; ; \; \gamma_{xz} = \frac{\partial u_x}{\partial z} + \frac{\partial u_z}{\partial x} \; ; \; \gamma_{yz} = \frac{\partial u_y}{\partial z} + \frac{\partial u_z}{\partial y} \tag{4.34}$$

These expressions for the strains in (4.33) and (4.34) are collected in a more compact matrix notation.

$$\boldsymbol{\varepsilon} = \widetilde{\boldsymbol{\nabla}}\mathbf{u} \tag{4.35}$$

Where:

$$\boldsymbol{\varepsilon} = \begin{bmatrix} \varepsilon_{xx} \\ \varepsilon_{yy} \\ \varepsilon_{zz} \\ \gamma_{xy} \\ \gamma_{xz} \\ \gamma_{yz} \end{bmatrix}; \quad \widetilde{\boldsymbol{\nabla}} = \begin{bmatrix} \frac{\partial}{\partial x} & 0 & 0 \\ 0 & \frac{\partial}{\partial y} & 0 \\ 0 & 0 & \frac{\partial}{\partial z} \\ \frac{\partial}{\partial y} & \frac{\partial}{\partial x} & 0 \\ \frac{\partial}{\partial z} & 0 & \frac{\partial}{\partial x} \\ 0 & \frac{\partial}{\partial z} & \frac{\partial}{\partial y} \end{bmatrix} \tag{4.36}$$

Expression (4.35) is referred to as the *kinematic relation*.

### *Linear elasticity*

Linear elasticity in one dimension is expressed by Hooke's law from 1676

$$\sigma = E \cdot \varepsilon \tag{4.37}$$

This relation also holds for linear elasticity with several stress and strain components. With the stress matrix $\boldsymbol{\sigma}$ and strain matrix $\boldsymbol{\varepsilon}$ as given in (4.31) and (4.36) respectively, (4.37) can be reformulated into

$$\boldsymbol{\sigma} = \mathbf{D}\boldsymbol{\varepsilon} \tag{4.38}$$

$\mathbf{D}$ is the constitutive matrix and consists of a symmetric $6 \times 6$ matrix, i.e. 21 independent elasticity coefficients. The expression (4.38) can be inverted to

$$\boldsymbol{\varepsilon} = \mathbf{C}\boldsymbol{\sigma}\ ;\ \mathbf{C} = \mathbf{D}^{-1} \qquad \textit{(4.39)}$$

If another direction of the coordinate system is chosen, the **D**-matrix changes. However there are materials with symmetry planes, i.e. materials for which the **D**-matrix is the same for two coordinate systems which are mirror to each other with respect to the symmetry plane. In the orthotropic material (timber) there are three such symmetry planes, and it can be shown that the **D**-matrix then can be reduced to consists of 9 independent coefficients. If the coordinate axes are parallel to these planes the **D**-matrix can be written as:

$$\mathbf{D} = \begin{bmatrix} D_{11} & D_{12} & D_{13} & 0 & 0 & 0 \\ D_{21} & D_{22} & D_{23} & 0 & 0 & 0 \\ D_{31} & D_{32} & D_{33} & 0 & 0 & 0 \\ 0 & 0 & 0 & D_{44} & 0 & 0 \\ 0 & 0 & 0 & 0 & D_{55} & 0 \\ 0 & 0 & 0 & 0 & 0 & D_{66} \end{bmatrix} \qquad \textit{(4.40)}$$

For the isotropic material (e.g. glass) the **D**-matrix is unchanged regardless of coordinate system. **D**-matrix can then be written with two independent variables; Young's modulus $E$ and Poisson's ratio $\nu$, as

$$\mathbf{D} = \frac{E}{(1+\nu)(1-2\nu)} \begin{bmatrix} 1-\nu & \nu & \nu & 0 & 0 & 0 \\ \nu & 1-\nu & \nu & 0 & 0 & 0 \\ \nu & \nu & 1-\nu & 0 & 0 & 0 \\ 0 & 0 & 0 & \frac{1}{2}(1-2\nu) & 0 & 0 \\ 0 & 0 & 0 & 0 & \frac{1}{2}(1-2\nu) & 0 \\ 0 & 0 & 0 & 0 & 0 & \frac{1}{2}(1-2\nu) \end{bmatrix} \qquad \textit{(4.41)}$$

The initial strains, due to e.g. temperature, that may exist in materials are dealt with in (4.38) by adding the initial strain vector $\boldsymbol{\varepsilon_0}$

$$\boldsymbol{\sigma} = \mathbf{D}(\boldsymbol{\varepsilon} + \boldsymbol{\varepsilon_0}) \qquad \textit{(4.42)}$$

To solve the equations (4.30), (4.35) and (4.42) boundary conditions expressed in terms of the traction vector **t** and/or the displacement vector **u** are needed. For a three dimensional problem over the boundary $S$, the boundary conditions are described as

$$\begin{aligned} &\mathbf{t} = \mathbf{h} \text{ on } S_h \\ &\mathbf{u} = \mathbf{g} \text{ on } S_g \\ &S_h + S_g = S \end{aligned} \qquad \textit{(4.43)}$$

### *Weak form of the FE-formulation*

To derive the weak form of the equilibrium equation (4.30), the arbitrary vector **v** is introduced given as

$$\mathbf{v} = \begin{bmatrix} v_x \\ v_y \\ v_z \end{bmatrix} \tag{4.44}$$

After multiplying the first equation of (4.29) with $v_x$ the second and third equations with $v_y$ and $v_z$ respectively, and integrating over the volume $V$, integration by parts is performed using the Green-Gauss theorem. The three expressions are then reduced by using the components of $t_x$, $t_y$ and $t_z$. Finally they are added together to form the weak form of the problem

$$\int_V \left(\tilde{\nabla}\mathbf{v}\right)^{\mathrm{T}} \boldsymbol{\sigma}\, \mathrm{d}V = \int_S \mathbf{v}^{\mathrm{T}}\mathbf{t}\, \mathrm{d}S + \int_V \mathbf{v}^{\mathrm{T}}\mathbf{b}\, \mathrm{d}V \tag{4.45}$$

### *FE-formulation of three dimensional elasticity.*

To obtain the FE formulation the displacement vector **u** is approximated by

$$\mathbf{u} = \mathbf{N}\mathbf{a} \tag{4.46}$$

where **N** contains of the global shape functions and **a** the displacements. With Galerkin's method the weight vector **v** is chosen according to $= \mathbf{N}\mathbf{c}$ , and as **v** is arbitrary the matrix **c** is also arbitrary, therefore

$$\tilde{\nabla}\mathbf{v} = \tilde{\nabla}\mathbf{N}\mathbf{c} = \mathbf{B}\mathbf{c} \text{ , where } \mathbf{B} = \tilde{\nabla}\mathbf{N} \tag{4.47}$$

Now (4.47) is inserted to (4.45) and as **c** is independent of coordinates and arbitrary it can be removed to form the balance principle of the body, given by

$$\int_V \mathbf{B}^{\mathrm{T}}\boldsymbol{\sigma}\, \mathrm{d}V = \int_S \mathbf{N}^{\mathrm{T}}\mathbf{t}\, \mathrm{d}S + \int_V \mathbf{N}^{\mathrm{T}}\mathbf{b}\, \mathrm{d}V \tag{4.48}$$

By inserting (4.46) and (4.47) into the expression (4.35) for strains the expression for stresses can be rewritten as:

$$\boldsymbol{\sigma} = \mathbf{D}\mathbf{B}\mathbf{a} - \mathbf{D}\boldsymbol{\varepsilon}_{\mathbf{0}} \tag{4.49}$$

The final FE formulation is then obtained by inserting (4.49) to (4.48) and applying the boundary conditions stated in (4.43)

$$\left(\int_V \mathbf{B}^{\mathrm{T}}\mathbf{D}\mathbf{B}\, \mathrm{d}V\right) a = \int_{S_h} \mathbf{N}^{\mathrm{T}}\mathbf{h}\, \mathrm{d}S + \int_{S_g} \mathbf{N}^{\mathrm{T}}\mathbf{t}\, \mathrm{d}S + \int_V \mathbf{N}^{\mathrm{T}}\mathbf{b}\, \mathrm{d}V + \int_V \mathbf{B}^{\mathrm{T}}\mathbf{D}\boldsymbol{\varepsilon}_{\mathbf{0}}\, \mathrm{d}V \tag{4.50}$$

To write the FE formulation in a more compact manner the following matrices are defined

$$\mathrm{K} = \int_V \mathbf{B}^{\mathrm{T}}\mathbf{D}\mathbf{B}\,\mathrm{d}V$$

$$\mathrm{f_b} = \int_{S_h} \mathbf{N}^{\mathrm{T}}\mathbf{h}\,\mathrm{d}S + \int_{S_g} \mathbf{N}^{\mathrm{T}}\mathbf{t}\,\mathrm{d}S \qquad \textit{(4.51)}$$

$$\mathrm{f_l} = \int_V \mathbf{N}^{\mathrm{T}}\mathbf{b}\,\mathrm{d}V$$

$$\mathrm{f_0} = \int_V \mathbf{B}^{\mathrm{T}}\mathbf{D}\boldsymbol{\varepsilon_0}\,\mathrm{d}V$$

resulting in the familiar standard FE formulation

$$\mathbf{K}\mathbf{a} = \mathbf{f} \qquad \text{where } \mathbf{f} = \mathbf{f_b} + \mathbf{f_l} + \mathbf{f_0} \qquad \textit{(4.52)}$$

**K** is called the stiffness matrix, **a** the displacement vector and **f** the load vector.

### 4.2.2 Linear buckling analyses with the finite element method

In order to explain the approach of the linear buckling analysis, the term *stress stiffening* should first be treated. Stress stiffening refers to the coupling between the out of plane stiffness of a structure and the state of in-plane stress (also called membrane stress). The bending stiffness of a plate, beam etc. is increased by a tensile in-plane stress, and decreased by a compressive in-plane stress. As descried in 4.1, a large compressive in-plane stress reduces the bending stiffness to zero which results in buckling. According to [21] stress stiffening is usually negligible for relatively massive bodies but could be of importance for thin-walled structures. Taking the stress stiffness in consideration, equation (4.52) can be written

$$[\mathbf{K} + \mathbf{K_\sigma}]\mathbf{a} = \mathbf{f} \qquad \textit{(4.53)}$$

where $\mathbf{K_\sigma}$ is the stress stiffness matrix, also called e.g. the differential stiffness matrix. If the stress stiffness matrix is calculated from an arbitrarily level of in-plane stress the matrix equation for a linear buckling analysis is

$$[\mathbf{K} + \lambda\mathbf{K_\sigma}]\{d\mathbf{a}\} = \mathbf{0} \qquad \textit{(4.54)}$$

where $\lambda$ is the factor by which $\mathbf{K_\sigma}$ must be multiplied with to reach the buckling load. At the bifurcation point there are at least two infinitesimally closely located equilibrium states that are possible, the unbuckled and at least one buckled state. $\{d\mathbf{a}\}$ are the displacement increments that exist just before buckling, and since the transition between the close points doesn't require any changes in applied loads the right side of the equation is the null vector **0**. [21] This equation can be solved as a generalized eigenvalue problem, i.e.

$$(\mathbf{A} - \lambda\mathbf{B})\mathbf{a} = 0 \qquad \textit{(4.55)}$$

for a non-trivial solution of (4.55) to exist, the following must apply

$$\det(\mathbf{A} - \lambda\mathbf{B}) = 0 \qquad \textit{(4.56)}$$

The solution of the eigenvalue problem means that the values of $\lambda$ that fulfill (4.56) are calculated. There can of course be several valid values of $\lambda$, these sets are called eigenvalues. For every eigenvalue $\lambda_i$ there is a corresponding eigenvector $\mathbf{a}_i$ that fulfills (4.55). The eigenvectors represent the various buckling modes of a structure.

At large deformations the stiffness matrices of (4.53) are the result of a linear perturbation of the loaded structure.

## 4.3 FE software Abaqus

Abaqus is a general finite element method analysis software. It can be used to calculate both dynamic and static problems in two or three dimensions. Abaqus can be used in a wide variety of engineering problems.

The Abaqus software consist of four main parts; Abaqus/CAE, Abaqus/Standard, Abaqus/Explicit and Abaqus/CFD. Abaqus/CAE is a user interface that can be used to visually and interactively create a model and view the results after the finite element analysis. In Abaqus/CAE the user can design the geometry, create and assign material properties, boundary and load conditions etc. Abaqus/CAE creates an input file containing the model data which can be read by the analysis software, e.g. Abaqus/Standard and Abaqus/Explicit. The analysis program creates a file containing the results which in turn can be read by the Abaqus/CAE.

Abaqus/Standard is ideal to use for static and low-speed dynamic calculations, where high accurate stress solutions are requested. Abaqus/Explicit effectively handles severe nonlinear behaviour, such as contact conditions, and it is in particular suited to simulate short transient events as e.g. a car crash. Abaqus/CFD is an application for advanced calculations within fluid dynamics such as laminar and turbulent flows, it also supports pre and post processing with Abaqus/CAE.

In this thesis Abaqus/CAE 6.12 is used for modelling, and Abaqus/standard is used for analysis calculations. When creating a model with Abacus/CAE the user follows a set of modules to create the necessary data for the input file. The modules are described below together with certain input possibilities that are of importance in this thesis.

**Part module** - the geometric entity is created. The part can be deformable, discrete rigid, analytical rigid, eulerian or electromagnetic. The deformable part can be any arbitrary shaped axisymmetric, two- or three –dimensional part that deforms under load. The discrete rigid part can be of arbitrary shape just like a deformable part but is used to model bodies that cannot deform i.e. are completely rigid, such parts are often used in contact analysis. An analytical discrete part has the same properties as a discrete rigid part but the shape cannot be chosen arbitrary.

**Property module** – sections and material properties are created and assigned to the parts, e.g. the orientation of the orthotropic material properties.

**Assembly module** – parts are inserted and arranged into a global domain. The parts are positioned by e.g. applying position constraints that align selected edges.

**Step module** – in this module the user creates the analysis steps and specifies output requests. In this thesis two different analysis steps are used, the static general procedure for regular stress analysis and the linear perturbation buckling procedure described in 4.3.1.

**Interaction module** – here the user defines e.g. the mechanical interactions between regions of a model or between the model and its surroundings. Springs can be created between two points or between a point on the model and a point of the ground.

**Load module** – definition of loads and boundary conditions.

**Mesh module** – definition of the element mesh. There are a variety of elements available in Abaqus, a small evaluation of two of these elements and their behaviour were made in this thesis, these elements are described in 4.3.2 and the evaluation in 5.1.

**Job module** – the setup for analysis. The input file is created then sent to, and analysed by e.g. Abaqus/Standard, as in this thesis.

**Visualization module** – The output file from Abaqus/Standard can be viewed and post processed.

### 4.3.1 Eigenvalue buckling analysis in Abaqus

Abacus provides the possibility to estimate the elastic buckling of a structure by making an eigenvalue extraction. In a stiff structure where the response prior to the buckling is linear, this estimation is a very useful tool.

Prior to the eigenvalue extraction, the structure is defined as being in its base state. This state is obtained by any response history, including nonlinear effects. In the base state the stresses $\boldsymbol{\sigma}^B$ are in equilibrium with the surface traction $\mathbf{t}^B$ and body forces $\mathbf{b}^B$. From this state a linear perturbation (incremental loading) i.e. is applied with additional surface traction $\Delta\mathbf{t}$, body forces $\Delta\mathbf{b}$ and boundary displacements $\Delta\mathbf{u}$. For the estimation of the buckling load to be reasonable the response to the perturbation loads must be linear until the estimated buckling load value. The linearity of the problem means that if the response to $\Delta\mathbf{t}$, $\Delta\mathbf{b}$ and $\Delta\mathbf{u}$ is $\Delta\boldsymbol{\sigma}$, then the response of $\lambda\Delta\mathbf{t}$, $\lambda\Delta\mathbf{b}$ and $\lambda\Delta\mathbf{u}$ will be $\lambda\Delta\ \boldsymbol{\sigma}$. For each distinct value of $\lambda$ there is a corresponding linear perturbation. In the linear perturbation analysis ABAQUS seeks for the values of $\lambda$ that allows for nontrivial incremental displacement fields with arbitrary magnitudes as valid solutions to the problem, these are referred to as the buckling modes.

In accordance with the standard FE method approach it is the stiffness matrix **K** that is evaluated to find the eigenvalues. In [22] the governing equation for buckling then takes the form

$$(K_0^{NM} + \lambda K_\Delta^{NM})v^M = 0$$

where $K_0^{NM}$ is the base state stiffness, which is the sum of the hypo elastic tangent stiffness, the initial stiffness and load stiffness. $K_\Delta^{NM}$ is the differential stiffness, which is the sum of the initial stiffness due to the perturbation stresses and the load stiffness due to the perturbation loads, i.e. $K_\Delta^{NM}$ is a function of the initial load vector associated with the predeformed base state.

If the resulting nodal loads from applied forces ( $\mathbf{t}^B$, $\mathbf{b}^B$ )and prescribed displacements ($\mathbf{u}^B$) are denoted $P^N$, and the nodal loads due to the additional loads ($\Delta\mathbf{t}$, $\Delta\mathbf{b}$, $\Delta\mathbf{u}$) are denoted $Q^N$, then the eigenvalues $\lambda_i$ are the multipliers that provide the estimated buckling load $P^N + \lambda_i Q^N$. The corresponding buckling mode is given by the corresponding eigenvector $v_i^N$. Note especially that with this general definition of buckling prediction, any state can be used as base state and that in general, the load patterns can be different, i.e. $P^N \neq k \cdot Q^N$.

### 4.3.2 Element types in Abaqus

The evaluated elements for this thesis were continuum (solid) and shell elements.

Continuum elements Shell elements

*Figure 4.9 Illustration of continuum and shell elements*

Continuum (solid) elements are general purpose elements that can be used to model a large variety of problem types. The continuum elements represent three dimensional blocks of material which can be connected to other elements on all its faces, making it possible to create almost any structure. Each node of the element has three translational degrees of freedom. In the present study hexahedral elements (bricks) are used. Both linear (eight node) and quadratic (20 node) elements were used. Reduced and fully integrated elements have also been compared. These different element types differ in the number of Gauss points that is used in the integration.

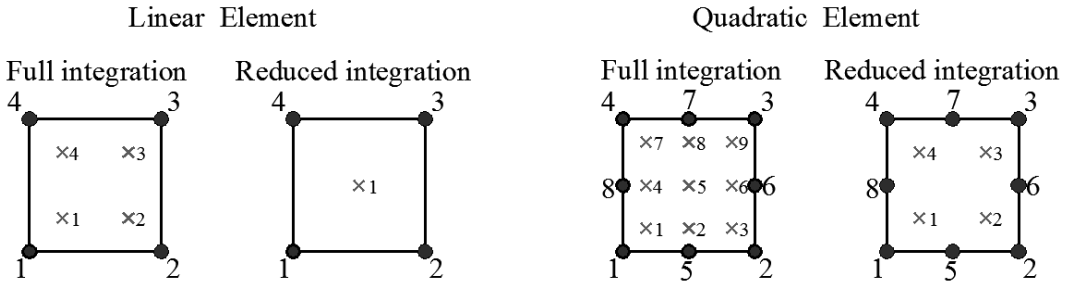


*Figure 4.10 Continuum elements with illustrated integration points*

Linear elements with full integration use two integration points in each direction, quadratic elements use three. This gives a total of $2^3$=8 and $3^3$=27 integration points for the linear and quadratic elements respectively. A problem with the fully integrated linear elements is shear locking, which causes the elements to behave much too stiff in bending. This is because the edges of a linear element can't curve when exposed to a bending moment, see Figure 4.11. In the deformed state the angles between the dotted lines have changed which misleadingly indicates that the shear strain (stress) is nonzero. Shear locking is only a problem in bending, otherwise the linear, fully integrated, elements work well in shear or direct loads. The hexahedral element of second order does not have this problem since the displacement approximation allows for a curvature within the element.

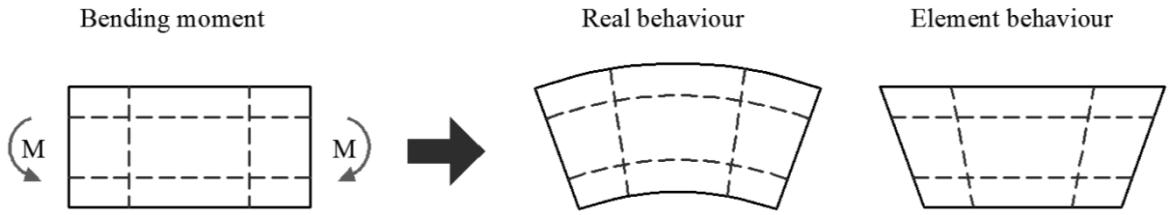


*Figure 4.11 Shear locking of fully integrated linear continuum element*

In reduced integration the element uses one less integration point in each direction, and thus only a single integration point is used for the linear element. In such cases linear elements can instead be too flexible because of another problem called hour-glassing. When the element in Figure 4.12 is subjected to the bending moment M, none of the dotted lines change length, the strain (and stress) monitored at the only integration point is therefore zero. Consequently, the deformation pattern shown in Figure 4.12 is possible without any strain energy being monitored – in other words the element possesses no stiffness to this hourglass-shaped deformation mode. Abaqus deals with this problem by adding a small amount of hourglass stiffness which limits the propagation of hourglass patterns in the mesh. This generates acceptable results but also requires a reasonably fine mesh to work well. The quadratic element in combination with reduced-integration can also create hourglass modes, but it is very unusual that this can propagate in a mesh and rarely becomes a problem.

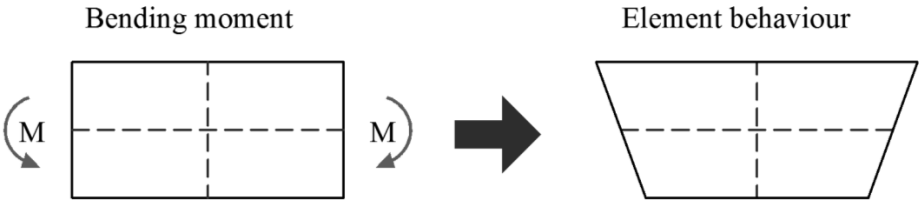


*Figure 4.12 Hour glassing effect in reduced integrated linear elements*

There is also another way to overcome the problems of shear locking in linear elements with full integration. In Abaqus so-called "Incompatible mode elements" are provided. In these elements additional degrees of freedom are introduced that enhance the element's deformation gradient, to account for bending modes.

Shell elements are preferably used to model structures were one dimension is significantly smaller than the others and stresses in the thickness direction are negligible. A guideline value is that the thickness, t, should be less than 1/10 of other global structural dimensions, for example the distance between supports. The conventional shell element discretizes a reference surface by defining its planar dimensions, its surface normal and initial curvature. The thickness of the element is defined by the section properties. By numerical integration the stresses and strains are calculated independently at each section point trough the thickness, which means that nonlinear material behavior can be allowed. The number of section points is by default set to five which is enough to cover most problems. By default the mid surface and the reference surface are equivalent.

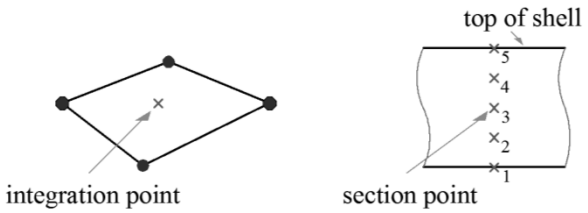


*Figure 4.13 Shell element with reduced integration and 5 section points*

# 5 Development of a representative FE-model

In this master thesis work a substantial time and effort has been spent in developing a representative model of the shear wall element in the FEM-program Abaqus. In this chapter the procedure of the development is presented to give a motivation for choices that have been made in the development of the model. This also gives a more detailed explanation of how Abaqus deals with buckling problems and what possibilities the user has in terms of various modeling approaches.

The first step in the development was to evaluate which types of elements to use, section 5.1. Abaqus gives some guidelines on what elements to use for different analyses but to gain more knowledge of how the elements behave for the present application, a parametric study of different element types was made comparing the estimated buckling load of a simply supported plate in Abaqus to an analytical solution.

The next step was to model the entire shear wall element and design the application of loads and boundary conditions to resemble the conducted experiments, described in 3.2, with the aim of achieving correlating results. The built up of the shear wall part and material properties are presented in 5.2, there after the development of boundary conditions, load applicators etc are presented in a chronological order. Initially the load and boundary conditions were applied with a constraint coupling interaction, section 5.3, thereafter rigid bodies were used to introduce the loads and boundary conditions, see section 5.4. With rigid bodies applying loads the boundary conditions were further analyzed, using springs to adjust the vertical and rotational stiffness, see section 5.5. The final adjustments of the model and analysis procedure to form the models which are the basis in producing the presented results is finally described in 5.5.3, this section also briefly describes the procedure of the analyses for achieving the aims and questions of this thesis.

## 5.1 Evaluation of different element types – Plate buckling

To evaluate the various elements available in Abaqus, a simply supported plate was modeled in Abaqus. Buckling analyses were performed and the results were compared to an analytical solution. The geometry and material properties of the plate used in the evaluation were set according to Table 5.1. Boundary conditions and application of load is illustrated in Figure 5.1 below.

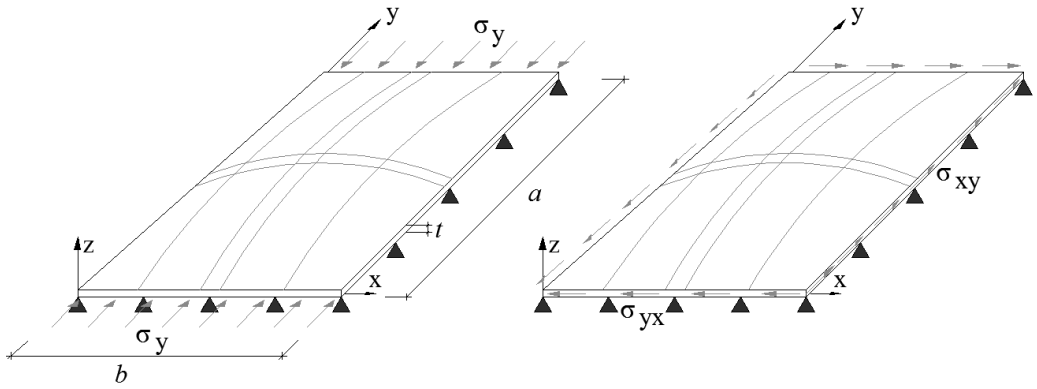


*Figure 5.1 Boundary condition and application of load in the element study, left figure under compressive stress, right figure under shear force.*

*Table 5.1 Geometry and material properties for element study*

| | | | |
|---|---|---|---|
| Hight | a = 2.4 (m) | Young's modulus | $E = 77 \cdot 10^9$ |
| Width | b = 1.2 (m) | Poissons ratio | $\nu = 0.23$ |
| Thickness | t = 0.01 (m) | | |

### 5.1.1 Analytical calculation:

*Compressive stress*

The compressive buckling stress, $\sigma_{cr}$, was calculated according to expression (4.15), with geometry and material properties according to Table 5.1. Buckling coefficient given by (4.13) with m=1,2,3,4,5, gives

*Table 5.2 Buckling loads (MPa) for a simply supported plate according to Table 5.1*

| Results of $\sigma_{cr}$ (MPa): | | | | |
|---|---|---|---|---|
| n=1, m=1 | n=1, m=2 | n=1, m=3 | n=1, m=4 | n=1, m=5 |
| 29.0222 | 18.5742 | 21.7989 | 29.0222 | 39.0523 |
| Result in order of stress level | | | | |
| 18.5742 | 21.7989 | 29.0222 | 29.0222 | 39.0523 |

*Shear stress*

The shear buckling stress, $\tau_{cr}$, was calculated according to expression (4.16), with geometry and material properties according to Table 5.1. Buckling coefficient given by (4.17), gives

$\tau_{cr} = 29.4402$ MPa

### 5.1.2 Parameter study

For the model with continuum elements the plate was created as a 3D deformable solid extrusion part with geometry and material properties according to Table 5.1. The part was then partitioned with a cutting plane through the mid plane of the plate. To mimic the conditions of the analytical calculation loads were applied to the plate as uniform pressure on the edges for compression and as surface tractions for shear, boundary conditions where applied along the mid plane around the plate's perimeter.

For the model with shell elements a planar shell part was created. Loads were applied to the plate as shell edge load, and boundary conditions were applied along the edges and corners.

The calculation of the buckling load was performed by a linear perturbation ("Buckle") analysis, described in 4.3.1. The various element types tested in the parameter study were

*Table 5.3 Element types used in parameter study.*

| Element | code |
|---|---|
| Continuum, linear, reduced integration | C3D8R |
| Continuum, linear, full integration | C3D8 |
| Continuum, quadratic, reduced integration | C3D20R |
| Continuum, quadratic, full integration | C3D20 |
| Continuum, linear, incompatible modes | C3D8I |
| Continuum shell | SC8R |
| Shell, linear, reduced integration | S4R |
| Shell, linear, full integration | S4 |
| Shell, quadratic, reduced integration | S8R |

In the table for calculated $\sigma_{cr}$ below the ratio of $\sigma_{cr.}$Abacus / $\sigma_{cr.}$Analytic is given for the second buckling mode (with a one-period sinusoidal curve in the height direction).

*Table 5.4 Results from parameter study. Buckling load ratios for compressive stress.*

| | Number of elements | | | t-dir × b-dir × a-dir / total number of elements | |
|---|---|---|---|---|---|
| | 2×24×48 | 2×60×120 | 2×120×240 | 4×24×48 | 4×60×120 |
| Element | 2304 | 14400 | 57600 | 4608 | 28800 |
| C3D8R | 7.559 | 0.923 | 0.760 | 28.131 | 1.630 |
| C3D8 | 5.701 | 1.646 | 1.067 | 5.792 | 1.737 |
| C3D20R | 0.994 | 0.994 | 0.994 | 0.994 | 0.994 |
| C3D20 | 0.998 | 0.995 | 0.994 | 0.997 | 0.995 |
| C3D8I | 1.006 | 0.998 | 0.996 | 1.006 | 0.997 |
| SC8R | 1.005 | 0.996 | 0.995 | 1.005 | 0.996 |
| | 1×6×12 | 1×12×24 | 1×24×48 | | |
| | 72 | 288 | 1152 | | |
| S4R | 1.048 | 1.010 | 1.000 | | |
| S4 | 1.039 | 1.008 | 1.000 | | |
| S8R | 0.991 | 0.994 | 0.994 | | |

*Table 5.5 Results from parameter study. Buckling load ratios for shear stress.*

| | Number of elements | | | t-dir × b-dir × a-dir / total number of elements | |
|---|---|---|---|---|---|
| | 2×24×48 | 2×60×120 | 2×120×240 | 4×24×48 | 4×60×120 |
| Element | 2304 | 14400 | 57600 | 4608 | 28800 |
| C3D8R | 5.298 | 0.898 | 0.783 | 18.634 | 1.448 |
| C3D8 | 6.665 | 1.834 | 1.142 | 1.276 | 1.929 |
| C3D20R | 1.030 | 1.030 | 1.029 | 1.030 | 1.029 |
| C3D20 | 1.033 | 1.030 | 1.030 | 1.033 | 1.030 |
| C3D8I | 1.047 | 1.032 | 1.031 | 1.047 | 1.032 |
| SC8R | 1.029 | 1.008 | 1.000 | 1.017 | 1.000 |
| | 1×6×12 | 1×12×24 | 1×24×48 | | |
| | 72 | 288 | 1152 | | |
| S4R | 1.227 | 1.076 | 1.048 | | |
| S4 | 1.256 | 1.081 | 1.043 | | |
| S8R | 1.038 | 1.029 | 1.029 | | |

### 5.1.3 Conclusions after parametric study

As expected, the linear continuum elements do not behave well, and do not show a clear convergence towards the analytical solution. Furthermore, the linear elements with full integration elements are too stiff. The quadratic continuum elements work well both with reduced and full integration. The continuum shell elements and elements with incompatible modes also work well. But there is a big difference in time of calculation. As an example the

time of calculation for the plate with 57600 elements took approximately one minute using the continuum shell elements but nearly fifteen minutes using the quadratic, fully integrated, continuum elements.

Shell elements behave in general well, showing conforming results with fewer elements compared with the case of using continuum elements. The calculation time is also a plus for these elements. The disadvantage of these elements is that the shell elements are planar in their geometry, i.e. without any thickness in the geometrical model, which complicates the build-up of a full 3D-model which includes adhesives layers and timber studs connected to the glass pane.

After these tests the continuum shell element was selected for the further development of an FE-model of the shear wall pane. These elements converge well towards the analytical solution and can save some calculation time. They will also be easy to model together with the 3D-geometry of the adhesive and the timber frame.

## 5.2 Model built-up

### 5.2.1 Creating the shear wall element part

The shear wall was modeled as a 3D deformable solid part of size 2404×1204×103 ($mm^3$). Instead of using the Abaqus tie option to assemble the different parts together, the entire shear wall was made as a single 3D deformable solid part which was shaped with cut extrudes and partitioned using cutting planes.

The geometry of the model is shown in Figure 5.2. In the FE model the glass pane was assumed to be of the same size as the frame, which differs slightly from the shear walls used in the experiments where the glass was 2400×1200×10 ($mm^3$) and a 2 mm thick PTFE (Teflon$^{TM}$) strip was used to fill the small gap.

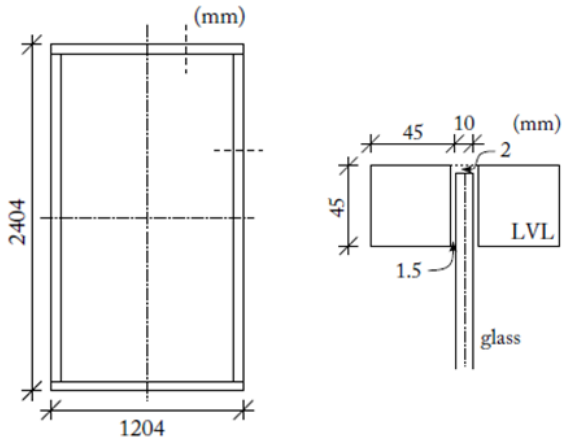


*Figure 5.2Geometry of the shear wall element [1]*

In Figure 5.3 below a corner of the part is shown, illustrating the cutting planes that partition the part into different sections. With this approach all section were perfectly connected, and the different sections could be given different material properties.

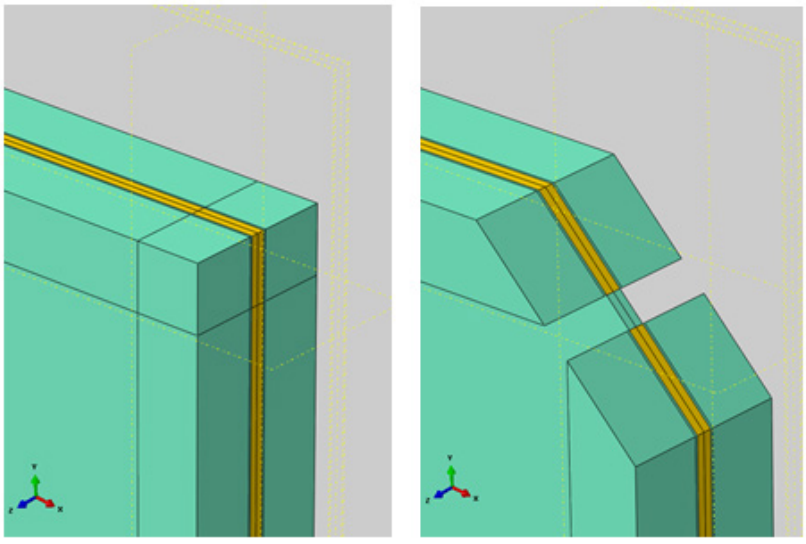

*Figure 5.3Illustration of cutting planes*

The sections of timber studs, adhesive and the glass between the adhesive frames were meshed with linear continuum elements with full integration, C3D8. The remaining glass pane section was a meshed with continuum shell elements, SC8R. The global element size was set to 0.02 m. With the partitioning of the corners all elements became rectangular in shape. With this element size the timber studs are made up of 2×2 elements over the cross-section.

During the development the timber studs were modeled both as being fully connected to each other at the corners and by assuming that there was no interaction at all between them. This latter modeling approach was achived by making a cut through the studs at the cornes. A very thin triangularly shaped cut was done through the vertical studs, so that the vertical studs were separated from the horizontal, see Figure 5.4.

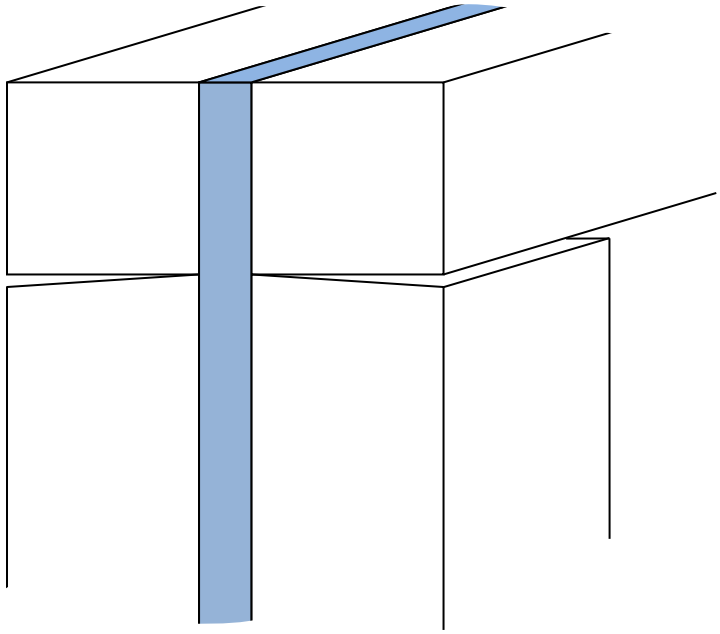

*Figure 5.4 Illustration of cut to separate studs (width of cut is exaggerated for clarity).*

### *Assembly in global coordinates*

The shear wall was inserted in the global coordinate system so the glass pane lies parallel to the x-y plane and the normal of the glass plane is oriented in the z-direction. The short edge of the glass pane is parallel to the x-axis. Boundary conditions and loads are denoted as follows

$u_x$, $u_y$, $u_z$ – displacement in x-, y- and z-direction

$ur_x$, $ur_y$, $ur_z$ – rotation around the x-,-y- and z-axis

$CF_x$, $CF_y$, $CF_z$ - concentrated force in x-, y- and z-direction

### 5.2.2 Material properties

Material properties were initially chosen in accordance with the materials used for the tested I-beams in [6] , assuming that approximately the same materials were used for the timber-glass shear wall. The properties of LVL in [6] are presented in Table 2.2 , Poisson's ratios for the LVL were questioned since $\nu_{lt} = \nu_{lr} = 1.1$ are much higher than what is given in other literature. These were therefor set initially to $\nu_{lt} = \nu_{lr} = 0$, the effect was assumed to be negligible. Properties of glass were Young´s modulus E = 77 GPa, and Poisson's ratio $\nu = 0.23$.

The orthotropic properties of the LVL were matched to the orientations of the LVL on the constructed timber-glass shear wall. The orientations of the material properties were set to the vertical and horizontal studs respectively according to Figure 5.5.

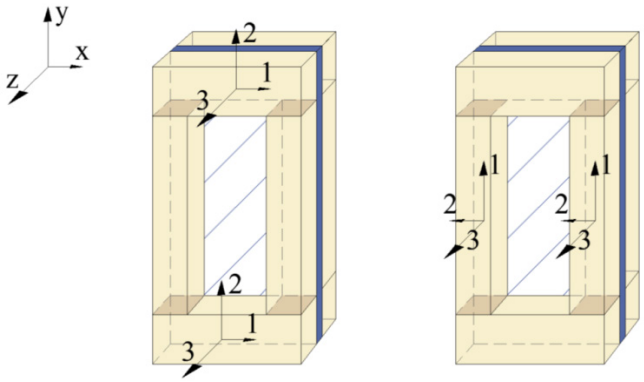


*Figure 5.5 Illustration of material orientation of LVL studs (horizontal on the right, vertical on the left)*

The directions 1,2 and 3 correspond to the longitudinal direction along the fibers, to the normal of the LVL-veneers plane, and parallel to the planes of the veneers, respectively.

In the development of a conforming model the FE-results were compared with the test results obtained with the shear walls with acrylate adhesive. The following material parameters were used initially

*Table 5.6 Material properties used in the model development.*

| | | | |
|---|---|---|---|
| Glass | E = 77 000 MPa | $\nu = 0.23$ | |
| Timber (LVL) | $E_1 = 16\,060$ MPa | $E_2 = 440$ MPa | $E_3 = 440$ MPa |
| | $G_{12} = 440$ MPa | $G_{13} = 440$ MPa | $G_{23} = 44.4$ MPa |
| | $\nu_{12} = 0$ | $\nu_{13} = 0$ | $\nu_{23} = 0.39$ |
| Adhesive | E = 80 MPa | $\nu = 0.4$ | |

To obtain comparable results throughout the development these material values were not initially changed although the values for timber and glass seemed high. During the process of developing this model it turned out that the boundary conditions at the horizontal load case had a much greater impact than first thought. The load application device used in the test (a rigid beam) was first thought of as being locked in the vertical direction and in rotation around the out of plane axis, however this boundary condition did not give correlating results. As will be seen in section 5.5 the adjustment of these two boundary conditions can calibrate the model to match the experimental results, using various material properties.

The analyses to study the interaction between the vertical and horizontal critical load in the combined load case were also made with the alternative timber properties according to Table 2.3, material properties used in this test are shown in Table 5.7

*Table 5.7 Alternative material properties, used in the final model to study the interaction in the combined load case.*

| | | | |
|---|---|---|---|
| Glass | $E = 77\ 000$ MPa | $\nu = 0.23$ | |
| Timber (LVL) | $E_1 = 13\ 800$ MPa | $E_2 = 130$ MPa | $E_3 = 430$ MPa |
| | $G_{12} = 600$ MPa | $G_{13} = 600$ MPa | $G_{23} = 60$ MPa |
| | $\nu_{12} = 0.5$ | $\nu_{13} = 0.5$ | $\nu_{23} = 0.5$ |
| Adhesive | $E = 80$ MPa | $\nu = 0.4$ | |

## 5.3 Shear wall model 1: Coupling constraints

In a surface-based coupling constraint, the displacements of selected nodes on a surface are governed by a reference node. The coupling constraint can be very useful in many situations, for example when a surface is constrained to a rigid body motion or to apply loads and boundary conditions. There is also the possibility to model end conditions, for example a rigid plate, or to constrain a planar section of a solid part to remain planar.

The reference node has both rotational and translational degrees of freedom. In Abaqus the user can choose which of these degrees of freedoms that will be coupled to the nodes on a surface. If all are selected the displacement of the coupled nodes are then determined by the expression (5.1) below (for small displacement increments).

$$\begin{aligned} u_x &= u_{P.x} + u_{P.Ry} \cdot \Delta z - u_{P.Rz} \cdot \Delta y \\ u_y &= u_{P.y} + u_{P.Rz} \cdot \Delta x - u_{P.Rx} \cdot \Delta z \\ u_z &= u_{P.z} + u_{P.Rx} \cdot \Delta y - u_{P.Ry} \cdot \Delta x \end{aligned} \qquad \textit{(5.1)}$$

where $u_i$ is the displacement in direction *i* for a node on the coupled surface located at ($\Delta x$, $\Delta y$, $\Delta z$) relative the reference node, and where $u_{p.i}$ and $u_{p.Ri}$ is the displacement in direction *i* and the rotation about axis *i* of the reference node, respectively.

### 5.3.1 Model built-up of shear wall with coupling constraint

For the coupling constraint the selected coupling nodes were the upper and the lower horizontal surfaces of the shear wall, respectively. The reference point was placed on the centroid of the respective surface. Boundary conditions were applied to the reference nodes only, and set to mimic the experimental setup. The analysis was conducted in two steps, an initial displacement with a static general procedure followed by a linear perturbation – buckling procedure. Analyses were conducted both with and without nonlinear geometry effects taken into account.

***Boundary conditions and loads*** (mm, N)

| **Vertical load case** | **Step 1- static general** | **Step 2 – linear perturbation** |
|---|---|---|
| Ref.point bottom | $u_x = u_y = u_z = 0$, $ur_y = ur_z = 0$ | $u_x = u_y = u_z = 0$, $ur_y = ur_z = 0$ |
| Ref.point top | $u_x = u_z = 0$, $ur_y = ur_z = 0$<br>$u_y = -0.01$ | $u_x = u_z = 0$, $ur_y = ur_z = 0$<br>$[CF_x, CF_y, CF_z] = [0,-1,0]$ |
| **Horizontal load case** | | |
| Ref.point bottom | $u_x = u_y = u_z = 0$, $ur_y = ur_z = 0$ | $u_x = u_y = u_z = 0$, $ur_y = ur_z = 0$ |
| Ref.point top | $u_x = 0.1$, $u_y = -0.01$<br>$u_z = 0$, $ur_y = ur_z = 0$ | $u_x = u_z = 0$, $ur_y = ur_z = 0$<br>$[CF_x, CF_y, CF_z] = [1,0,0]$ |

### 5.3.2 Results and conclusions for further development.

*Table 5.8 Buckling loads obtained from models with coupling constraints.*

| **Vertical load** | Nlgeom | Horizontal preload (kN) | Critical load $V_{cr}$ (kN) |
|---|---|---|---|
| Model-1a | OFF | 0 | 176.83 |
| Model-1b | ON | 0 | 176.86 |
| **Horizontal load** | Nlgeom | Vertical preload (kN) | Critical load $H_{cr}$ (kN) |
| Model-1c | OFF | 4.32 | 229.71 |
| Model-1d | ON | 4.32 | 233.85 |
| Model-1e | OFF | 8.64 | 221.19 |
| Model-1f | ON | 8.64 | 221.20 |

Compared to the experimental results in Table 3.1 the vertical buckling load was about the same magnitude. The horizontal buckling load on the other hand was much higher than in the conducted experiments where the highest registered horizontal load was 71.3 kN. A probable explanation to the much overestimated buckling load in the FE-analyses is that the entire element interacted completely with the load and boundary conditions due to the constraint coupling. In the coupling constraint the horizontal surface was kept plane and horizontal and there was no transverse motion of the nodes at the surface. Another explanation can be that the timber studs were perfectly connected in the corners which also adds stiffness to the frame in the FE-model.

To obtain a closer fit to the experimental results in terms of horizontal buckling load, a more refined model of the loading device was necessary. Instead of a coupling constrain the idea arose that a rigid part could be used to apply loads and boundary conditions. This could give a more realistic behavior of the shear wall.

## 5.4 Shear wall model 2 & 3: Introducing rigid parts

Rigid parts can be used when parts in a model come in contact and some parts are much stiffer so that the deformation of these can be neglected.

### 5.4.1 Model 2, built-up with rigid parts

The shear wall was created in the same manner as in 5.2.1, with material properties according to Table 5.6. The rigid parts modeling the loading devices were created as 3D analytical rigid parts. The rigid parts were given a reference point which was placed so that it would lie at the center of the top and bottom surfaces, respectively. The heel which applies the horizontal load is 50 mm high, resembling the experimental set up.

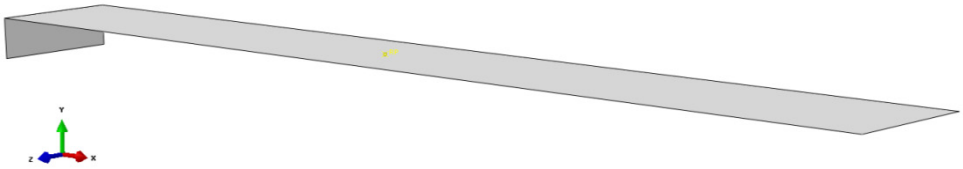

*Figure 5.6 Rigid part - model 2*

To simulate the contact between the loading device and the shear wall, an interaction criterion was defined. This included a frictional interaction constraint between the surfaces allowing for some slip between the surfaces. In Abaqus a surface-to-surface contact interaction was created, with the rigid part as master surface and the corresponding shear wall surfaces as slave surfaces. The interaction property was set to hard contact (no penetration of the slave surface into the master surface) with the tangential behavior defined by a penalty formulation. This is a stiffness method that allows for elastic slip, i.e. allows some relative motions of the surface when they are in contact. The magnitude of the slip is controlled by the elastic slip. The friction coefficient was set to 0.3.

Analyses were made both with and without nonlinear geometry behavior. Boundary conditions were applied to the reference nodes of the rigid parts, according to 5.3.1. In order to ensure converging results during the first calculation step (i.e. to establish contact without any rigid body motions), two additional nodes were pinned (locked in all directions) in the first step, these were two points on the timber frame. After the contact was established these pinned boundary conditions were released

To evaluate the bifurcation load two different methods were used, a linear perturbation buckling analysis and a general, static large displacement analysis applying the full load and evaluating the associated load-displacement diagram. The buckle analysis used a displacement acting as reference “load”. The buckling load was then calculated by controlling the reaction forces in the reference node after step one and adding to these the eigenvalue multiplied with this preload and the ratio between the “buckling reference displacement” and the “pre-displacement”. This assumes a linear relation between load and displacement at the end of the preload step, and to control this assumption a few tests were made with a concentrated force instead. These showed only small differences that could be neglected.

When the model was subjected to the full load, a larger vertical displacement (with nonlinear geometry in the calculations), the aim was first that the calculations would fail at a level corresponding to the bifurcation point, but the results turned out to be perfectly linear. To trigger instability a small transverse uniform pressure was therefore added on the panel. The vertical reaction force (RF2) was plotted against the displacement in the z-direction of a node at the center of the pane.

A number of analyses were made to study the influence of the vertical preload on the horizontal critical load. In step 1 in these models the horizontal displacement was 0.1 mm and the vertical displacement was varied from 0.08 mm to 0.4 mm. In step 2 a reference displacement was given in the horizontal direction and a buckling analysis was made.

### 5.4.2 Model 2-Results and conclusions for further development

*Table 5.9 Vertical critical load with buckling analysis*

| | | Step 1 | | | Step 2 | | Bifurcation value |
|---|---|---|---|---|---|---|---|
| Vertical | Nlgeom | U2 (mm) | RF 1 (kN) | RF2 (kN) | U2 (mm) | Eigen value | $V_{cr}$ (kN) |
| Model-2a | OFF | -0.1 | 0.25 | -42.42 | -1 | 0.31357 | 175.42 |
| Model-2b | ON | -0.1 | 0.25 | -42.42 | -1 | 0.31358 | 175.44 |

*Table 5.10 Approximated vertical critical load from a load-displacement plot*

| | | Step 1 | Step 2 | | | Bifurcation value |
|---|---|---|---|---|---|---|
| Vertical | Nlgeom | U2 (mm) | Transversal pressure | U2 (mm) | Transversal pressure | Approximated $V_{cr}$ (kN) |
| Model-2c | ON | -0.1 | ON | -5 | ON | 208.6 |
| Model-2d | ON | -0.1 | ON | -10 | ON | 210.6 |
| Model-2e | ON | -0.1 | ON | -10 | OFF | 210.6 |

The vertical critical load was about the same with this model as with the model with the coupling constraints, see 5.3.2. There were no larger differences between the models with or without nonlinear geometry behavior taken into account.

The model using a larger displacement can carry a vertical load larger than the estimated critical value, and thus it is difficult to estimate when the buckling load has been passed. It was also shown that a transverse load was needed to trigger the instability and that with the linear perturbation buckling analysis the results were closer to the values from the experiments.

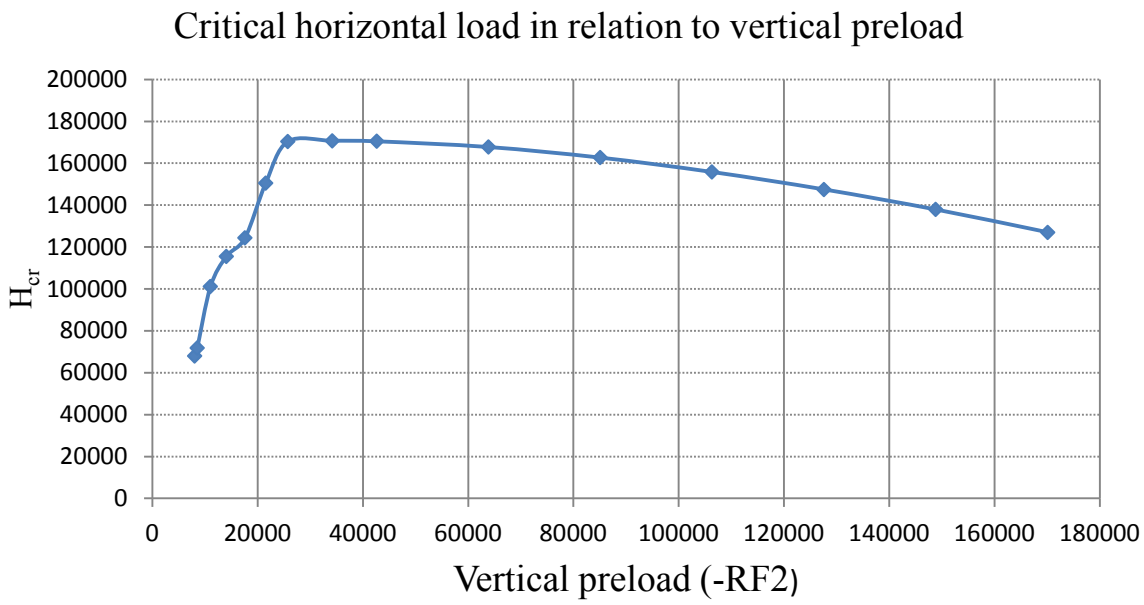


*Figure 5.7 Horizontal critical load, obtained with buckling analysis under varied vertical preload*

The horizontal critical load was now lower and closer to the experimental results with the linear perturbation analysis used, but there were some questions raised. After the first analysis step, the contact between the rigid body and the shear wall was not enough to keep it in place and the corners of the shear wall not in contact with the loading device (and thus no friction being built up), moved in the out of plane direction. The conducted test with a larger horizontal displacement in step 2 could not be used in a comparison because the corners not in contact with the rigid body moved out of plane which changed the geometry to much in comparison with the buckle analysis made. The rigid bodies could not capture the boundary conditions from the experiments. According to the Abaqus manual, the use of contact constraints is indeed allowed even for linear perturbation analyses such as the Buckle procedure. The contact constraints at the reference node state are, however, not updated during eigen value extraction (since contact constrains are nonlinear boundary conditions this would contradict the assumption of a linear behavior).

Tests made to study the impact of the initial vertical load showed that the horizontal stiffness is enhanced initially but then decreases. This is explained by the fact that a larger part of the ends of the glass come in contact with the loading devices i.e. the rigid bodies, but if the preload is too large, the transverse stiffness is reduced already by the vertical preload. The bifurcation point when combining different stresses is according to theory, discussed in 4.1.2, depending on the interaction of $\sigma/\sigma_{cr}$ and $\tau/\tau_{cr}$. With this in mind the horizontal load capacity should have decreased towards zero more clearly as $\sigma/\sigma_{cr}$ approached 1.

Compared to the experiments, the buckling load using a small vertical preload matched the results better. All this highlights the importance that to be able to compare the FE-results with experiments the same vertical preload must be used, and the horizontal to vertical force ratio in which the shear wall was actually loaded is of great importance.

### 5.4.3 Shear wall model 3: Clamped edges and cut stud connections

To resolve the problem of the out of plane movement the rigid bodies were redesigned, and a 30 mm edge around the rigid body was added. At this point two more influencing variables were added to the development of the model.

The stud connections had so far been perfectly bonded which contributed to the horizontal stiffness. Images from experiments show that a small crack appeared in these connections. To evaluate the significance of this a very thin part was cut out from the vertical studs creating a gap between the vertical and horizontal studs, see Figure 5.4.

Another influencing condition that had to be taken in consideration was the distance from the glass pane to the point of rotation. This variable was tested by moving the reference points positions according to the experimental set up described in Figure 3.4.

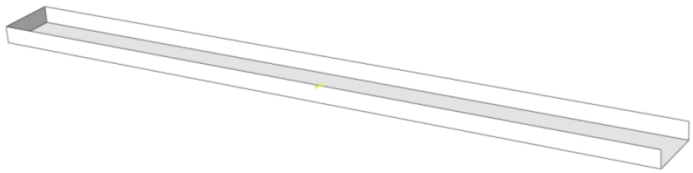

*Figure 5.8 Rigid part - model 3*

To establish a good initial contact, the width of the rigid body was set to 102.9 mm, i.e. 0.1 mm smaller than the width of the shear wall, and in the first step of the analysis the interaction is established by gradually removing slave node overclosure. This meant that the timber studs shrank 0.05 mm on each side to fit inside the loading device. This compression remained during the second and third calculation step and counteracts the out of plane movements by ensuring contact between the sides of the loading device and the timber frame sides. In step one the top and bottom reference nodes were locked in all directions and rotations.

***Boundary conditions and loads*** (mm,N)

| | **Step 2- static general** | **Step 3 – linear perturbation** |
|---|---|---|
| **Vertical load case** | | |
| Ref.point bottom | $u_x = u_y = u_z = 0$, $ur_y = ur_z = 0$ | $u_x = u_y = u_z = 0$, $ur_y = ur_z = 0$ |
| Ref.point top | $u_x = u_z = 0$, $ur_y = ur_z = 0$<br>$u_y = -0.01$ | $u_x = u_z = 0$, $ur_y = ur_z = 0$<br>$[CF_x, CF_y, CF_z] = [0,-1,0]$ |
| **Horizontal load case** | | |
| Ref.point bottom | $u_x = u_y = u_z = 0$, $ur_y = ur_z = 0$ | $u_x = u_y = u_z = 0$, $ur_y = ur_z = 0$ |
| Ref.point top | $u_x = 0.1$, $u_y = -0.01$<br>$u_z = 0$, $ur_y = ur_z = 0$ | $u_x = u_z = 0$, $ur_y = ur_z = 0$<br>$[CF_x, CF_y, CF_z] = [1,0,0]$ |
| **Combined load case** | | |
| Ref.point bottom | $u_x = u_y = u_z = 0$, $ur_y = ur_z = 0$ | $u_x = u_y = u_z = 0$, $ur_y = ur_z = 0$ |
| Ref.point top | $u_x = 0.1$, $u_y = -0.01$<br>$u_z = 0$, $ur_y = ur_z = 0$ | $u_x = u_z = 0$, $ur_y = ur_z = 0$<br>$[CF_x, CF_y, CF_z] = [F_x, F_y, 0]$ |

### 5.4.4 Results and conclusions for further development

*Table 5.11 Vertical critical load with buckling analysis*

| | Step 2 | | | | Step 3 | | Bifurcation value |
|---|---|---|---|---|---|---|---|
| **Vertical** | U1 (mm) | U2 (mm) | RF 1 (kN) | RF2 (kN) | U2 (mm) | Eigen value | $V_{cr}$ (kN) |
| Model-3a | 0 | -0.1 | 0.21 | -42.45 | -1 | 0.31526 | 176.29 |
| **With eccentric reference points** | | | | | | | |
| Model-3b | 0 | -0.1 | 0.09 | -42.43 | -1 | 0.31529 | 176.22 |
| **With eccentric reference points and stud connections cut** | | | | | | | |
| Model-3c | 0 | -0.1 | 0.21 | -42.08 | -1 | 0.30278 | 169.47 |

*Table 5.12 Horizontal critical load with buckling analysis*

| | Step 2 | | | | Step 3 | | Bifurcation value |
|---|---|---|---|---|---|---|---|
| **Horizontal** | U1 (mm) | U2 (mm) | RF 1 (kN) | RF2 (kN) | U1 (mm) | Eigen value | $H_{cr}$ (kN) |
| Model-3d | 0.1 | -0.01 | 3.27 | -8.29 | 1 | 2.8368 | 96.15 |
| Model-3e | 0.1 | -0.1 | 5.15 | -42.67 | 1 | 3.3843 | 179.44 |
| Model-3f | 0.1 | -0.4 | 5.96 | -169.29 | 1 | 2.2317 | 139.06 |
| **With eccentric reference points** | | | | | | | |
| Model-3g | 0.1 | -0.01 | 3.27 | -8.29 | 1 | 2.8215 | 95.65 |
| **With connection cut** | | | | | | | |
| Model-3h | 0.1 | -0.01 | 3.20 | -8.20 | 1 | 2.5959 | 86.32 |
| **With eccentric reference points and connection cut** | | | | | | | |
| Model-3i | 0.1 | -0.01 | 3.20 | -8.20 | 1 | 2.5941 | 86.27 |

*Table 5.13 Buckling load at combined load, stud connection cut*

| | Step 2 | | | | Step 3 | | Bifurcation value | |
|---|---|---|---|---|---|---|---|---|
| **Combined** | U1 (mm) | U2 (mm) | RF 1 (kN) | RF2 (kN) | $F_x$ / $F_y$ | Eigen value | $H_{cr}$ (kN) | $V_{cr}$ (kN) |
| Model-3j | 0.1 | -0.01 | 3.27 | -8.29 | 0.4 / -1 | 65130 | 68.33 | 171.02 |
| Model-3k | 0.1 | -0.01 | 3.27 | -8.29 | 0.6 / -1 | 63001 | 101.00 | 171.20 |
| Model-3l | 0.1 | -0.01 | 3.27 | -8.29 | 0.8 / -1 | 139416 | 114.73 | 142.61 |
| Model-3m | 0.1 | -0.01 | 3.27 | -8.29 | 1 / -1 | 121014 | 124.22 | 129.21 |

*Table 5.14 Approximated horizontal critical load from a load-displacement plot*

| Studs connected, no eccentric reference points | | | | | | | | | |
|---|---|---|---|---|---|---|---|---|---|
| | Step 2 | | | | Step 3 | | | | Bifurcation value |
| | U1 (mm) | U2 (mm) | RF 1 (kN) | RF2 (kN) | U1 (mm) | U2 (mm) | RF 1 (kN) | RF2 (kN) | Approximated $H_{cr}$ (kN) |
| Model-3n | 0.1 | -0.01 | 3.33 | -8.40 | 10 | -0.1 | 99.43 | -203.72 | 65-70 |

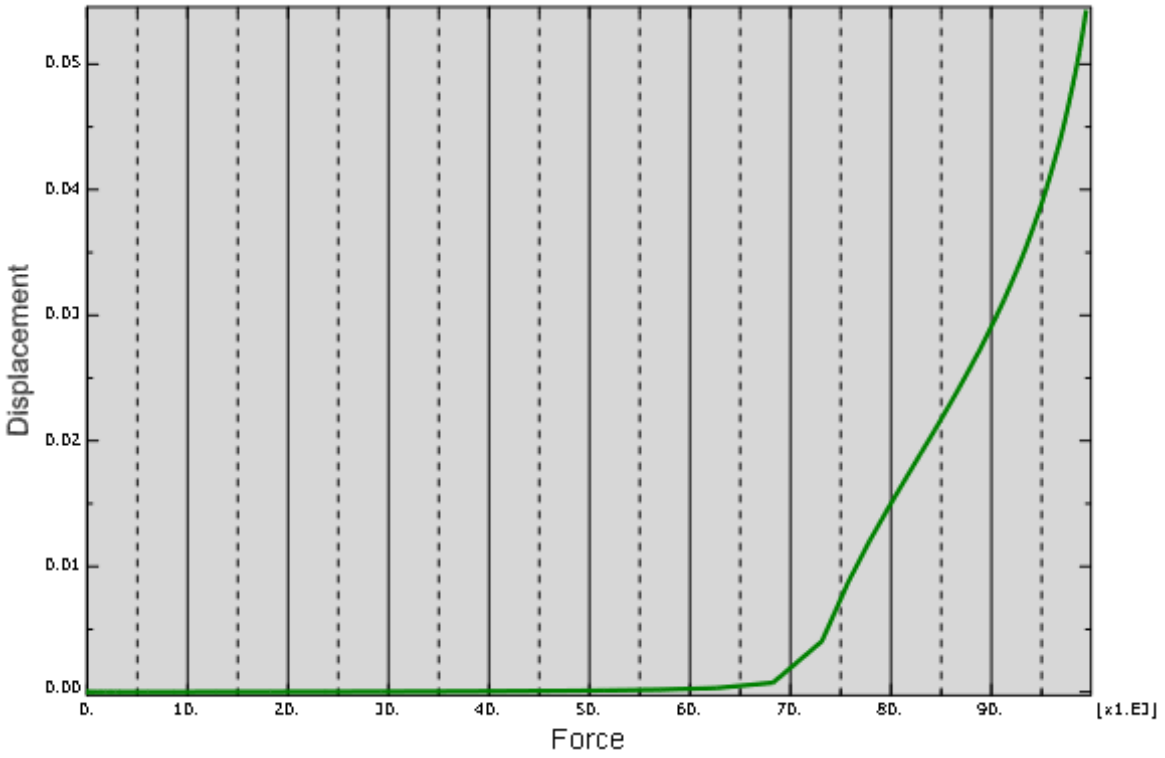


*Figure 5.9 Plot of out of plane displacement of a node at the center of the pane versus reaction force in Y-dir, Model-3n*

The vertical critical load was not affected in any significant manner by the redesign or the eccentric reference points of the rigid bodies. But the critical value was lowered when the stud connections was cut.

The horizontal critical load for Model-3d, 3e and 3f was increased in comparison with results of the model without clamped edges. This is explained by the fact that there was no transverse movement of the shear wall edges with the clamped edges. The vertical preload has the same effect on the horizontal critical load with or without the clamped edges. Comparing Model-3d with experiments (the vertical preload on Model 3d is closest to the preload level in experiments) shows that Model-3d has a higher horizontal critical load.

The force-displacement plot from Model-n displayed in Figure 5.9 above shows that at the horizontal force of about 65-70 kN the out of plane displacement escalates in the center of the

glass pane. This is a reasonable bifurcation point when compared to the experiments. Since glass has a very brittle behavior, especially in tension, the escalating out of plane movement can probably not be hindered by the glass.

Aslo noticed for this model is that when the stud connections were cut the critical buckling load was significantly reduced, and the load case of combined loads resulted in to high critical loads.

In the Abaqus analysis of the horizontal buckling load, the shapes of the buckling modes, Figure 5.10, do not match the shapes that could be observed in the experiments, see Figure 3.6.

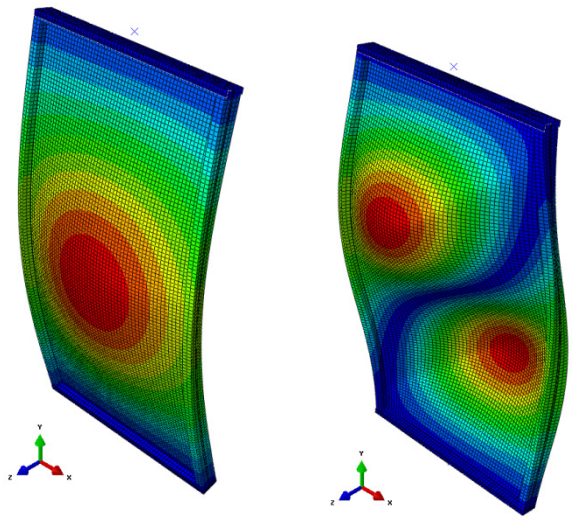

Mode-shape a Mode-shape b

*Figure 5.10 Eigenmode shapes from Model-3*

In the analyses either mode a or b according to Figure 5.10 was the mode shape corresponding to the lowest eigen value. In the horizontal load cases and the combined load case with the vertical to horizontal load ratio of 1:0.4, mode shape a was the first buckling mode. The other vertical to horizontal load ratios gave mode shape b at the lowest buckling load

## 5.5 Final corrections for a satisfying model

In studying the results from analyses in Abaqus it was noticed that at a horizontal displacement the vertical reaction force and the reaction moment counteracting the rotation of the upper rigid part increased to a very high level. This did not correspond at all to the measurements during the experiments. In the experiments evaluating horizontal loads, the vertical load applier was intended to be kept horizontal and at a constant level, but this was not really obtained. In a first trial to correlate the model towards this movement two springs were introduced, allowing vertical displacement and rotational movement around the out of plane axis. The shape of the buckling mode had not yet been taken into any larger consideration, due to the introduction of the springs also the buckling shapes turned out more similar to experiments.

After evaluating the results from analyses with models using springs the models that would be used to form the results of this thesis could be designed with a thorough knowledge of the impact of various variables.

### 5.5.1 Shear wall model 4 – Springs tuning the boundary conditions

Springs can be used in Abaqus to model a physical spring and to idealize axial or torsional movement, springs are also used in e.g. modal damping. There are two ways to insert a spring, either between two nodes or between one node and ground. There are three different elements available in Abaqus, “spring 1”, “spring 2” or “springA”. Spring1 is used to connect one node to ground, Spring 2 is used to connect two nodes, these are acting in a fixed direction i.e. the user specifies the line of direction. SpringA also acts between two nodes, however the spring stiffness acts always along the current line of action (i.e. the line connecting the two nodes) for this element.

A reference point (denoted RP-spring) was inserted at the coordinates of the top rigid body’s reference point (denoted RP-top) between these reference points two spring2 elements were inserted, these were determined to act in $u_y$ and $ur_z$.

The vertical stiffness of the structure, i.e vertical load (N) per vertical displacement (mm), was adjusted by inserting a spring stiffness $k_{vert}$ into degree of freedom 2, i.e. y-direction between RP-top and RP-spring. The vertical displacement boundaries were then set on node RP-spring, thus introducing at RP-top an elastic boundary condition.

The vertical stiffness of the structure tested in the experiments was estimated by observing Pontos measurements on the load applying beam from the experiments, the stiffness of the Abaqus model was determined with a force displacement graph. The stiffness of the vertical spring could then be estimated to give the Abaqus model the same total stiffness as the structure tested in experiments. Observe that by structure is meant both the shear wall element and other devices such as holding supports. These calculations are presented in Appendix B. The rotational stiffness $k_{rot}$ was difficult to estimate from the experimental set up or from the results, this therefore had to be estimated in an iterative manner with respect to obtained buckling load and buckling mode shape.

The Abaqus analyses were made in three steps, according to 5.4.3. In step 1 (removal of contact node over closure) reference points were locked in all degrees of freedom.

***Boundary conditions and loads*** (mm, N)

| **Vertical load case** | **Step 2- static general** | **Step 3 – linear perturbation** |
|---|---|---|
| RP-bottom | $u_x = u_y = u_z = 0$, $ur_y = ur_z = 0$ | $u_x = u_y = u_z = 0$, $ur_y = ur_z = 0$ |
| RP-top | $u_x = u_z = 0$, $ur_y = 0$ | $u_x = u_z = 0$ , $ur_y = 0$ |
| RP-spring | $u_y = -0.01$<br>$ur_z = 0$ | $ur_z = 0$<br>$[CF_x, CF_y, CF_z] = [0,-1,0]$ |
| **Horizontal load case** | | |
| RP-bottom | $u_x = u_y = u_z = 0$, $ur_y = ur_z = 0$ | $u_x = u_y = u_z = 0$, $ur_y = ur_z = 0$ |
| RP-top | $u_x = 0.1$<br>$u_z = 0$, $ur_y = 0$ | $u_z = 0$, $ur_y = 0$<br>$[CF_x, CF_y, CF_z] = [1,0,0]$ |
| RP-spring | $u_y = -0.01$ , $ur_z = 0$ | $u_y = 0$, $ur_z = 0$ |
| **Combined load case** | | |
| RP-bottom | $u_x = u_y = u_z = 0$, $ur_y = ur_z = 0$ | $u_x = u_y = u_z = 0$, $ur_y = ur_z = 0$ |
| RP-top | $u_x = 0.1$, $u_z = 0$<br>$ur_y = 0$ | $u_z = 0$, $ur_y = 0$<br>$[CF_x, CF_y, CF_z] = [1, 0, 0]$ |
| RP-spring | $u_y = -0.01$<br>$ur_z = 0$ | $ur_z = 0$<br>$[CF_x, CF_y, CF_z] = [0, -2.5, 0]$ |

In order to estimate the impact of the spring's stiffness several models with various vertical and rotational spring stiffness values were analyzed, using material properties according to Table 5.6. The results from these are presented in Figure 5.11 where in each series one of the two springs were kept constant and the other varied.

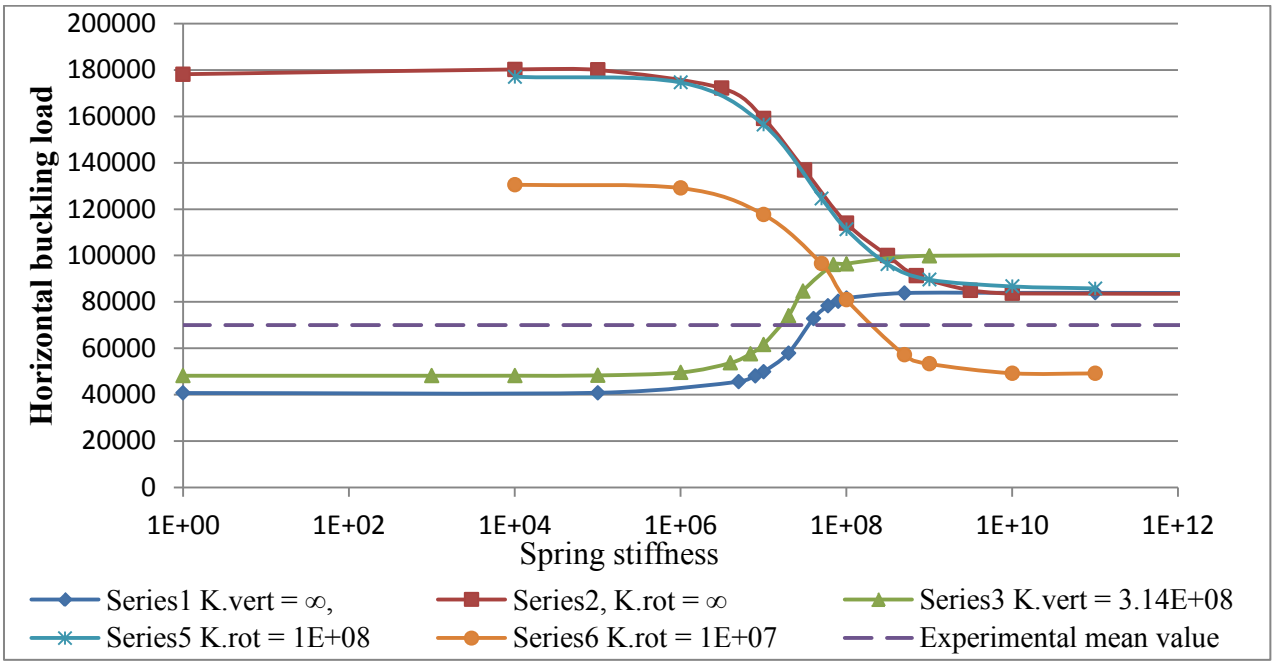


*Figure 5.11 Model 4, Results from varying spring stiffness of top boundary condition, in each series either $k_{rot}$ or $k_{vert}$ were kept constant the other varied.*

With the material properties according to Table 5.6 the estimating calculation, see Appendix B, of vertical spring stiffness resulted in $k_{vert}=3.14\cdot10^{8}$ and by fine-tuning the rotational spring stiffness to $k_{rot}=1.7\cdot10^{7}$, the results of Table 5.15 were obtained.

*Table 5.15 Model 4. Buckling load at vertical, horizontal and combined load case, using rotational and vertical springs.*

| | Step 2 | | | | Step 3 | | Bifurcation value | |
|---|---|---|---|---|---|---|---|---|
| Load case | U1 (mm) | U2 (mm) | RF 1 (kN) | RF2 (kN) | $F_x$ / $F_y$ | Eigen value | $H_{cr}$ (kN) | $V_{cr}$ (kN) |
| Vertical | 0 | -0.01 | 0 | 1.79 | - / 1 | 168.59 | - | 170.38 |
| Horizontal | 0.1 | -0.01 | 1.06 | -3.71 | 1 / - | 69359 | 70.42 | - |
| Combined | 0.1 | -0.01 | 1.06 | -3.71 | 1 / -2.5 | 58651 | 59.72 | 150.34 |

The values of horizontal and vertical load cases are reasonable well correlated to experimental values of Table 3.1. Also the shape of the buckling modes were well correlated. The combined load case is however too high, but after fine tuning the springs stiffness also this value could be correlated. However when further analyses were made with the combined load cases, varying the vertical to horizontal load ratios, the analyses did not give accurate results as can be seen in Figure 5.12. As the vertical load was decreased the horizontal buckling load increased far beyond the critical loading point given by the horizontal load case.

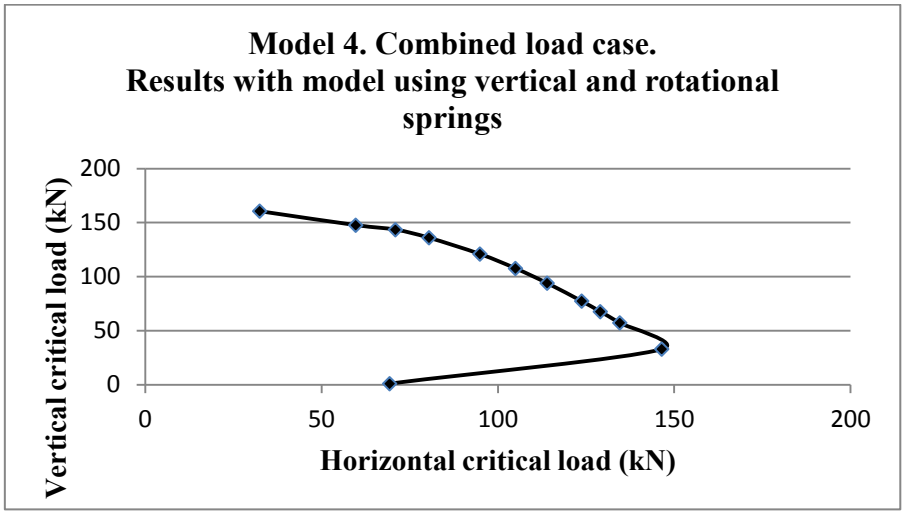


*Figure 5.12 Buckling load of model using springs, combined lod case.*

The puzzling results showed in Figure 5.12 turned out to depend on the boundary conditions set in the linear perturbation, buckle, analysis step. Since the boundary conditions of the reference node RP-spring in the horizontal load case was set to $u_y= 0$, the vertical force build-up in the spring increased to higher levels than those load values that were set as a concentrated force, CF2, in the combined load case. Since the linear perturbation analysis only makes the eigenvalue extraction the reaction forces is not presented in the results of this analysis, therefore it is not possible to predict how large the vertical force was at the bifurcation point.

### 5.5.2 Shear wall model 5 – Final adjustments and conclusions

The impact of the springs stiffness on the buckling load level shows the importance of carefully taking the displacements and rotations of the shear wall element into account to obtain correlating results. There are however a few disadvantages when using these springs as a boundary condition in the linear perturbation, buckle, step, as the results in Figure 5.12 show.

To deal with this problem the boundary conditions in the linear perturbation step was changed. The new approach was to apply the desired vertical force, then release the vertical boundary condition in the linear perturbation step to ensure that the vertical reaction force did not increase further. With this approach the resulting vertical force in a combined load case can be more exactly controlled.

To evaluate the effect of this approach loads and displacements were applied directly to RP-top, and rotation around the z-axis was set free. The Abaqus analyses were made in three steps, according to 5.4.3. In step 1 (removal of node over closure) reference points were locked in all degrees of freedom.

*Table 5.16 Model5, boundary conditions and results*

| **Boundary condition** | **Step 2- static general** | **Step 3 – linear perturbation** |
|---|---|---|
| RP-bottom | $u_x = u_y = u_z = 0$, $ur_y = ur_z = 0$ | $u_x = u_y = u_z = 0$, $ur_y = ur_z = 0$ |
| RP-top | $u_x = U1$, $u_y = U2$, $u_z = 0$, $ur_y = 0$ | $u_z = 0$, $ur_y = 0$ $[CF_x, CF_y, CF_z] = [F_x, F_y, 0]$ |

| **Results** | Step 2 | | | | Step 3 | | Bifurcation value | |
|---|---|---|---|---|---|---|---|---|
| Model | U1 (mm) | U2 (mm) | RF 1 (kN) | RF2 (kN) | $F_x$ / $F_y$ (kN) | Eigen value | $H_{cr}$ (kN) | $V_{cr}$ (kN) |
| Model5-a | 0.2 | 0 | 1.73 | -8.19 | 1 / 0 | 89.256 | 91.0 | 8.2 |
| Model5-b | 0.2 | -0.02 | 2.54 | -13.3 | 1 / -0.1 | 82.749 | 85.3 | 21.6 |
| Model5-c | 0.2 | -0.2 | 4.41 | -84.33 | 1 / -1 | 45.664 | 50.1 | 130.0 |
| Model5-d | 0.02 | -0.2 | 0.56 | -84.32 | 0.1 / -1 | 84.316 | 9.0 | 168.5 |
| Model5-e | 0 | -0.2 | 0.13 | -84.20 | 0 / -1 | 85.413 | 0.1 | 169.6 |

These results are corresponding well to the expected interaction effect. The horizontal critical value of Model5-a was too high compared to experiments, thus two trials were made with springs inserted in the same manner as explained in 5.5.1.

In the first trial a rotational spring was inserted in Model5-a, to control the rotational stiffness of RP-top in step 2. The boundary condition of RP-spring was set to $ur_z = 0$ in the initial displacement, step 2. Thereafter the spring was deactivated in the linear perturbation step.

In the second trial a vertical spring was inserted in Model5-a, to control the vertical displacement of RP-top in step 2. Thereafter the spring was deactivated in the linear perturbation step. Different values of the spring stiffness were used

*Table 5.17 Model5-a, results varying rotational stiffness of RP-top*

| | Step 2 | | | | Step 3 | | Bifurcation value | |
|---|---|---|---|---|---|---|---|---|
| Spring stiffness | U1 (mm) | U2 (mm) | RF 1 (kN) | RF2 (kN) | $F_x$ / $F_y$ (kN) | Eigen value | $H_{cr}$ (kN) | $V_{cr}$ (kN) |
| $10^8$ | 0.2 | 0 | 3.74 | -9.23 | 1 / 0 | 88.483 | 92.2 | 9.2 |
| $10^7$ | 0.2 | 0 | 2.10 | -8.24 | 1 / 0 | 89.342 | 91.4 | 8.2 |
| $10^6$ | 0.2 | 0 | 1.77 | -8.20 | 1 / 0 | 89.266 | 91.0 | 8.2 |
| $10^5$ | 0.2 | 0 | 1.74 | -8.20 | 1 / 0 | 89.257 | 91.0 | 8.2 |

*Table 5.18 Model5-a, results varying the vertical stiffness of RP-top*

| | Step 2 | | | | Step 3 | | Bifurcation value | |
|---|---|---|---|---|---|---|---|---|
| Spring stiffness | U1 (mm) | U2 (mm) | RF 1 (kN) | RF2 (kN) | $F_x$ / $F_y$ (kN) | Eigen value | $H_{cr}$ (kN) | $V_{cr}$ (kN) |
| $10^9$ | 0.2 | 0 | 1.46 | -6.69 | 1 / 0 | 90.177 | 91.6 | 6.7 |
| $10^8$ | 0.2 | 0 | 0.65 | -2.73 | 1 / 0 | 92.032 | 92.7 | 2.7 |
| $10^6$ | 0.2 | 0 | 0.1 | -0.17 | 1 / 0 | 93.671 | 93.7 | 0.2 |

The results of Table 5.17 and Table 5.18 show that the use of springs in this manner did not give the ability to correlate the results. But more importantly they show that the displacement and rotation of the shear wall element at the base state of the linear perturbation has a large impact on the critical value. With this insight the vertical force, vertical displacement and rotation around the z-axis after the initial displacement step was set to match the experimental elements just before the bifurcation point.

By observing experimental and Pontos measurements, see Appendix A and Appendix B, the total vertical force and vertical displacement were determined. To place the element in this state an extra static general analysis step was made after the initial displacement, where the vertical force was applied instead of the boundary condition.

| **Boundary condition** | **Step2 - static general** | **Step3 - static general** | **Step4 – linear perturbation** |
|---|---|---|---|
| RP-bottom | $u_x = u_y = u_z = 0$<br>$ur_y = ur_z = 0$ | $u_x = u_y = u_z = 0$<br>$ur_y = ur_z = 0$ | $u_x = u_y = u_z = 0$<br>$ur_y = ur_z = 0$ |
| RP-top | $u_x = 1$<br>$u_y = - 0.2$<br>$u_z = 0$, $ur_y = 0$ | $u_x = 5$<br>$CF_y = - 9.4$<br>$u_z = 0$, $ur_y = 0$ | $u_z = 0$, $ur_y = 0$<br>$[CF_x, CF_y, CF_z] = [1, 0, 0]$ |

| **Results** | Step 2 | | Step 3 | | Step 4 | | Bifurcation value | |
|---|---|---|---|---|---|---|---|---|
| Model | RF 1 (kN) | RF2 (kN) | RF 1 (kN) | CF2 (kN) | $F_x$ / $F_y$ (kN) | Eigen value | $H_{cr}$ (kN) | $V_{cr}$ (kN) |
| Model5-f | 12.79 | -67.10 | 2.28 | -9.4 | 1 / 0 | 69.372 | 71.65 | 9.4 |

The results from this model are very close to experimental values, the buckling mode shape also correspond to experiments.

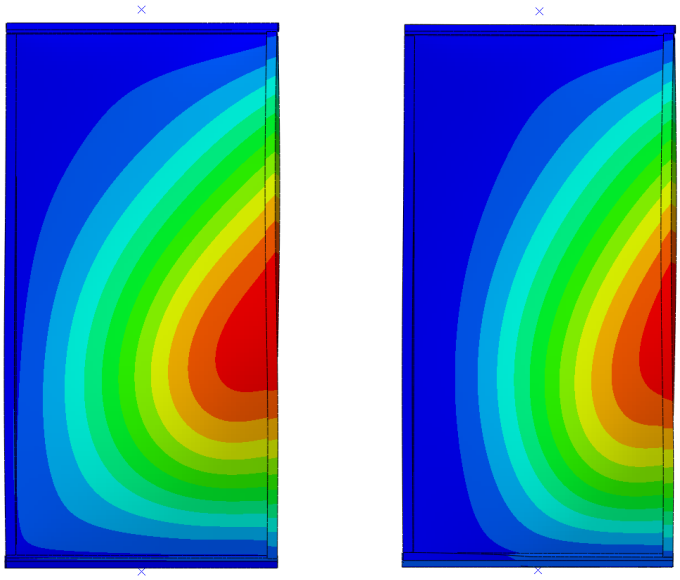

Model5-a Model5-f

*Figure 5.13 Buckling mode shapes, Model5-a and Model5-f*

The decrease of the horizontal buckling load is probably due to the larger vertical displacement of the lower left corner of the shear wall element. When the contact area of the bottom edge decreases, the compression forces gets more concentrated to the right side of the element, which means a higher compressive stress level and therefore a lower bifurcation point. This is also demonstrated by the shape of the buckling mode shapes shown in Figure 5.13, as the out of plane displacements are more concentrated to the right in Model5-f than in Model5-a. This reasoning also explains why a higher rotational stiffness generates a higher buckling load, i.e. increased rotational stiffness means less rotation of the upper edge, which in turn, by the bottom left corner not lifting, gives a more uniform distribution of the compressive stress through the element.

### 5.5.3 Models used as basis for results

At this stage it was difficult to in advance determined how large the displacement and rotation would be at different combined vertical and horizontal load ratios. And as shown in previous discussions the initial displacement is of great importance. Due to this fact the interaction in the combined load case was analyzed with Model5-a,-b,-c,-d and -e as basis. In these model the initial displacements is reasonably constant. The analysis procedure and boundary condition of these models are presented in section 5.5.2 and Table 5.16, to evaluate a larger variety of load ratios the reference loads ($CF_x$, $CF_y$) in the buckling step were altered. These analyses are presented in graphs with a corresponding estimation of an appropriate trend line, like the super ellipse equation (3.1) or the interaction equation (4.20).

The effect of altering material properties will be studied in the horizontal load case with Model5-a as basis, and the vertical load case with Model5-e as a basis. The analyses are conducted according to section 5.5.2 with boundary conditions according to Table 5.16, only material properties are changed in the models.

# 6 Results

## 6.1 Impact of adhesive stiffness

With Model5-a and Model5-f acting as a basic model in the horizontal and the vertical load case, respectively, changes of material properties ,i.e. stiffness, of Adhesive gave the following results.

*Table 6.1 Results – Horizontal and vertical buckling load, at various Adhesive stiffness.*

| Adhesive<br>E – modulus (MPa) | Horizontal<br>Buckling load (kN) | Vertical<br>Buckling load (kN) |
|---|---|---|
| 1.1 | 11.55 | 87.43 |
| 2 | 15.69 | 98.96 |
| 5 | 27.81 | 121.78 |
| 10 | 46.08 | 139.44 |
| 40 | 67.38 | 163.55 |
| 80 | 71.65 | 169.61 |
| 1000 | 76.68 | 177.04 |
| 5000 | 77.42 | 178.05 |

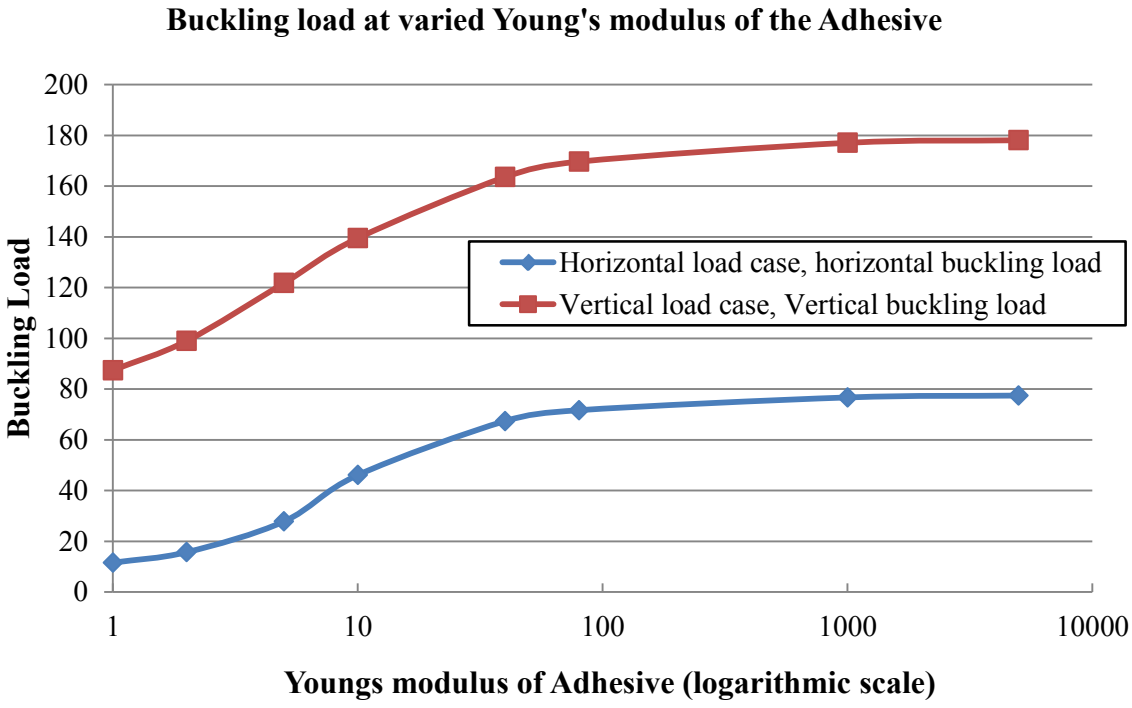


*Figure 6.1Buckling load, when varying adhesive stiffness (Young's modulus varied).*

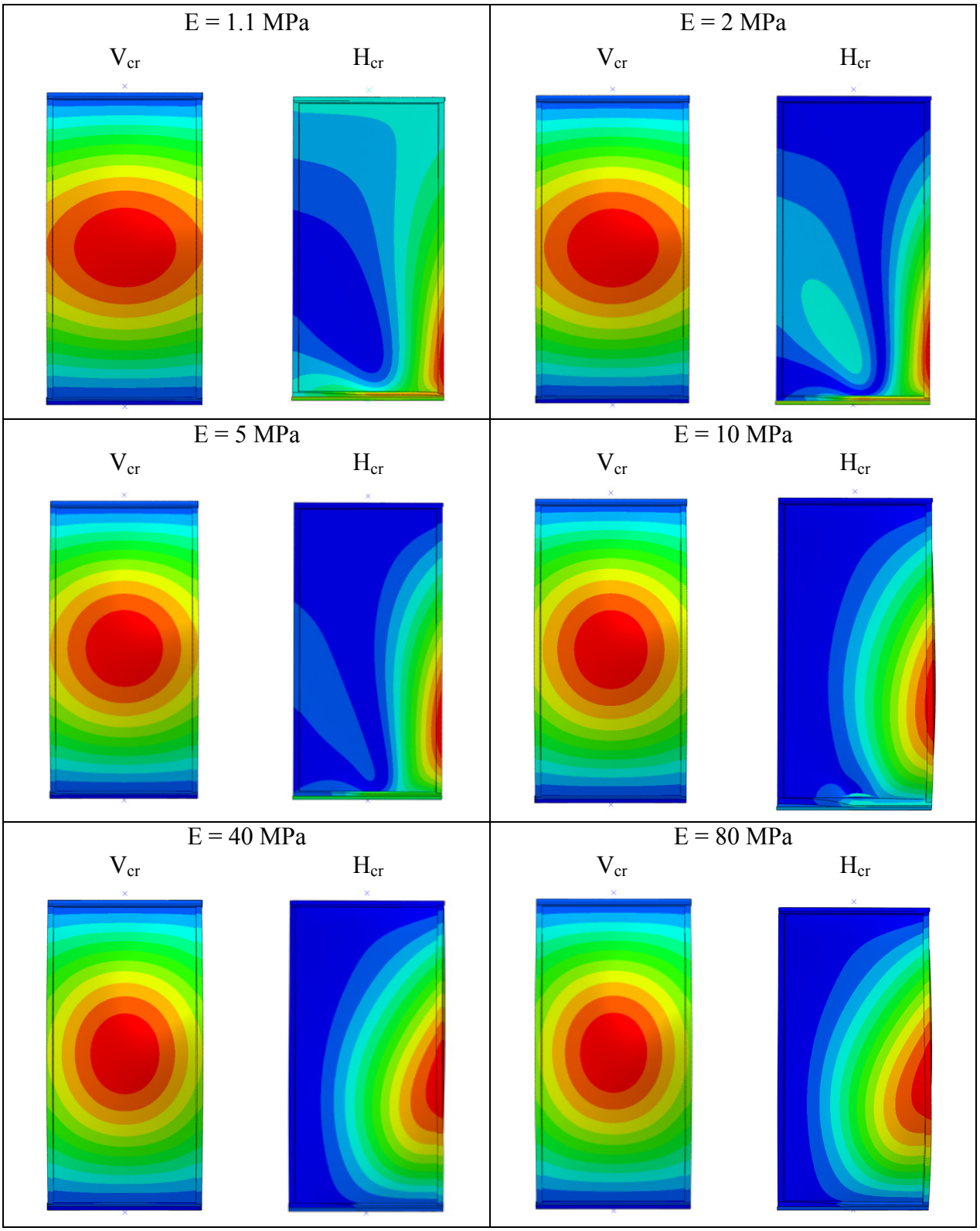


*Figure 6.2 Contour plots of the Buckling mode shapes, when varying adhesive stiffness. (Red equals the largest out of plane displacement).*

## 6.2 Impact of Glass stiffness

With Model5-a and Model5-f acting as a basic model in the horizontal and the vertical load case, respectively, changes of material properties ,i.e. stiffness, of Glass gave the following results.

*Table 6.2 Results - Impact of Glass stiffness*

| Glass<br>E – modulus (GPa) | Horizontal<br>Buckling load (kN) | Vertical<br>Buckling load (kN) |
|---|---|---|
| 7 | 27.70* | 77.55 |
| 60 | 67.31 | 158.54 |
| 70 | 69.95 | 165.32 |
| 77 | 71.65 | 169.61 |
| 90 | 74.19 | 176.81 |
| 500 | 132.10 | 292.68 |

** this was the third buckling mode, the first two were not valid buckling modes.*

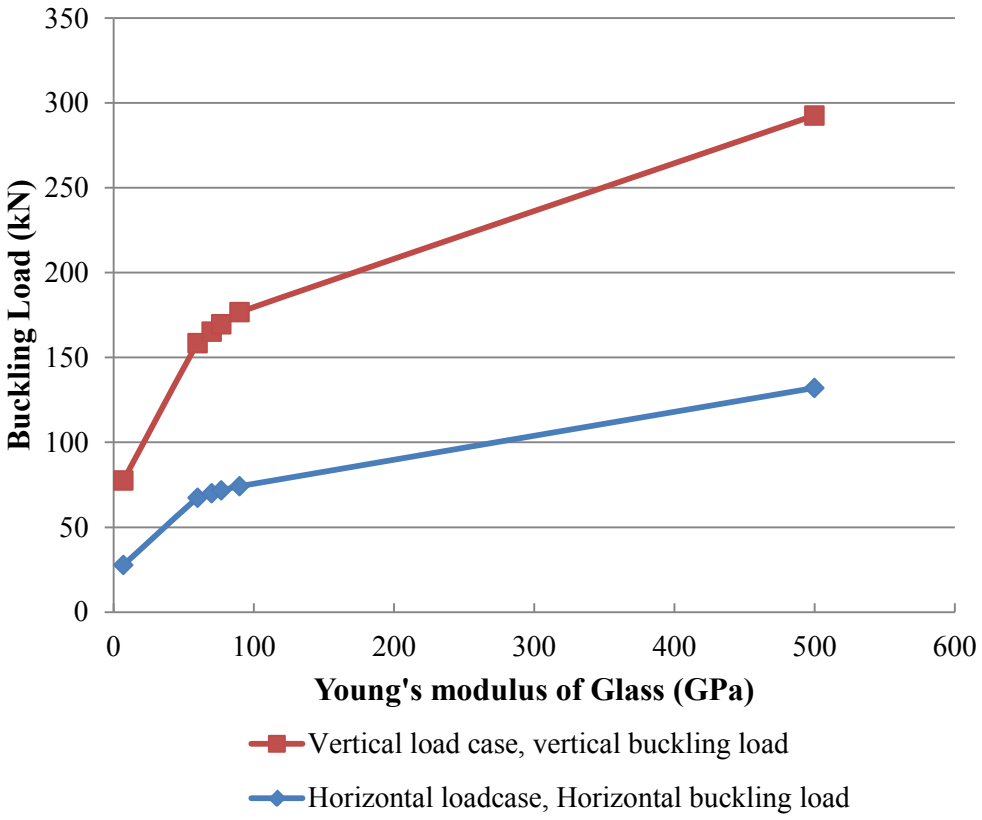


*Figure 6.3Buckling load, when varying Glass stiffness (Young's modulus varied).*

**Buckling shapes**

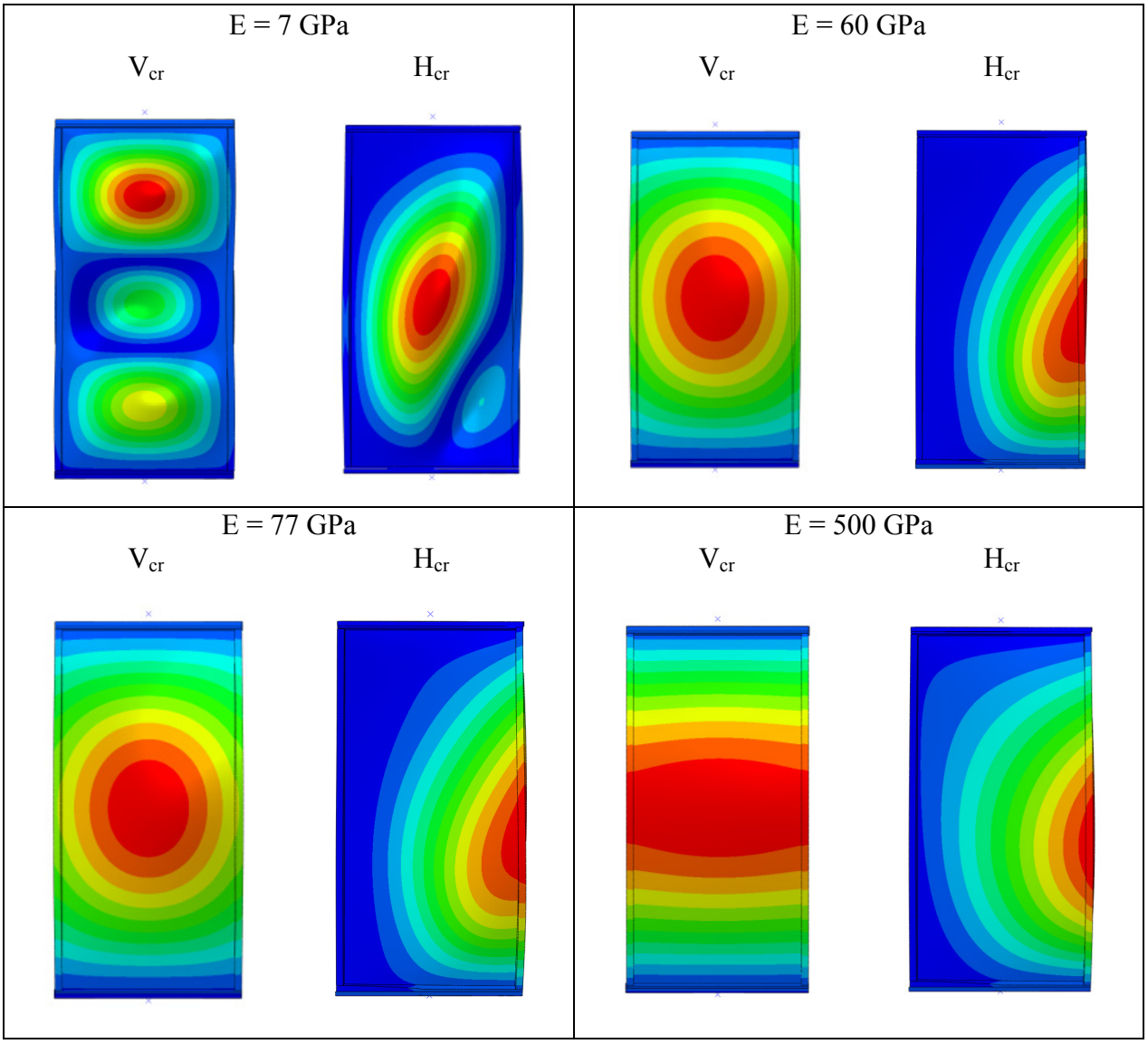


*Figure 6.4 Contour plot of the Buckling mode shapes, when varying Glass stiffness. (Red equals the largest out of plane displacement).*

## 6.3 Combined load case - Interaction effect

With material properties according to Table 5.6 and Table 5.7, Model5-a,-b,-c,-d and -e acting as a basic model, the combined load case gave the following results for different load ratios

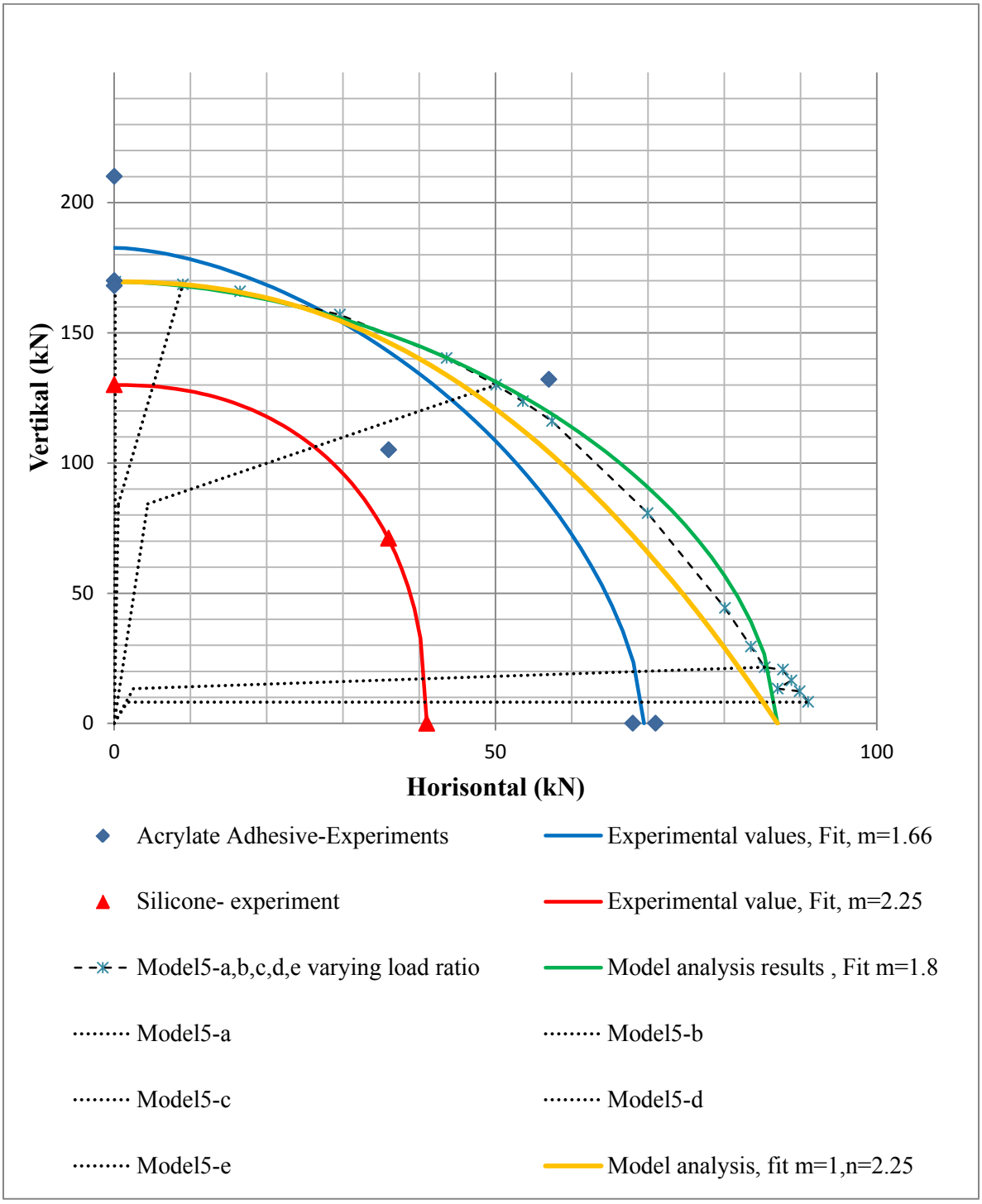


*Figure 6.5Buckling loads at combined load case, material properties according to Table 5.6*

*Fitted curves are calculated according to the super ellipse equation (3.1), and the interaction formula according to* $\left(\frac{V}{V_{cr}}\right)^m + \left(\frac{H}{H_{cr}}\right)^n = 1$.

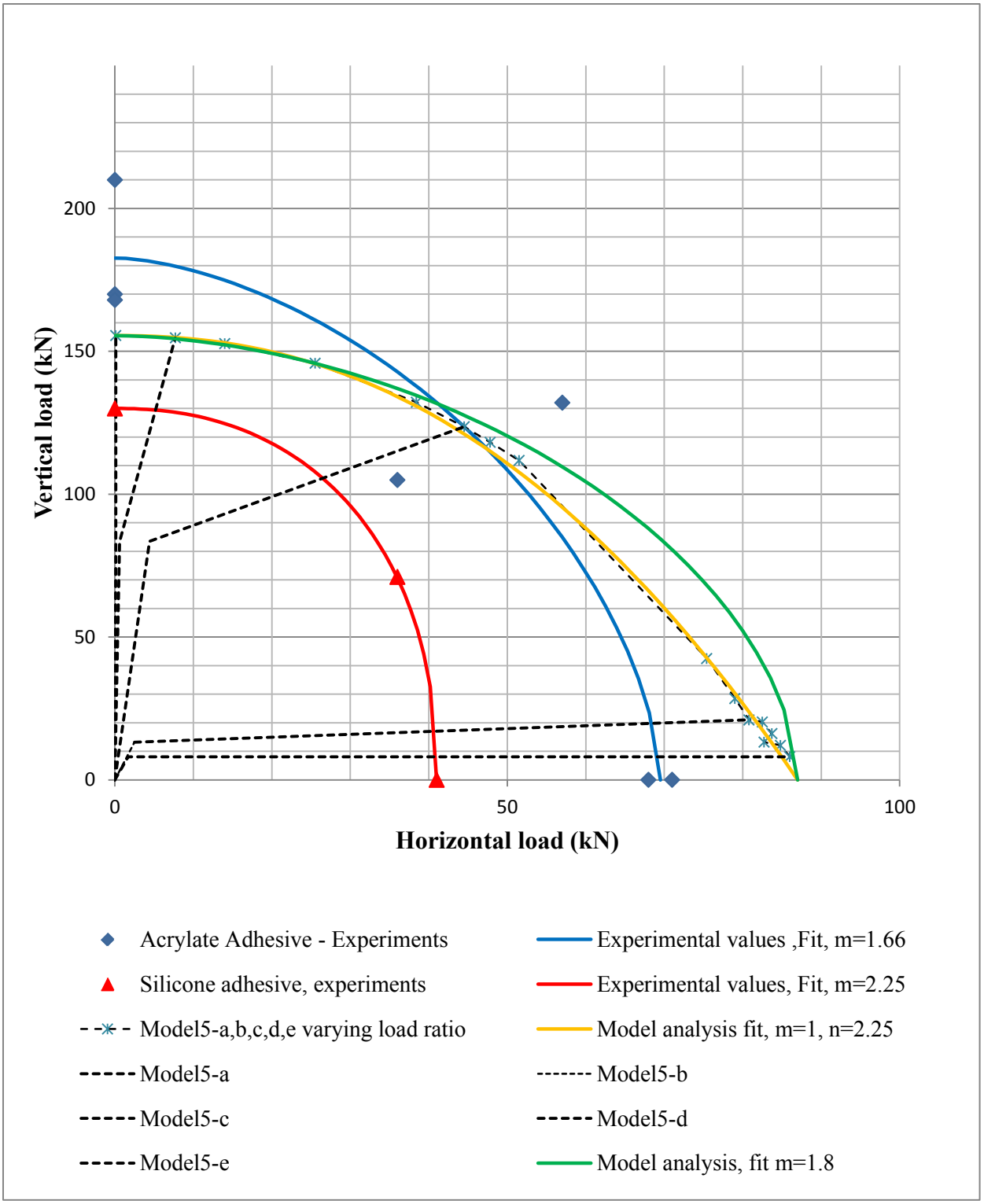


*Figure 6.6Buckling loads at combined load case, material properties according to Table 5.7 Fitted curves are calculated according to the super ellipse equation (3.1), and the interaction formula according to* $\left(\frac{V}{V_{cr}}\right)^m + \left(\frac{H}{H_{cr}}\right)^n = 1$.

# 7 Concluding remarks and discussion

The impact of the adhesive stiffness on the buckling load appears to have a decreasing effect as the adhesive stiffness increases over about 100 MPa. The buckling shape in Figure 6.2 for E = 1.1 MPa resembles the buckling shapes when the relative elastic stiffness of timber studs was decreased in relation to the glass stiffness in *Figure 6.4*. A probable cause is that not enough stiffness of the timber studs can be transferred to support the glass edge in an adequate manner.

The timber studs have a larger relative impact on the stability of the shear wall element, which can be seen when comparing the results of Table 6.2, Figure 6.5 and Figure 6.6. When decreaseing the elastic modulus $E_1$ of the timber the vertical buckling load decreases from 169.9 kN to 155.5 kN, when decreasing the glass elastic modulus in the same proportion the buckling load change from 169.9 kN to 165.3 kN.

The buckling shape is strongly dependent on the ratio between the stiffness of glass and the stiffness of the vertical timber studs. If the ratio in this model is given by [E-modulus Glass / E-modulus timber], then a larger ratio means that the buckling shape tends more to the shape of a column. This is illustrated in *Figure 6.4*. Considering the buckling load there is a significantly large difference in the capacity of a plate supported on two sides (i.e. slender column) or a plate simply supported around all edges. The timber studs should therefore be design to contribute with a large bending stiffness to stiffen the plate edge, thus the capacity of the glass plate increases

The horizontal buckling load can be increased by improving the corner ties. This would increase the timber frame's horizontal stiffness as well as increasing the bending stiffness of the vertical edge of the plate.

The fitted curves to the results of varying load ratios in Figure 6.5 and Figure 6.6 correspond approximately to the interaction formula (4.20) discussed in 4.1 and to earlier experimental values fitted with the super ellipse curve. However more analyses need to be done in order to draw any conclusions about the most appropriate formula.

The linear perturbation buckling analyses was in the end, after a lot of work, a good tool to use when estimating the critical load limit of the timber glass shear wall. However, the boundary conditions have showed to be of great importance in order to get an accurate result. When using the rigid bodies there must be a carefully chosen preload and pre displacement in order to calculate a correct eigenvalue, since the nonlinear behaviour in the contact condition is not included in the eigenvalue analysis.

# 8 Suggestions for Further work

When using this type of shear wall element as a horizontal stabilizer the vertical “hold down support” is of importance. How to practically solve this would be an interesting problem for further studies. If for example the timber frame is bolted into the floor structure, what kind of stresses occurs in the adhesive bond lines and which stiffness would be appropriate to use? There is also the question of what happens when several elements are connected and the vertical sides can interact.

The brittle behavior of glass has been discussed in this thesis, and it would be of interest to evaluate if a laminated glass plate could give the shear wall element increased capacity. Like the steel plate that has the ability to carry load after the bifurcation point, perhaps the laminate sheet could prevent the propagation of cracks and create a redundant structure.

# References


[1] L. Blyberg, "Timber/glass adhesive bonds for structural applications," Linnæus University, Växjö, 2011.

[2] O. e. a. Carling, Dimensionering av träkonstruktioner, Solna: AB svensk Byggtjänst, 1992.

[3] M. Johansson, "Structural properties of sawn timber and engineered wood products," in *Design of timber structures*, Stockholm, Swedish Wood, 2011.

[4] T. Isaksson and A. Mårtensson, Byggkonstruktion - Regel- och formelsamling, Lund: Studentlitteratur AB, 2010.

[5] S. Ormarsson, Numerical analysis of moisture-related distortions in sawn timber, Göteborg: Department of Structural Mechanics, Chalmers University of Technology, 1999.

[6] L. Blyberg and E. Serrano, "Timber/Glass adhesively bonded I-beams.," Linnæus University, Växjö, 2011.

[7] Glafo, Boken om glas, Växjö: Glafo, 2005.

[8] R. Nijsse, Glass in structures, Basel: Birkhäuser, 2003.

[9] F. A. Veer, "The strength of glass, effect of edge quality," in *Glass processing days, Conference proceedings*, Tampere, 2003.

[10] H. McArthur and D. Spalding, Enginrering materials science, Chichester: Horwood, 2004.

[11] F. Cobb, Structural Engineer's Pocket Book, Oxford: Elsevier Butterworth-Heinemann, 2004.

[12] A. Kott, "Remaining structural capacity of broken laminated safety glass," in *Glass processing days, Conference proceedings*, Tampere, 2003.

[13] W. Winter, W. Hochhauser and K. Kreher, "Load bearing and stiffening timber-glass-composites," in *WCTE 2010 Conference proceedings*, 2010.

[14] L. Blyberg, E. Serrano, B. Enquist and M. Sterley, "Adhesive joints for timber/glass applications - Part 1: Mechanical properties in shear and tension," Linnæus University, Växjö, 2011.

[15] P. Niedermaier, "Shear-strength of glass panel elements in combination with timber frame constructions," in *Glass processing days-Conference proceedings*, Tampere, 2003.

[16] S. Timoshenko and J. Gere, Theory of elastic stability, 2nd Edition, Stanford: McGraw-Hill Internationall Book Company, 1963.

[17] K. Runesson, A. Samuelsson and N.-E. Wiberg, Byggnadsmekanik - Knäckning, Lund: Studentlitteratur, 1992.

[18] B. Åkesson, Buckling - Ett instabilitetsfenomen att räkna med, Lund: Studentlitteratur, 2005.

[19] P. Bulson, The stability of flat plates, London: Chatto & Windus Ltd, 1970.

[20] N. Ottosen and H. Petersson, Introduction to the finite element method, Prentice Hall, 1992.

[21] R. Cook, Finite element modeling for stress analysis, John Wiley & sons, Inc, 1995.

[22] Dassault systèmes, "Abaqus 6.12 Online documentation," 13 February 2012. [Online]. Available: http://itchy:2080/v6.12/index.html. [Accessed Jan-May 2013].

# Appendix A

## Graphs generated from the experimental measurements.

### Vertical load case:

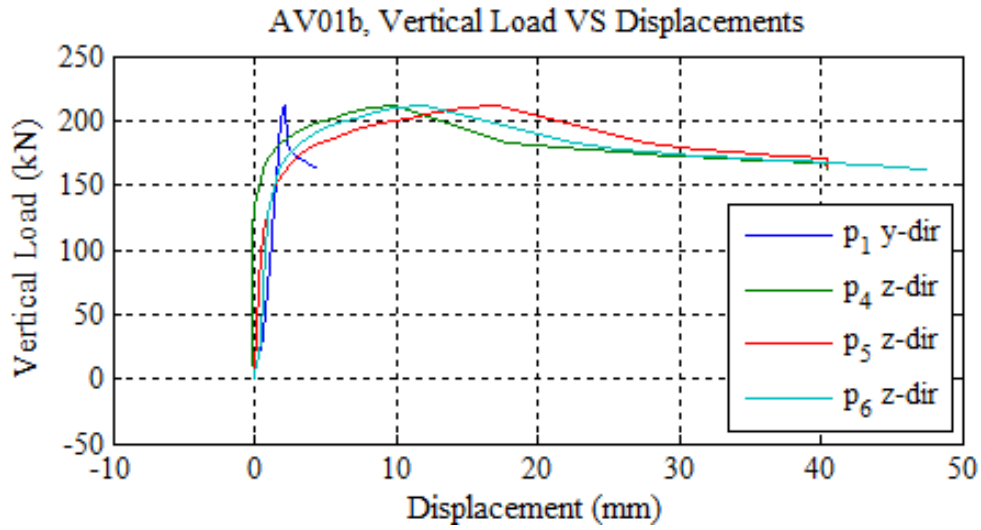


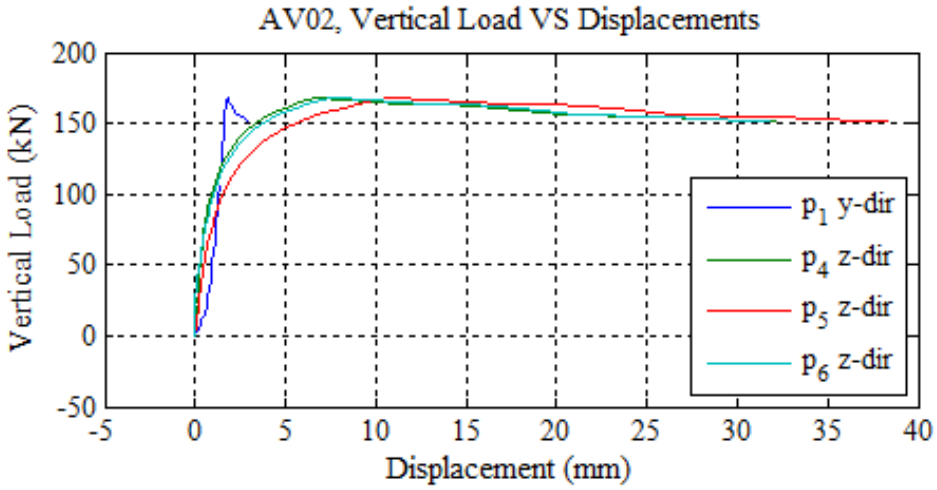


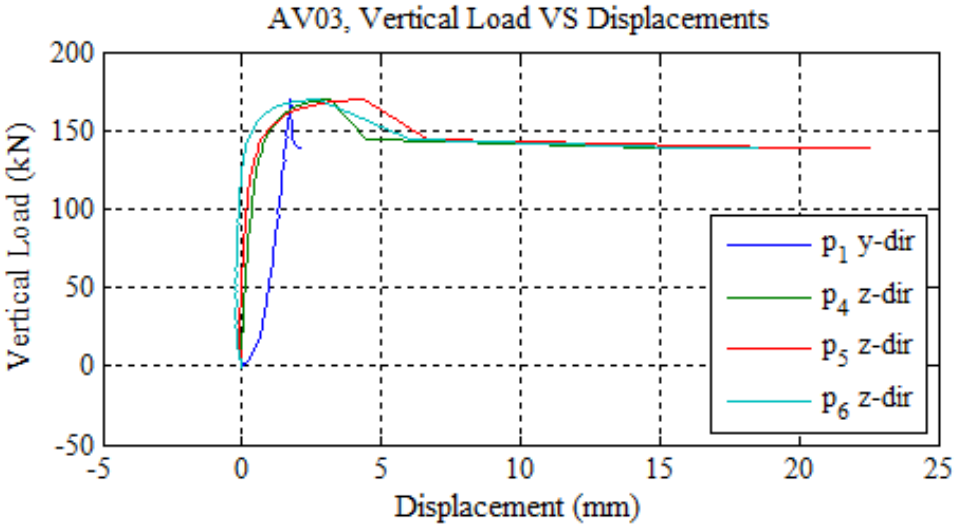

**Horizontal load case:**

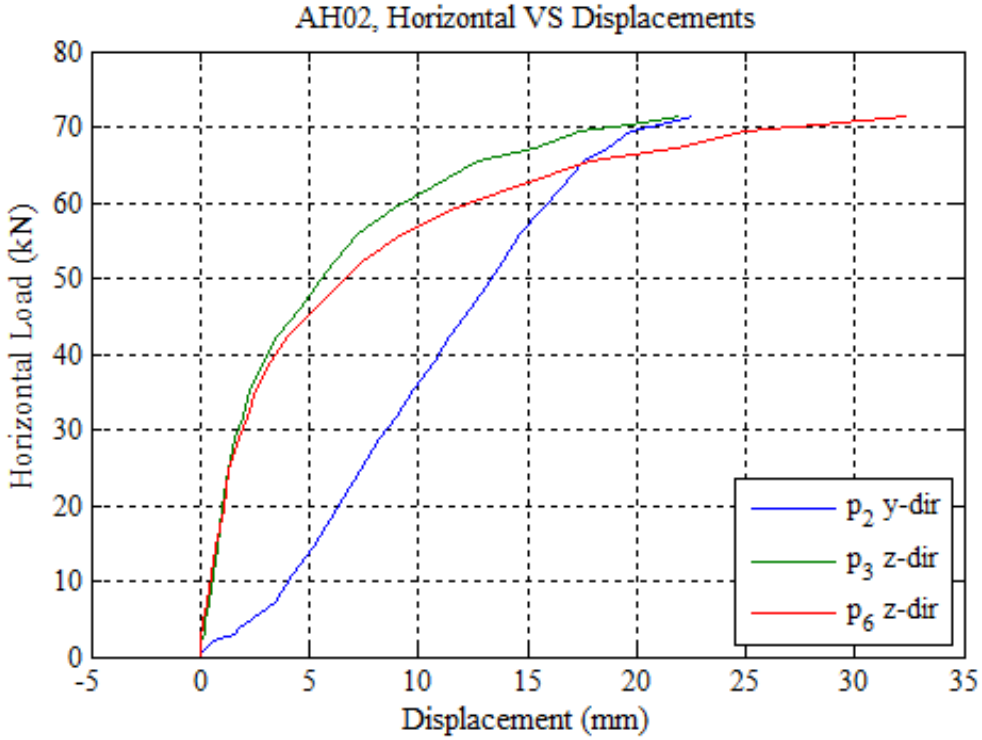


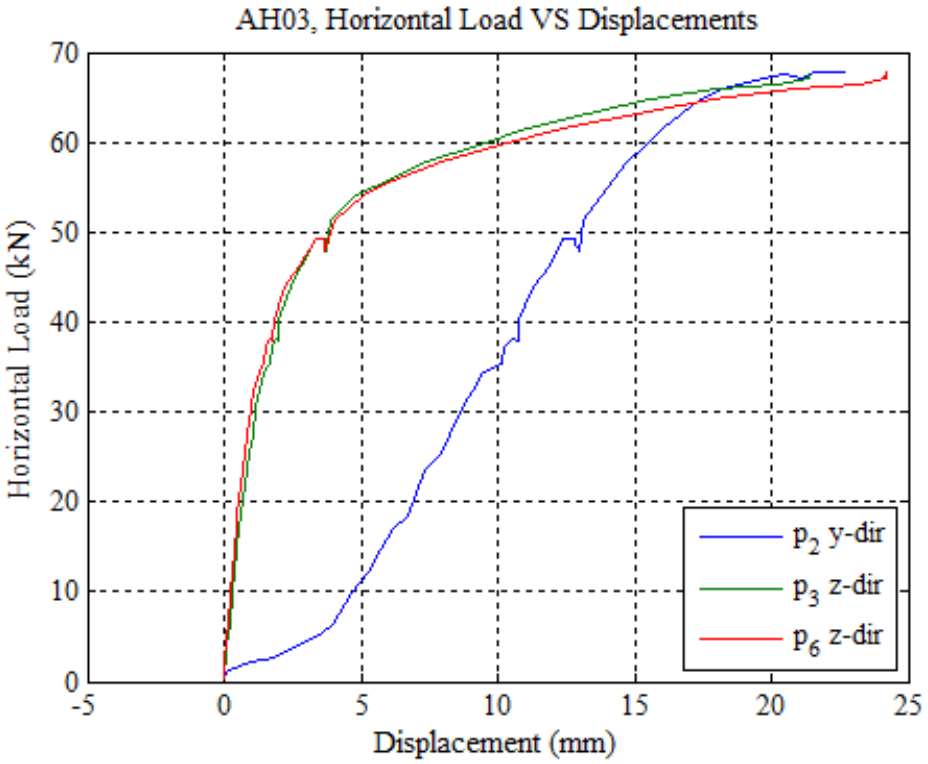

## Combined load case

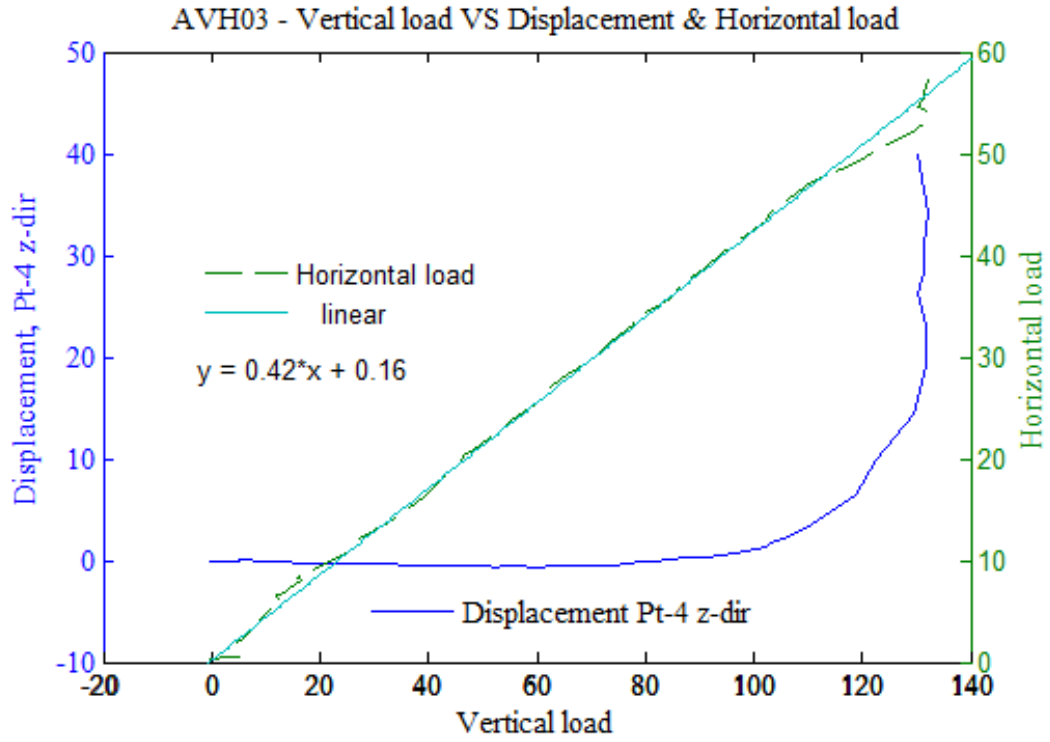


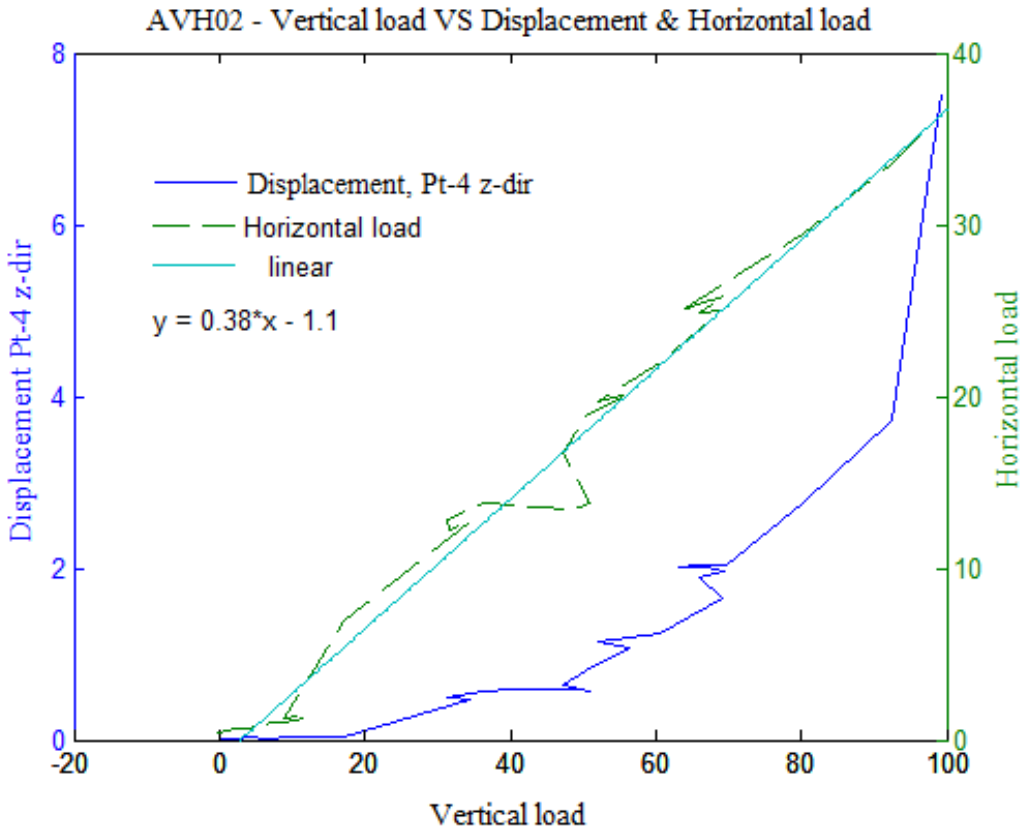

## Loading ratios:

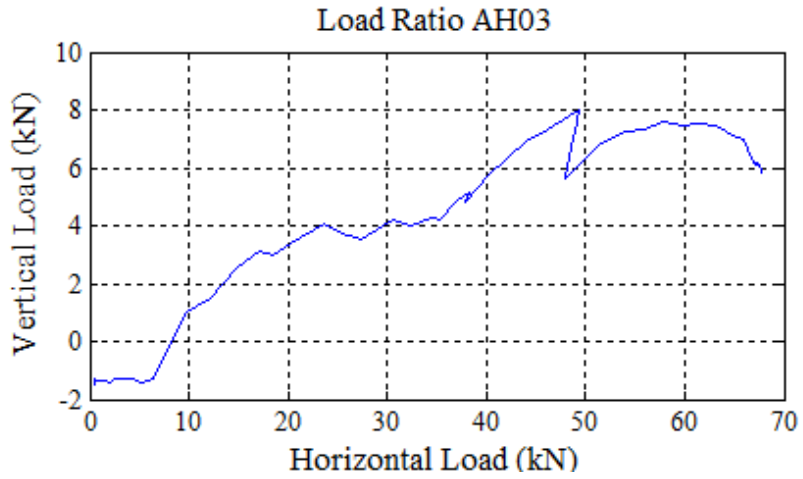


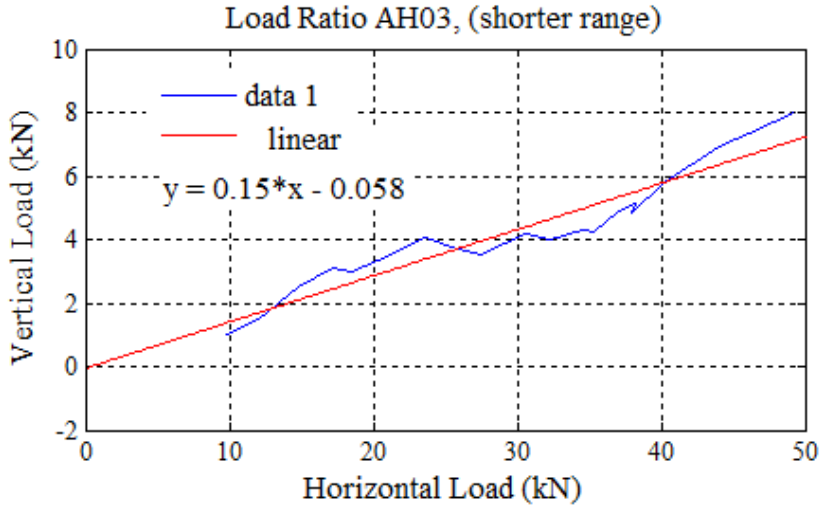


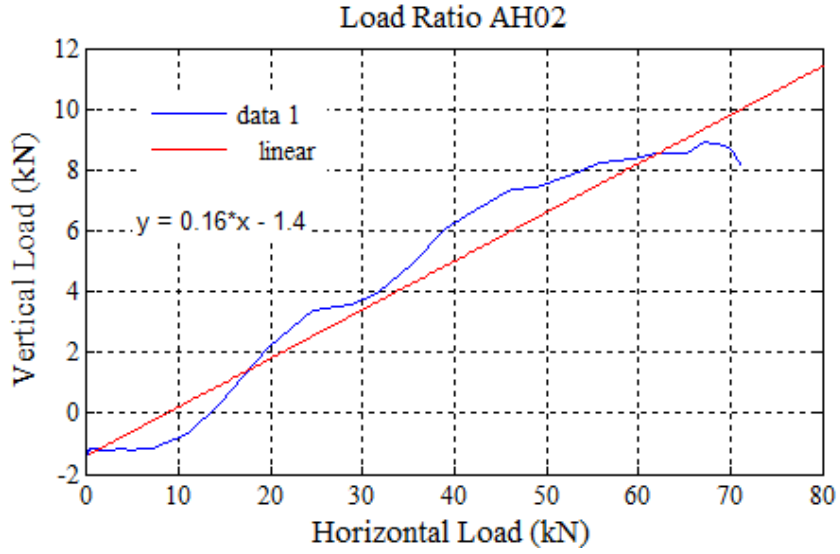

# Appendix B

## Determining vertical spring stiffness from Pontos measurements.

The load applying beam with measuring points

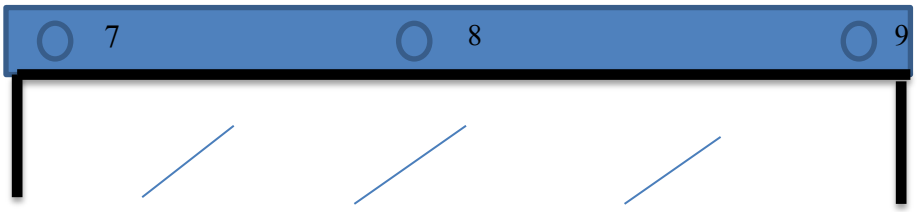


Values from the Pontos measurements were picked to estimate the vertical stiffness.

| Element | Vert. force | dY 7 | dV/dy | dY 8 | dV/dy | dY 9 | dV/dy |
|---|---|---|---|---|---|---|---|
| AV01b | 40 | -0.516 | | -0.525 | | -0.489 | |
| | | | -141 | | -142 | | -183 |
| | 80 | -0.799 | | -0.807 | | -0.708 | |
| | | | -215 | | -183 | | -177 |
| | 120 | -0.985 | | -1.025 | | -0.934 | |
| | mean | -174 | | | | | |
| AV02 | 30 | -0.741 | | -0.585 | | -0.44 | |
| | | | -211 | | -162 | | -161 |
| | 60 | -0.883 | | -0.77 | | -0.626 | |
| | | | -179 | | -207 | | -132 |
| | 90 | -1.051 | | -0.915 | | -0.853 | |
| | mean | -175 | | | | | |
| AV03 | 30 | -1.041 | | -0.73 | | -0.357 | |
| | | | -244 | | -222 | | -155 |
| | 60 | -1.164 | | -0.865 | | -0.551 | |
| | | | -259 | | -172 | | -200 |
| | 90 | -1.28 | | -1.039 | | -0.701 | |
| | mean | -209 | | | | | |
| | mean | 186 | kN/mm | | | | |

To correlate the vertical stiffness of the model so that it better match the real shear wall, a spring is added. The stiffness of the added spring is calculated as illustrated below:

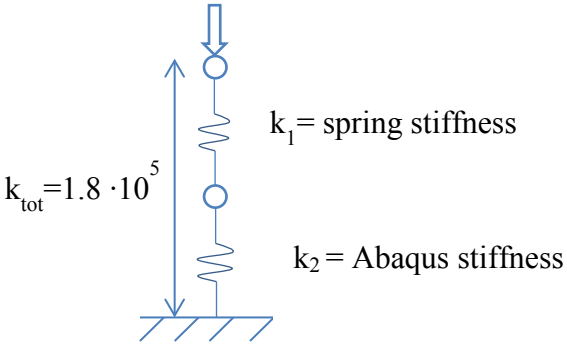


$$\frac{1}{\mathrm{k}_{tot}} = \frac{1}{k_1} + \frac{1}{k_2} \rightarrow k_1 = \frac{1}{\frac{1}{\mathrm{k}_{tot}} - \frac{1}{k_2}}$$

The vertical stiffness in the Abacus models were found by making a vertical displacement $\Delta u_y$ and observing the reactionforce $\Delta F_2$, this gives $k_2 = \Delta F_2/\Delta u_y$. Models with different material properties were evaluated.

Material properties according to Table 5.6 gives:

$$k_2 = \Delta F_2/\Delta u_y = 105.3\ (\mathrm{kN})/0.25(\mathrm{mm}) = 421\ \mathrm{kN/mm}$$

$$k_1 = \frac{1}{\frac{1}{1.8 \cdot 10^5} - \frac{1}{4.21 \cdot 10^5}} = 3.14 \cdot 10^5\ \mathrm{N/mm}$$

Material properties according to Table 5.7 gives:

$$k_2 = \Delta F_2/\Delta u_y = 117.6\ (\mathrm{kN})/0.3(\mathrm{mm}) = 392\ \mathrm{kN/mm}$$

$$k_1 = \frac{1}{\frac{1}{1.8 \cdot 10^5} - \frac{1}{3.92 \cdot 10^5}} = 3.33 \cdot 10^5\ \mathrm{N/mm}$$

## Determining vertical displacements in horizontal load case, from Pontos measurements.

| Element | H. force | Y 7 (mm) | Δy(mm) | Y 8 (mm) | Δy(mm) | Y 9 (mm) | Δy(mm) |
|---|---|---|---|---|---|---|---|
| AH02 | 0 | -0.03 | 0 | -0.039 | 0 | 0.02 | 0 |
| | | 0.392 | 0.422 | 0.061 | 0.1 | 0.008 | -0.012 |
| | | 1.789 | 1.819 | 0.625 | 0.664 | 0.008 | -0.012 |
| | | 3.165 | 3.195 | 1.494 | 1.533 | 0.282 | 0.262 |
| | $H_{cr}$ | 4.154 | 4.184 | 2.322 | 2.361 | 0.961 | 0.941 |

# Appendix C

## Tables associated with the results.

**Impact of Adhesive stiffness**

Vertical

Basic model5-e

| Model | U1 | U2 | RF 1 | RF2 | $F_x$ / $F_y$ | Eigen value | $H_{cr}$ | $V_{cr}$ |
|---|---|---|---|---|---|---|---|---|
| | (mm) | (mm) | (kN) | (kN) | (kN) | | (kN) | (kN) |
| Model5-e | 0 | -0.2 | 0.13 | -84.2 | 0 / -1 | 85.413 | 0.1 | 169.6 |

| Mod num | Emodulus | RF 1 | RF2 | Eigen value | $V_{cr}$ |
|---|---|---|---|---|---|
| | Mpa | N | N | | (kN) |
| 1 | 1 | 156 | 79245 | 8.1824 | 87.43 |
| 2 | 2 | 153 | 79846 | 19.109 | 98.96 |
| 3 | 5 | 146 | 81083 | 40.698 | 121.78 |
| 4 | 10 | 140 | 82108 | 57.333 | 139.44 |
| 5 | 40 | 131 | 83712 | 79.833 | 163.55 |
| Basic | 80 | 130 | 84200 | 85.413 | 169.61 |
| 6 | 1000 | 127 | 84981 | 92.062 | 177.04 |
| 7 | 5000 | 133 | 85378 | 92.667 | 178.05 |

Horizontal

Basis model5-f

| **Results** | Step 2 | | Step 3 | | Step 4 | | Bifurcation value | |
|---|---|---|---|---|---|---|---|---|
| Model | RF 1 | RF2 | RF 1 | CF2 | $F_x$ / $F_y$ | Eigen value | $H_{cr}$ | $V_{cr}$ |
| | (kN) | (kN) | (kN) | (kN) | (kN) | | (kN) | (kN) |
| Model5-f | 12.79 | -67.1 | 2.28 | -9.4 | 1 / 0 | 69.372 | 71.65 | 9.4 |

| Mod num | Emodulus | RF 1 | RF2 | Eigen value | $H_{cr}$ |
|---|---|---|---|---|---|
| | Mpa | N | N | | (kN) |
| 1 | 1 | 2273 | 9400 | 9.2767 | 11.55 |
| 2 | 2 | 2274 | 9400 | 13.416 | 15.69 |
| 3 | 5 | 2275 | 9400 | 25.536 | 27.81 |
| 4 | 10 | 2276 | 9400 | 43.801 | 46.08 |
| 5 | 40 | 2278 | 9400 | 65.102 | 67.38 |
| Basic | 80 | 2280 | 9400 | 69.372 | 71.65 |
| 6 | 1000 | 2281 | 9400 | 74.403 | 76.68 |
| 7 | 5000 | 2281 | 9400 | 75.134 | 77.42 |

**Impact of Glass stiffness**

Vertical

Basic model5-e

| Model | U1 | U2 | RF 1 | RF2 | $F_x$ / $F_y$ | Eigen value | $H_{cr}$ | $V_{cr}$ |
|---|---|---|---|---|---|---|---|---|
| | (mm) | (mm) | (kN) | (kN) | (kN) | | (kN) | (kN) |
| Model5-e | 0 | -0.2 | 0.13 | -84.2 | 0 / -1 | 85.413 | 0.1 | 169.6 |

| Mod num | E-modulus | RF 1 | RF2 | Eigen value | $V_{cr}$ |
|---|---|---|---|---|---|
| | Gpa | N | N | | (kN) |
| 1 | 7 | 2 | 13018 | 64.535 | 77.55 |
| 2 | 60 | 95 | 67276 | 91.268 | 158.54 |
| 3 | 70 | 114 | 77238 | 88.086 | 165.32 |
| Basic | 77 | 130 | 84200 | 85.413 | 169.61 |
| 4 | 90 | 154 | 97124 | 79.682 | 176.81 |
| 5 | 500 | 590 | 267141 | 25.543 | 292.68 |

Horizontal

Basis model5-f

| **Results** | Step 2 | | Step 3 | | Step 4 | | Bifurcation value | |
|---|---|---|---|---|---|---|---|---|
| Model | RF 1 | RF2 | RF 1 | CF2 | $F_x$ / $F_y$ | Eigen value | $H_{cr}$ | $V_{cr}$ |
| | (kN) | (kN) | (kN) | (kN) | (kN) | | (kN) | (kN) |
| Model5-f | 12.79 | -67.1 | 2.28 | -9.4 | 1 / 0 | 69.372 | 71.65 | 9.4 |

| Mod num | Emodulus | RF 1 | RF2 | Eigen value | $H_{cr}$ |
|---|---|---|---|---|---|
| | Gpa | N | N | | (kN) |
| 1 | 7 | 2211 | 9400 | 25.49* | 27.70 |
| 2 | 60 | 2269 | 9400 | 65.036 | 67.31 |
| 3 | 70 | 2275 | 9400 | 67.672 | 69.95 |
| Basic | 77 | 2280 | 9400 | 69.372 | 71.65 |
| 4 | 90 | 2280 | 9400 | 71.912 | 74.19 |
| 5 | 500 | 2284 | 9400 | 129.82 | 132.10 |

* Third mode, first two negative